


2011

Numerical Simulations of Heat Transfer Processes in a Dehumidifying Wavy Fin and a Confined Liquid Jet Impingement on Various Surfaces

Mutasim Mohamed Sarour Elsheikh
University of South Florida, melsheikh@mail.usf.edu

Follow this and additional works at: <http://scholarcommons.usf.edu/etd>

 Part of the [American Studies Commons](#), and the [Mechanical Engineering Commons](#)

Scholar Commons Citation

Elsheikh, Mutasim Mohamed Sarour, "Numerical Simulations of Heat Transfer Processes in a Dehumidifying Wavy Fin and a Confined Liquid Jet Impingement on Various Surfaces" (2011). *Graduate Theses and Dissertations*.
<http://scholarcommons.usf.edu/etd/3090>

This Thesis is brought to you for free and open access by the Graduate School at Scholar Commons. It has been accepted for inclusion in Graduate Theses and Dissertations by an authorized administrator of Scholar Commons. For more information, please contact scholarcommons@usf.edu.

Numerical Simulations of Heat Transfer Processes in a Dehumidifying Wavy Fin and a
Confined Liquid Jet Impingement on Various Surfaces

by

Mutasim Mohamed Sarour Elsheikh

A thesis submitted in partial fulfillment
of the requirements for the degree of
Master of Science in Mechanical Engineering
Department of Mechanical Engineering
College of Engineering
University of South Florida

Major Professor: Muhammad M. Rahman, Ph.D.
Frank Pyrtle, III, Ph.D.
Stuart Wilkinson, Ph.D.

Date of Approval:
March 23, 2011

Keywords: Fully-Confined Fluid Jet Impingement, Steady State, Transient Analysis,
Conjugates Heat Transfer, Heat Flux

Copyright © 2011, Mutasim Mohamed Sarour Elsheikh

Dedication

To God.

In the name of Allah, Most Gracious, Most Merciful,

I bear witness that there is no God but Allah, and Mohamed is the Messenger of Allah.

To my mother, Azeeza,

thank you for everything that you have done, for all of your love and support.

I also wish to thank my wife, Haifa, and our lovely kids, Azeeza and Magdi,

and my dear brother Magdi.

I dedicate this thesis especially in memory of my father, Mohamed Sarour.

Finally, to my Major Professor Muhammad Mustafizur Rahman,

thank you for your enormous tolerance and guidance. Without your guidance and

persistent help, this thesis would not have been materialized.

Acknowledgements

Apart from individual effort, the success of any project depends largely on the encouragement and guidance of many others. I take this opportunity to express my gratitude to the people who have been instrumental in the successful completion of this project.

I would like to express my sincere appreciation to Mr. Bernard Batson for his support and encouragement. I would like to also thank Donovan Industries (Tampa, FL) and the generous support from the National Science Foundation S-STEM grant DUE #0807023.

Also, I would like to thank Professor Frank Pyrtle and Professor Stuart Wilkinson for being my committee members. I am grateful for their constant support and help.

Special thanks to Dr. Luis Rosario and Dr. Jorge C. Lallave, for their guidance and valuable support.

In addition, I sincerely thank Professor Ashok Kumar for his help and guidance. I wish to thank John Shelton and Daniel Miller for their help in revising my thesis. Last but not least, I would like to thank Sue Britten, Shirley Tervort, and Wes Frusher for their help.

Table of Contents

List of Tables	ii
List of Figures	iii
List of Symbols	vi
Abstract	x
Chapter 1: Introduction and Literature Review	1
1.1 Introduction (Heat Transfer in a Wavy Fin Assembly)	1
1.2 Literature Review (Heat Transfer in a Wavy Fin Assembly)	2
1.3 Introduction (Heat Transfer by Jet Impingement)	6
1.4 Literature Review (Heat Transfer by Jet Impingement)	7
Chapter 2: Heat Transfer Analysis of Wavy Fin Assembly with Dehumidification	12
2.1 Physical Description of Wavy Fin Heat Exchangers	12
2.2 Mathematical Model	18
2.3 Results and Discussion	23
Chapter 3: Conjugate Heat Transfer Analysis of a Confined Liquid Jet Impingement on Concave and Convex Surfaces	36
3.1 Modeling and Simulation	36
3.2 Results and Discussion	41
Chapter 4: Conclusions	62
References	65
Appendices	70
Appendix A: Q-Basic Heat Transfer Code of a Wavy Fin Analysis	71
Appendix B: FIDAP Code for Analysis of Heat Transfer by Jet Impingement	79

List of Tables

Table 2.1	Geometric dimensions of sample wavy fin-and-tube heat exchangers.	16
Table 2.2	Geometric dimensions of sample fin-and-tube heat exchangers.	17

List of Figures

Figure 2.1	Most evaporator uses in air condition systems.	12
Figure 2.2	Schematic diagram of evaporator.	13
Figure 2.3	Some types of fins.	13
Figure 2.4	Side views of a wavy fin assembly.	14
Figure 2.5	Side views of the physical wavy model.	14
Figure 2.6	Side views of the physical street radial model.	15
Figure 2.7	Variation of dimensionless temperature distribution with the variation in relative humidity.	24
Figure 2.8	Variation of dimensionless temperature distribution with variation in cold fluid temperature at relative humidity 50%.	25
Figure 2.9	Variation of dimensionless temperature distribution with variation in surrounding air dry bulb temperature at relative humidity 50%.	27
Figure 2.10	The present model with and without insulation in the fin tip, and at 50% RH.	28
Figure 2.11	Comparison of rectangular and wavy models for dry and 50% RH.	29
Figure 2.12	Comparison between present model and Kazeminejad [6]; and Rosario and Rahman [10].	30
Figure 2.13	$(Aug)_{dry}/(Aug)_{wet}$ variation with change in T_1 .	31
Figure 2.14	$(Aug)_{dry}/(Aug)_{wet}$ variation with change in T_2 .	32
Figure 2.15	$(Aug)_{dry}/(Aug)_{wet}$ variation with change in RH.	33

Figure 2.16	Comparison of 1-D and 2-D radial models for dry and 50% RH.	34
Figure 2.17	Comparison of the wavy model and the converted rectangular model at dry and 50% RH.	35
Figure 3.1	Two-dimensional liquid jet impingement on a uniformly heated concave surface.	36
Figure 3.2	Velocity vector distribution for jet impingement on a curved copper plate.	41
Figure 3.3	Solid–fluid interface temperature for different number of elements in x and y directions ($Re = 1,000$, $b = 30$, $w = 0.6$ cm).	42
Figure 3.4	Dimensionless interface temperature and Local Nusselt number distribution for (a) concave and (b) convex copper plate at different Reynolds numbers and water as the cooling fluid.	44
Figure 3.5	Average Nusselt number at different Reynolds numbers for (a) concave (b) convex copper plate with water as the cooling fluid ($R = 6.21, 6.61, 7.01$, and ∞ cm).	46
Figure 3.6	Solid–fluid interface distance and (a) dimensionless interface temperature distribution (b) Local Nusselt number distribution for a concave copper wafer at different radius, and water as the cooling fluid ($R = 6.21, 6.61, 7.01$, and ∞ cm).	48
Figure 3.7	Solid–fluid interface distance and (a) dimensionless interface temperature distribution (b) Local Nusselt number distribution for a convex copper wafer at different radius, and water as the cooling fluid ($R = 6.21, 6.61, 7.01$, and ∞ cm).	49
Figure 3.8	Solid–fluid interface distance and (a) dimensionless interface temperature distribution (b) Local Nusselt number distribution for different material thickness ($H = 1, 1.5, 2, 2.5$, and 3 cm).	51
Figure 3.9	Solid–fluid interface distance and (a) dimensionless interface temperature distribution (b) Local Nusselt number distribution for different spacing of concave curvature ($D = 0.1, 0.2, 0.3, 0.4$, and 0.5 cm).	53

Figure 3.10	Solid–fluid interface distance and (a) dimensionless interface temperature distribution (b) Local Nusselt number distribution for different spacing of convex curvature ($D = 0.1, 0.2, 0.3, 0.4,$ and 0.5 cm).	54
Figure 3.11	Solid–fluid interface distance and (a) dimensionless interface temperature distribution (b) Local Nusselt number distribution for different materials (copper, silicon, aluminum, and Constantan).	56
Figure 3.12	Dimensionless interface temperature and Local Nusselt number distribution for (a) concave and (b) convex silicon plates at different Reynolds numbers and water as the cooling fluid.	59
Figure 3.13	Stagnation Nusselt number comparison of Rahman et al. [49], Inoue et al. [40], with actual numerical results under different Reynolds numbers ($w = 4$ mm, $d = 2$ mm).	61

List of Symbols

b	Inner solid thickness [m]
Bi	Fin Biot number, h_2t/k_f
Bi ₁	Cold fluid Biot number, h_1p/k_w
Bi ₂	Ambient Biot number, h_2p/k_w
c _{pa}	Specific heat of dry air [J/kg °C]
d	Channel spacing [m]
h	Heat transfer coefficient [W/m ² K], $q_{int}/(T_{int}-T_j)$
h ₁	Cold fluid heat transfer coefficient [W/m ² °C]
h ₂	Ambient heat transfer coefficient [W/m ² °C]
h _d	Mass transfer coefficient [kg/m ² s]
h _m	Mass transfer coefficient [J/kg]
h _n	Height of the nozzle from the plate [m]
h _{fg}	Latent heat of condensation [J/kg]
H	Outer solid thickness
k	Thermal conductivity [W/m K]
k _f	fin thermal conductivity [W/m°C]
k _w	Wall thermal conductivity [W/m°C]
K	Thermal conductivity ratio (fin-wall), (k_f/k_w)
	Mass flow rate of air [kg/s]

Nu	Nusselt number, $(h \cdot d_n) / k_f$
Nu _{av}	Average Nusselt number for the entire surface, $(h_{av} \cdot d_n) / k_f$
p _t	Half fin pitch [m]
p	Pressure [Pa]
P	Aspect ratio, $(t/p)_q$ Heat flux [W/m ²]
q _c	latent heat flux [W]
q _s	Sensible heat flux [W]
q _t	Total heat flux, $q_s + q_c$ [W]
r	Radial coordinate [m]
R	Ratio of sensible to total heat transfer calculated at fin temperature
R _b	Ratio of sensible to total heat transfer rate at fin base temperature
R _l	Ratio of sensible to total heat transfer rate at fin tip temperature
R ₀	Outer radius of curvature [m]
R _i	Inner radius of curvature [m]
Re	Reynolds number, $(V_j \cdot w) / \nu_f$
RH	Relative humidity
R _T	Fin tip radius [m]
t	Half fin thickness [m]
T	Temperature [°C]
T ₁	Cold fluid temperature [°C]
T ₂	Ambient dry bulb temperature [°C]
V _j	Jet velocity [m/s]
w	Wall thickness [m]

w_n	Nozzle width [m]
	Humidity ratio at the surface
	Humidity ratio at any point
W	Dimensionless wall thickness $(w)/p$
x	x- coordinate [m]

Greek Symbols

Δ	Dimensionless fin thickness (δ_o/p)
ρ_{ma}	Mosit air density $[\text{kg}/\text{m}^3]$
θ_1	Fin angle [$^\circ$]
η	Fin efficiency
Θ_1	Dimensionless temperature $(T-T_2)/(T_1-T_2)$
α	Thermal diffusivity $[\text{m}^2/\text{s}]$
β	Channel spacing ratio, b/d
ε	Thermal conductivity ratio, k_s/k_f
ϕ	Angular coordinate [rad]
Φ	Solid thickness to curvature ratio, b/R_o
ν	Kinematic viscosity $[\text{m}^2/\text{s}]$
θ	Angular coordinate [rad]
Θ	Dimensionless temperature, $2 \cdot k_f (T_{int} - T_j) / (q \cdot w)$
ρ	Density $[\text{kg}/\text{m}^3]$
ψ	Radius of curvature, R_o / d

Subscripts

1	Cold fluid side
2	Air side
avg	Average
e	Outer edge of the fin
f	Fin
f	Fluid
i	Interfacial location
int	Solid-fluid interface
j	Jet or inlet
max	Maximum
n	Nozzle
s	Solid
w	Wall
δ	Condensate film

Abstract

This thesis consists of two different research problems. In the first one, the heat transfer characteristic of wavy fin assembly with dehumidification is carried out. In general, fin tube heat exchangers are employed in a wide variety of engineering applications, such as cooling coils for air conditioning, air pre-heaters in power plants and for heat dissipation from engine coolants in automobile radiators. In these heat exchangers, a heat transfer fluid such as water, oil, or refrigerant, flows through a parallel tube bank, while a second heat transfer fluid, such as air, is directed across the tubes. Since the principal resistance is much greater on the air side than on the tube side, enhanced surfaces in the form of wavy fins are used in air-cooled heat exchangers to improve the overall heat transfer performance. In heating, ventilation, and air conditioning systems (HVAC), the air stream is cooled and dehumidified as it passes through the cooling coils, circulating the refrigerant. Heat and mass transfer take place when the coil surface temperature in most cooling coils is below the dew point temperature of the air being cooled. This thesis presents a simplified analysis of combined heat and mass transfer in wavy-finned cooling coils by considering condensing water film resistance for a fully wet fin in dehumidifier coil operation during air condition. The effects of variation of the cold fluid temperature ($-5^{\circ}\text{C} - 5^{\circ}\text{C}$), air side temperature ($25^{\circ}\text{C} - 35^{\circ}\text{C}$), and relative humidity (50% – 70%) on the dimensionless temperature distribution and the augmentation factor are investigated and compared with

those under dry conditions. In addition, comparison of the wavy fin with straight radial or rectangular fin under the same conditions were investigated and the results show that the wavy fin has better heat dissipation because of the greater area. The results demonstrate that the overall fin efficiency is dependent on the relative humidity of the surrounding air and the total surface area of the fin. In addition, the findings of the present work are in good agreement with experimental data.

The second problem investigated is the heat transfer analysis of confined liquid jet impingement on various surfaces. The objective of this computational study is to characterize the convective heat transfer of a confined liquid jet impinging on a curved surface of a solid body, while the body is being supplied with a uniform heat flux at its opposite flat surface. Both convex and concave configurations of the curved surface are investigated. The confinement plate has the same shape as the curved surface. Calculations were done for various solid materials, namely copper, aluminum, Constantan, and silicon; at two-dimensional jet. For this research, Reynolds numbers ranging from 750 to 2000 for various nozzle widths channel spacing, radii of curvature, and base thicknesses of the solid body, were used. Results are presented in terms of dimensionless solid-fluid interface temperature, heat transfer coefficient, and local and average Nusselt numbers. The increments of Reynolds numbers increase local Nusselt numbers over the entire solid-fluid interface. Decreasing the nozzle width, channel spacing, plate thickness or curved surface radius of curvature all enhanced the local Nusselt number. Results show that a convex surface is more effective compared to a flat or concave surface. Numerical simulation results are validated by comparing them with experimental data for flat and concave surfaces.

Chapter 1: Introduction and Literature Review

1.1 Introduction (Heat Transfer in a Wavy Fin Assembly)

In traditional refrigeration and air conditioning systems, finned tube heat exchangers are used to cool and dehumidify air. An air stream is cooled and dehumidified by the refrigerant that is circulating through the coil tube. The evaporation of the refrigerant within the coil removes heat from the air stream. The efficiency of the fin attached to the outer surface of the coil tube is directly related to the effectiveness of the heat exchanger. The cooling process occurs by the removal of sensible heat followed by condensation of water vapor contained within the air, as the moist air passes through the coil. Simultaneously, a condensation process entails heat transfer with phase change and the cooling takes place by the removal of sensible as well as latent heat. An important quantity that controls the heat transfer rate during a dehumidification process is the ratio of sensible to total heat transfer, which is mostly used in sizing cooling coils for air conditioning units.

The current work is carried out through a one dimensional analysis and modeling of a wavy fin as used in a cooling coil (dehumidifier) of an air conditioner. The focus of the analysis is on the fully wet condition. Since, the coil surface temperature in most cooling coils is below the dew point temperature of the air being cooled, simultaneous heat and mass transfer takes place. Moisture condensation on the fin surface affects the overall fin efficiency. In an air conditioner, the cooling coils are used for the removal of

heat and moisture from the occupied space. Condensation of moist air bursts onto these cooling coils located within the air conditioning units. The metal fin attached to the tube improves the heat conduction. A number of physical parameters affect the thermal performance of the cooling coils such as geometry, material properties, psychrometric conditions, and the efficiency of the fin. The fin efficiency may be affected when moist air is condensed on the fin. This happens when the fin temperature is below that of the dew point temperature of the arriving air passing through the cooling coil. The improvement of the efficiency of the cooling coils directly contributes to the improvement of the performance of heating ventilation air conditioning system (HVAC), leading to big energy savings. The condensation process involves both heat and mass transfer; simultaneous cooling occurs by the removal of sensible as well as latent heat. An important quantity that used in the design and sizing of cooling coils for air conditioning units is the ratio of sensible to total heat transfer.

1.2 Literature Review (Heat Transfer in a Wavy Fin Assembly)

Lunardini and Aziz [1] presented a review of the analytical and experimental progress made in understanding the process of condensation on extended surfaces. They discussed the topic of dehumidification of air on finned cooling coils. Their review is focused on rectangular fins. They reviewed models based on classical fin theory for dry fin, introducing some modifications to take into account the effect of mass transfer. They concluded that although progress has been made in understanding condensation of cooling coils, more theoretical and experimental works are needed. Experimental data for the overall performance of dry and fully wet cooling coils with dehumidification have

been reported by various investigators (Kays and London [2], Wang et al. [3], Leu et al. [4]). These studies confirmed that the performance of cooling finned coils is significantly reduced when condensation takes place. This is a consequence of lower fin efficiency for wet conditions. It was shown that fully wet fin efficiency was lower than that of dry fin. However, only a few theoretical works have been reported on condensation assuming fully wet fins or fin assemblies (Webb [5]). Kazeminejad [6] presented a simple model for simultaneous heat and mass transfer to a cooling and dehumidifying rectangular fin. He showed an analysis of rectangular one-dimensional fin assembly heat transfer with dehumidification under fully wet conditions, incorporating the ratio of sensible to total heat transfer. Salah El-Din [7] presented an analytical solution for the performance of partially-wet rectangular fin assembly. His model was useful in prediction of wet and dry parts of the fin assembly, besides the effect of the various parameters, including the assembly dimensions on the thermal performance. However, most dehumidifier cooling coils have annular fins in contrast to rectangular fins.

Liang et al. [8] examined the efficiency of a plate-fin-tube heat exchanger using 1-D and 2-D models. The 2-D model considered the complex fin geometry and the variation of the moist air properties over the fin. Rosario and Rahman [9] presented a one dimensional radial fin assembly model with condensation. Their findings indicated that the heat transfer rate increased in increments in both dry bulb temperature and relative humidity of the air. Rosario and Rahman [10] presented the 1-D analysis of heat transfer in a partially wet circular fin assembly during dehumidification. These models assumed that droplets can drain off the fin under the influence of the gravitational force neglecting the thermal resistance of the condensate.

Threlkeld [11] proposed a rectangular fin model assuming that the fin was covered with a uniform condensate film. He developed an analytical expression for the overall fin efficiency by using the enthalpy difference as the driving potential for simultaneous heat and mass transfer. He assumed a linear relationship between the ambient air temperature and the corresponding saturated air temperature. His model showed that the wet fin efficiency was only slightly affected by the air relative humidity. ARI Standard 410-81 [12] used an approach similar to Threlkeld [11], but neglecting the presence of the water film on the fin surface. McQuiston [13] developed an expression for wet fin efficiency for the case of a plane fin by approximating the saturation curve on the psychrometric chart by a straight line over small range of temperatures. Coney et al. [14] presented a numerical solution for condensation over a rectangular fin, taking into account the thermal resistance of the condensate film and using a second-degree polynomial to relate the humidity ratio with dry bulb temperature. He assumed a linear temperature profile for the condensate film. The results showed that there is negligible effect of condensate thermal resistance on the fin temperature distribution. Srinivasan and Shah [15] presented a summary of previous studies on condensation over rectangular fins.

Elmahdy and Biggs [16] obtained the overall fin efficiency of a circular fin by taking into consideration the temperature distribution over the fin surface. Their work treated heat transfer and mass transfer separately by considering their respective driving force and then assumed a linear relationship between the humidity ratio of the saturated air on the fin surface and its temperature. Their numerical results indicate that the fin efficiency strongly depends on the relative humidity. As the relative humidity of air

increases, the driving potential for mass transfer increases; this leads to a higher latent heat transfer and higher temperature. McQuiston and Parker [17] presented an analysis of circular fins using an approximation proposed by Schmidt [18]. Their model assumed a linear relationship between the humidity ratio and the dry bulb temperature. Hong and Webb [19] derived an analytical formulation of fin efficiency of fully wet surface for circular fins. Their formulation was based on the exact solution of the governing differential equation after incorporating a linear relationship between the humidity ratio and the dry bulb temperature (McQuiston [13], McQuiston and Parker [17]). Wang et al. [3] derived a fully wet fin efficiency for circular fins using the formulation given by Threlkeld [11]. They obtained an analytical expression for the fully wet fin efficiency by utilizing the enthalpy difference as the driving force for the combined heat and mass transfer process. Lin et al. [20] presented an experimental study on the performance of a rectangular fin in both dry and wet conditions. They observed that the dehumidification phenomenon can be classified into four regions. One of those regions had a thin film of condensate. Heggs and Ooi [21] presented a mathematical model for a radial rectangular fin. They presented charts that can be used to rate or design specific radial rectangular fins for a particular heat transfer specification. However, their model did not take into account any condensate effect. Lin and Jang [22] presented a 2-D analysis for the efficiency of an elliptic fin under the dry, partially wet and fully wet conditions for a range of axis ratios. One limiting condition was the circular fin.

The objective of the present work is to develop an analytical solution for heat and mass transfer in a wavy fin assembly under wet conditions, considering that the fin is covered with a uniform condensate film. This analysis also studies the effects of variation

of cold fluid temperature ($-5^{\circ}\text{C} - 5^{\circ}\text{C}$), air side temperature ($25^{\circ}\text{C} - 35^{\circ}\text{C}$), and relative humidity ($50\text{C} - 70\text{C}$) on the dimensionless temperature distribution and the augmentation factor compared with those under dry condition. The results are expected to be meaningful for the design of cooling coils for air conditioning.

1.3 Introduction (Heat Transfer by Jet Impingement)

There are numerous experimental and theoretical studies on the characteristics and heat transfer associated with confined jet impingement on surfaces. These studies have considered both single impinging jet and jet arrays. Martin [23] and Viskanta [24] reviewed earlier studies of impingement heat transfer. Jet impingement has been demonstrated to be an effective means of providing high heat/mass transfer rates in industrial processes where rapid heating, cooling, or drying is necessary. These include surface coating and cleaning, cooling of electronic components, fire testing of building material, annealing of metal and plastic sheets, tempering glass, chemical vapor deposition, avionics cooling, cooling of turbine blades, and drying of textiles, according to Hong et al. [25]. The principal virtue of this method of cooling is the large rate of heat transfer and the relative ease with which both the heat transfer rate and distribution can be controlled.

There are only a few studies on concave and convex surfaces, while several studies of impinging jets are for flat surfaces. If the fluid is discharged from a nozzle or orifice into a body of surrounding fluid that is the same as the jet itself, then it is called submerged. Confined submerged liquid jets find use in both axisymmetric and planar configurations. Both configurations share the common feature of a small stagnation zone

at the impingement surface, whose size is of the order of the nozzle diameter or slot dimension, with the subsequent formation of a wall jet region. The fluid impingement and boundary layer behaviors that control the convective heat transfer will be examined for two-dimensional under confinement conditions in the present investigation.

1.4 Literature Review (Heat Transfer by Jet Impingement)

The following is a summary of most related literature pertaining to confined and semi-confined jet impingement over flat, concave, and convex surfaces. Glauert [26] considered the flow due to jet spreading out over a plane surface, either radially or in two dimensions. Solutions to the boundary layer equations were sought for a laminar flow using similarity transformation. McMurray et al. [27] studied convective heat transfer to an impinging plane jet from a uniform heat flux wall. To fit their data, they based heat transfer correlations on the stagnation flow in the impingement zone and on the flat plate boundary layer in the uniform parallel flow zone. Metzger et al. [28] experimentally studied the effects of Prandtl number on heat transfer to a liquid jet for a uniform surface temperature boundary condition. Thomas et al. [29] measured the film thickness across a stationary and rotating horizontal disk using the capacitance technique, where the liquid was delivered to the disk by a controlled impinging jet. Faghri and Rahman [30] experimentally, analytically, and numerically studied the heat transfer effect from a heated stationary or rotating horizontal disk to a liquid film from a controlled impinging jet, under partially confined conditions for different volumetric flow rates and inlet temperatures for both supercritical and subcritical regions. Hung and Lin [31] proposed an axisymmetric sub-channel model for evaluating local surface heat flux for confined

and unconfined cases. Garimella and Rice [32] presented experimental results for the distribution of local heat transfer coefficient during confined submerged liquid jet impingement with fluoroinert (FC-77) as the working fluid. Webb and Ma [33] presented a comprehensive review of studies on jet impingement heat transfer. Ma et al. [34] reported experimental measurements for local heat transfer coefficient during impingement of a circular jet perpendicular to a target plate. Both confined and free jet configurations were used. Garimella and Nenaydykh [35], Li et al. [36], and Fitzgerald and Garimella [37], all considered a confining top plate for a submerged liquid jet. Their studies used FC-77 as the working fluid at different volumetric flow rates. Morris and Garimella [38] computationally investigated the flow fields in the orifice and the confinement regions of a normally impinging, axisymmetric, confined and submerged liquid jet. Tzeng et al. [39] numerically investigated confined impinging turbulent slot jets. Eight turbulence models, including one standard and seven low Reynolds number $k-\epsilon$ models were employed and tested to predict the heat transfer performance of multiple impinging jets. Inoue et al. [40, 41] experimentally investigated and proposed conceptual designs for the cooling of the diverter under critical heat flux (CHF) loads for two-dimensional confined planar jet on flat and concave surfaces as a function of distance from the center, flow velocity and curvature. The obtained results show that the centrifugal force on the concave surface under CHF is not significant due to an existence of counter wall to suppress the splash of liquid film, which is quite different from planar jet cooling with free surface. Li and Garimella [42] experimentally investigated the influence of fluid thermo-physical properties on the heat transfer from confined and submerged impinging jets. Generalized correlations for heat transfer were proposed based

on their results. Rahman et al. [43] numerically evaluated the conjugate heat transfer of a confined jet impingement over a stationary disk using liquid ammonia as the coolant. Ichimiya and Yamada [44] studied the heat transfer and flow characteristics of a single circular laminar impinging jet including buoyancy effect in a narrow space with a confining wall. Temperature distribution and velocity vectors in the space were obtained numerically. Dano et al. [45] investigated the flow and heat transfer characteristics of confined jet array impingement with cross-flow. Digital particle image velocimetry and flow visualization were used to determine the flow characteristics. Rahman and Mukka [46] developed a numerical model for the conjugate heat transfer during vertical impingement of a two-dimensional (slot) submerged confined liquid jet using liquid ammonia as the working fluid. Robinson and Schnitzler [47] experimentally investigated the heat transfer and pressure drop characteristics of liquid jet arrays impinging on a heated surface for both confined-submerged and free-surface flow configurations. For the submerged jet arrays, a strong dependence on both jet-to-target and jet-to-jet spacing was found and correlated to adequately predict the experimental measurements. Their results revealed that submerged and free jet configurations are not susceptible to changes in heat transfer when the nozzle is in close proximity ($2 \leq H/d_n \leq 3$) to the heated surface. Conversely, their results showed how the heat transfer deteriorated monotonically with the increment of the jet-to-target spacing ($5 \leq H/d_n \leq 20$) and spacing between jets. Whelan and Robinson [48] experimentally studied the cooling capabilities of a square water jet array of 45 jets under fixed jet-to-jet spacing and jet-to-target distance for six different nozzle geometries. The confined-submerged jet array tests yielded greater heat transfer coefficients when compared with their free jet array counterparts.

Rahman et al. [49] numerically studied the heat transfer characteristics of a free liquid jet discharging from a slot nozzle and impinging vertically on a curved cylindrical shaped plate of finite thickness. The model included the entire fluid jet impingement region and flow spreading out over the convex plate under a uniform heat flux boundary condition. Computations were done for a series of parameters, such as: jet Reynolds numbers, nozzle to target spacing ratios, inner plate radius of curvature, plate thickness, and for different nozzle widths using water, fluoroinert, and oil as working fluids. Their results were presented for dimensionless solid–fluid interface and maximum temperature in the solid, including local and average Nusselt numbers. Numerical simulation results were validated by comparing with experimental measurements.

Chang and Liou [50] presented an experimental study of heat transfer of impinging jet-array onto concave- and convex-dimpled surfaces with effusion. The results obtained showed the enhancement in heat transfer by each dimpled surface with and without effusion.

From the above literature review it can be noticed that even though confined jet impingement heat transfer has been quite extensively investigated, most of these are for flat surfaces. Only a few attempted to produce local heat transfer distribution of concave or convex surfaces in combination with two–dimensional confined liquid jet impingement. In addition, none of the studies have attempted to explore conjugate heat transfer effect of a convex surface during two-dimensional confined liquid jet impingement.

Therefore, the intent of this research is to carry out a comprehensive investigation of local conjugate heat transfer with a steady flow for a two–dimensional confined liquid

jet impingement over flat, concave, and convex surfaces. Computations using water (H₂O) as the working fluid were carried out for several combinations of geometrical surfaces, a variety of jet Reynolds numbers, different solid thickness to curvature ratios, four channel spacing ratios, and four radii of curvature of both concave and convex surfaces. The thermal conductivity effect was studied with the implementation of four different disk materials: copper, silicon, aluminum, and Constantan. Results offer a better understanding of the fluid mechanics and heat transfer behavior of confined liquid jet on bodies with a current boundary. Even though no new numerical technique has been developed, results obtained in the present investigation are entirely new. The numerical results showing the quantitative effects of different parameters, as well as the correlation for average Nusselt numbers, will be practical guides for engineering design.

Chapter 2: Heat Transfer Analysis of Wavy Fin Assembly with Dehumidification

2.1 Physical Description of Wavy Fin Heat Exchangers

The most widely used types of condensers and evaporators are shell-and-tube heat exchangers and finned-coil heat exchangers (Figure 2.1). Figure 2.2 shows the schematic diagram of the evaporator. In the air conditioning system, the most important heat exchanger is the evaporator, because the useful processes of a refrigeration cycle occur in the evaporator. Now days the coolant fluid on the automobile radiator is glycol (antifreeze), because it has high efficiency in removing heat from the car engine.

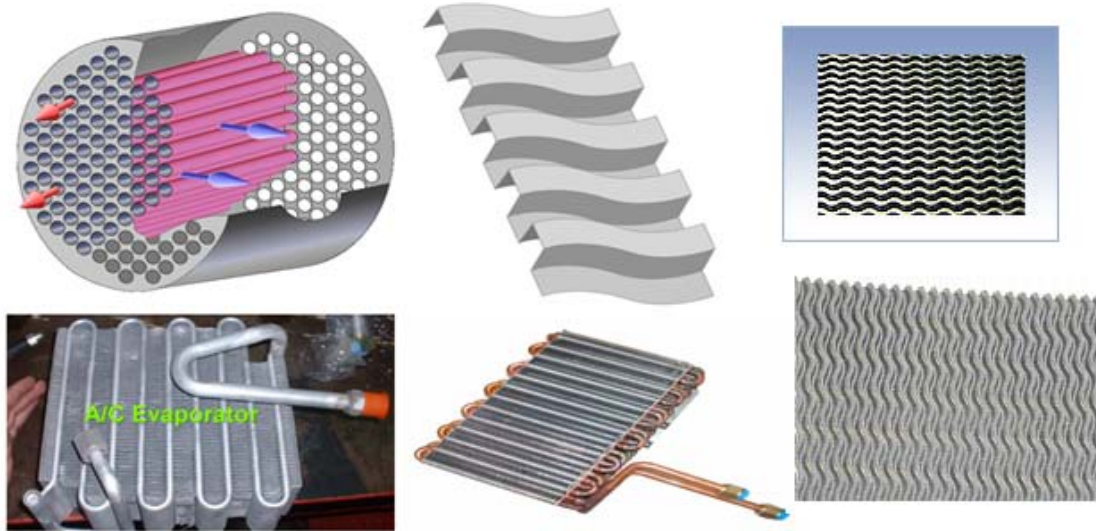


Figure 2.1 Most evaporator uses in air condition systems.

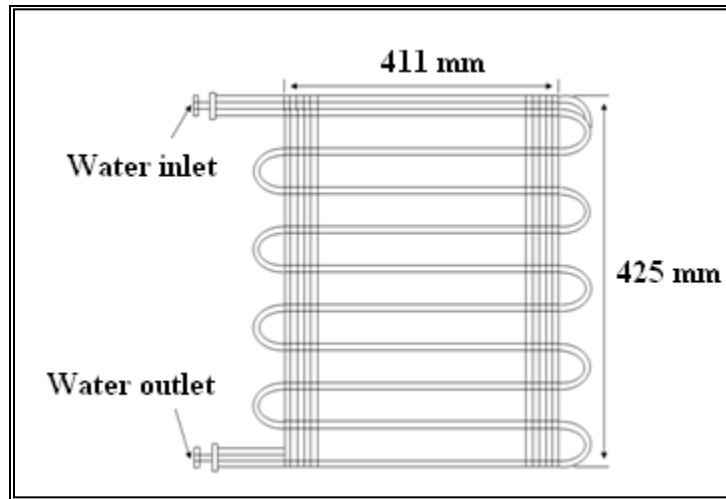


Figure 2.2 Schematic diagram of evaporator.

In real life, there are too many different types of fin evaporators, such as square, rectangular, longitudinal, radial, and wavy as shown in Figure 2.3.

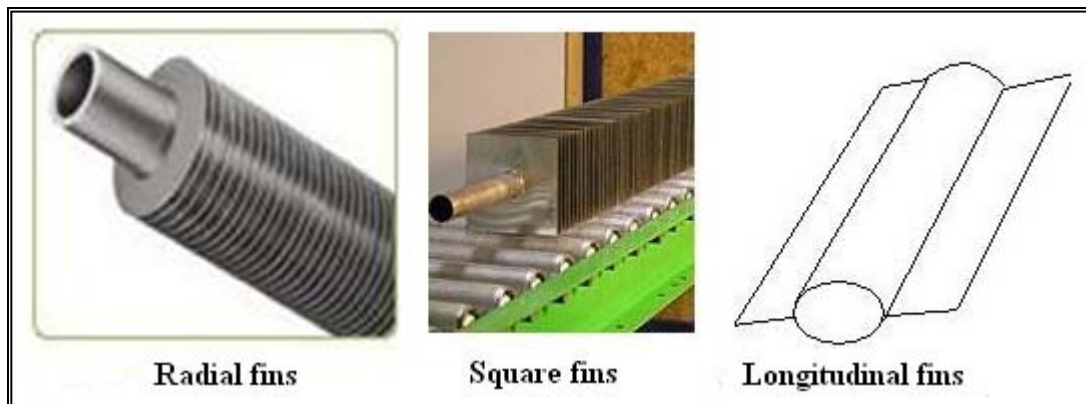


Figure 2.3 Some types of fins.

In general, the wavy fin is more efficient because it has more area, as shown in Figure 2.4. The current work represents part of a wavy fin (Figure 2.5). Because of the axisymmetric model, we assume that the fin tip is insulated or $dT/dR = 0$ when R equal to R_T , the results compared with uninstalled fin tip under the same conditions.

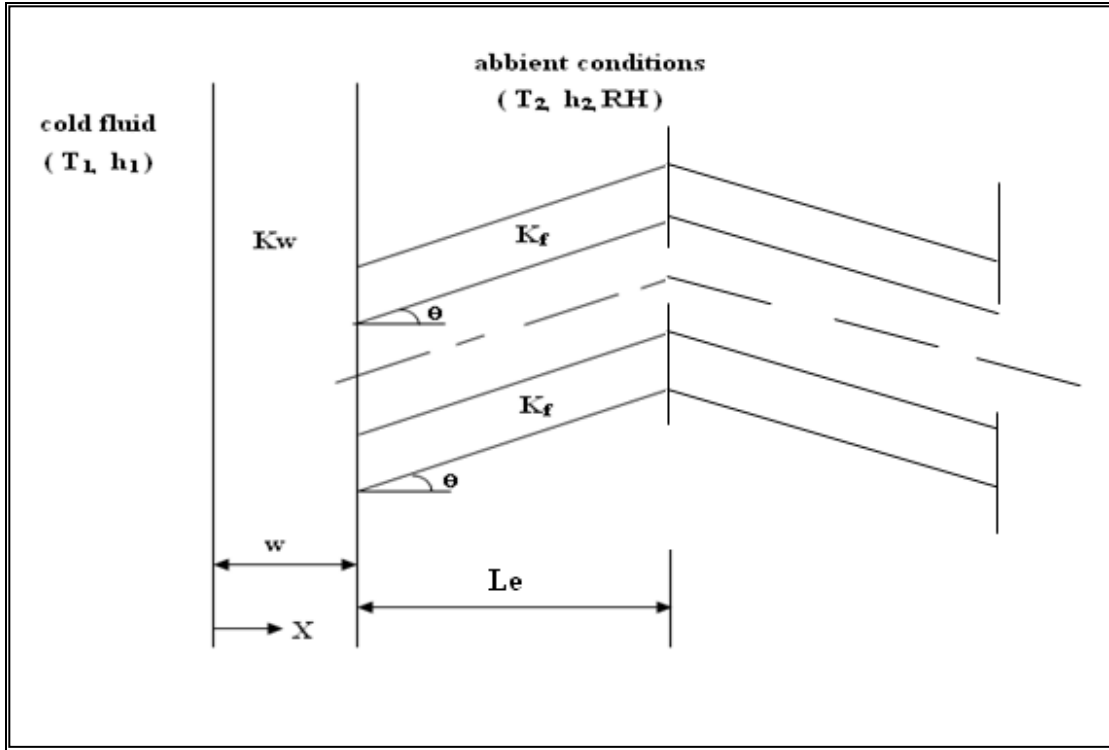


Figure 2.4 Side views of a wavy fin assembly.

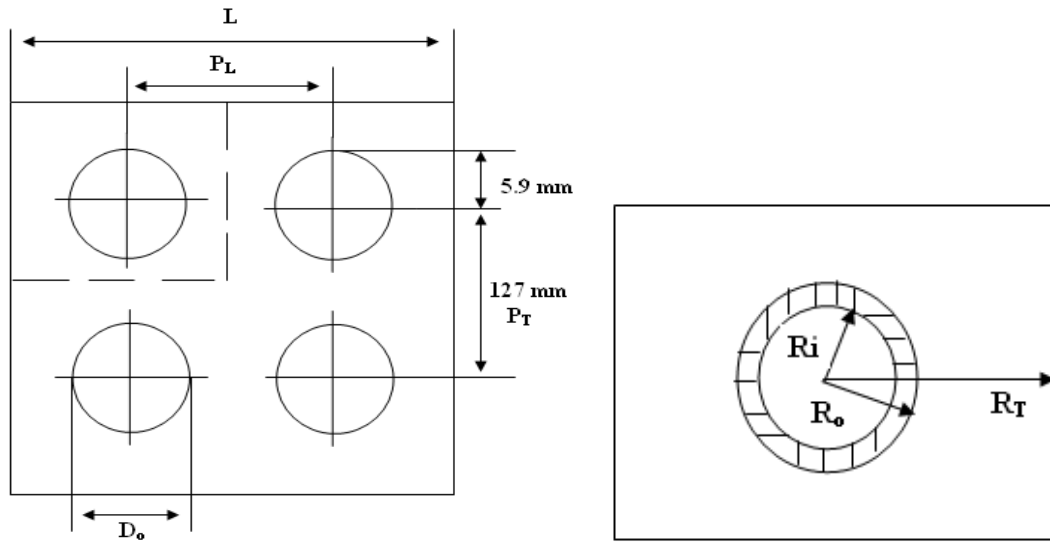


Figure 2.5 Side views of the physical wavy model.

Furthermore, the wavy fin has been converted to straight radial fin, by taking the equivalent length of the wavy fin and using it as a real length of the straight radial fin, as shown in Figure 2.6. In addition, some calculations have been done for some types of fin. The dimensions of a real wavy fin of current work are shown in Table 2.1 and Table 2.2. Also Table 2.2 show that there are two types for surfaces treatment, such as un-coated surface (present model), and Hydrophilic coating. Hydrophilic coating has an affinity to water and is usually charged or has polar side groups to their structure that will attract water.

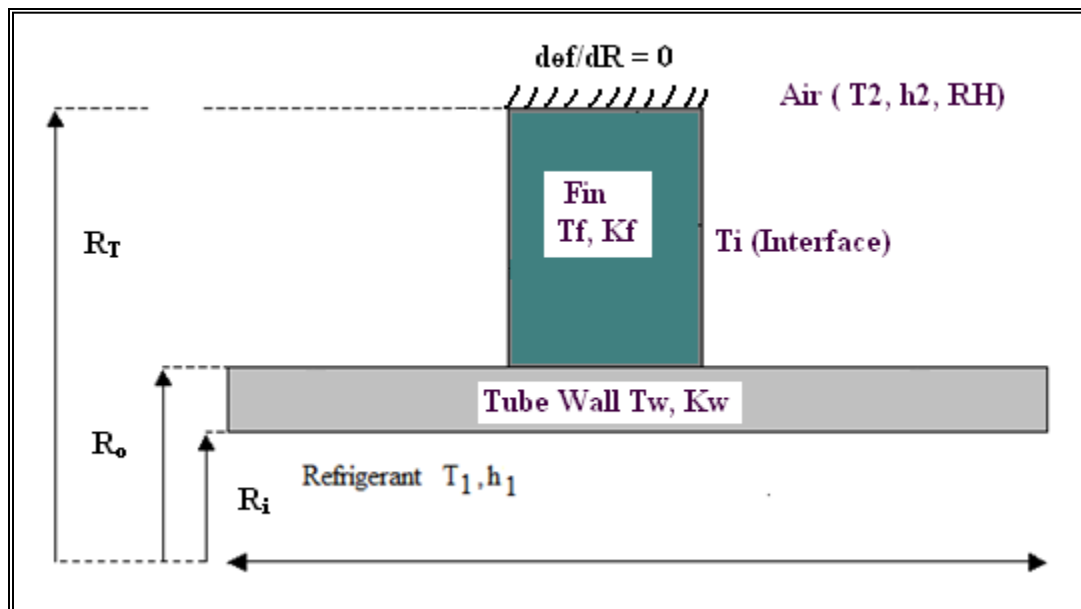


Figure 2.6 Side views of the physical street radial model.

Table 2.1 Geometric dimensions of sample wavy fin-and-tube heat exchangers.

No	Do	Dc	P _T	P _L	Fp	δ _f	N
	(mm)	(mm)	(mm)	(mm)	(mm)	(mm)	
1	9.53	9.76	25.4	19.05	1.41	0.115	2
2	9.53	9.76	25.4	19.05	1.81	0.115	2
3	9.53	9.76	25.4	19.05	2.54	0.115	2
4	9.53	9.76	25.4	19.05	2.54	0.115	4
5	9.53	9.76	25.4	19.05	2.54	0.115	6
6	9.53	10.03	25.4	19.05	1.41	0.250	2
7	9.53	10.03	25.4	19.05	1.81	0.250	2
8	9.53	10.03	25.4	19.05	2.54	0.250	2
9	9.53	10.03	25.4	19.05	2.54	0.250	4
10	9.53	10.03	25.4	19.05	2.54	0.250	6

Note: Tubes are made of copper with a wall thickness of 0.3 mm.

Table 2.2 Geometric dimensions of sample fin-and-tube heat exchangers.

No	Dc (mm)	P _T (mm)	P _L (mm)	Fp (mm)	δ _f (mm)	N	Surface treatment	Fin type
1	7.64	21	12.7	1.27	0.115	2	Un-coated	Slit
2	7.64	21	12.7	1.28	0.115	2	Hydrophilic coating	Slit
3	6.93	17.7	13.6	1.21	0.115	1	Un-coated	Plain
4	6.93	17.7	13.6	1.99	0.115	1	Un-coated	Plain
5	7.53	21	12.7	1.23	0.115	2	Hydrophilic coating	Plain
6	7.53	21	12.7	1.23	0.115	2	Un-coated	Plain
7	7.53	21	12.7	1.78	0.115	2	Hydrophilic coating	Plain
8	7.53	21	12.7	1.78	0.115	2	Un-coated	Plain

2.2 Mathematical Model

In the current study we consider a wavy fin assembly of uniform cross section and pitch under wet condition, as shown in Figure 2.4. The water condenses at the surface as filmwise, dropwise, or mixed mode when a humid air contacts to the surface at below its dew point temperature. The differences between them depend on the surfaces. For instance, clean surfaces tend to promote filmwise, and treated surfaces dropwise, condensation. The created film is greatly thinner than the boundary layer in the dehumidification process, this makes the condensate thermal resistance to heat transfer flow negligible. Consider a uniform heat exchanger wavy fin attached to a plane wall, as shown in Figure 2.5. To complete the development of the formulation model, simplifying assumptions are made as follows:

1. The heat flow in the fin and the temperature at any point on the fin remain constant with the time.
2. The fin material is homogenous; its thermal conductivity, the condensate film, and the wall are constant.
3. There is no contact resistance between fins in the configuration or between the fin at the base of the configuration and the prime surface.
4. The convective heat transfer coefficients between the fin and the surrounding medium are uniform and constant over the entire surface of the fin.
5. The temperature of the medium surrounding the fin is uniform.
6. The fin width is so small compared with its height that temperature gradients across the fin width may be neglected.
7. The temperature of the base of the fin is uniform.

8. There are no heat sources within the fin itself.
9. Heat transfer to or from the fin is proportional to the temperature excess between the fin and the surrounding medium.
10. Condensation occurs when the surrounding air dew point temperature is reached.

Assume that the fin is dissipating heat to the surrounding environment at temperature T_s , heat is transferring from cold fluid T_1 , and the temperature distribution at any point is $T(x)$. Because there is no heat generation in steady state, the energy required for heat entering and leaving the element (Δx) must equal the heat dissipated by convection over the two fin faces, each with area (Δx), so that the total surface area for convective dissipation is $\Delta s = (2L\Delta x)$.

At steady state condition for one-dimension with no heat generation, the energy balance through the wall becomes:

$$\frac{d^2\theta_w}{dx^2} = 0 \quad (1)$$

The heat transfer by conduction is equal to the difference between the heat entering and leaving the elements, Δx , according to Fourier law.

$$\Delta q = kA \frac{dT_x}{dx} I_x - kA \frac{dT_x}{dx} I_{x+\Delta x} \quad (2)$$

For $\theta(x) = T(x) - T_s$, and $d\theta_x = dT_x$

The minus sign in the Fourier law means the direction of heat flow is in a direction opposed to the positive sense of the coordinate system:

$$q = -kA \frac{dT_x}{dx} \quad (3)$$

The total heat that is dissipated from the two faces of the fin over the element Δx , is equal to:

$$\Delta q = h[T_{(x)} - T_{(s)}]q_s + m_a \cdot (w_x - w_s)h_{fg} \quad (4)$$

$$m_a (w_x - w_s)h_{fg} = q_c \equiv \text{Latent heat flux} \quad (5)$$

$$h[T_{(x)} - T_{(s)}]q_s \equiv \text{Sensible heat flux} \quad (6)$$

Now the steady state energy balance can be used to combine equations 1 and 2 so that

$$\Delta q = kA \frac{dT_x}{dx} I_x - kA \frac{dT_{x+\Delta x}}{dx} I_{x+\Delta x} - h[T_{(x)} - T_{(s)}]h_{fg} + m_a \cdot (w_x - w_s)h_{fg} \quad (7)$$

$$\lim_{\Delta x \rightarrow 0} \left[\Delta q = kA \frac{dT_x}{dx} I_x - kA \frac{dT_{x+\Delta x}}{dx} I_{x+\Delta x} \right] = \frac{d^2 \theta_w}{dx^2} \quad (8)$$

$$\therefore kA \frac{d^2(\theta_f)X}{dx^2} - [q_c + q_s] = 0 \quad (9)$$

The ratio of sensible to total heat transfer calculated at fin temperature is R, then:

$$R = \frac{q_s}{q_c + q_s} \Rightarrow q_c + q_s = \frac{q_s}{R}, \text{ substitute in equation 4}$$

$$\frac{d^2(\theta_f)X}{dx^2} - \frac{q_s}{k_f A_f R} = 0 \quad (10)$$

We use the manipulation to develop energy balance from simultaneous heat and mass transfer from the humid air to the condensate film.

$$\frac{d^2(\theta_f)X}{dx^2} - \frac{B_i}{P^2 R_{(\theta_f)}} \theta_f(x) = 0 \quad (11)$$

The boundary conditions are the following.

- At $x = 0$

$$kA \frac{dT_w}{dx} = 2ph(T_w - T_1) \quad (12)$$

$$(T_1 - T_2) \frac{d\theta_w}{pdx} = \frac{h}{k_w} [(T_w - T_2) - (T_1 - T_2)] \quad (13)$$

$$\frac{d\theta_w(x)}{pdx} = \frac{ph}{k_w} \left[\left(\frac{(T_w - T_2)}{(T_1 - T_2)} \right) - \left(\frac{(T_1 - T_2)}{(T_1 - T_2)} \right) \right] \quad (14)$$

$$\frac{d\theta_w(x)}{pdx} = -B_i(1 - \theta_w(x)) \quad (15)$$

- At $X = R_0$,

$$\theta_w(x) = \theta_f(z) \quad (16)$$

$$\frac{d\theta_w(x)}{pdx} = kp \frac{d\theta_f(z)}{pdz} - \frac{B_{i2}}{R_b} (1 - p)\theta_w(x) \quad (17)$$

- At $R = R_T$

$$\frac{d\theta_f}{dR} = 0 \quad (18)$$

The ratio of the sensible heat flux to the total heat flux $q_s/(q_s + q_c)$ is given by the equation:

$$R(\theta) = \frac{q_s}{q_t} = \left[1 + (\rho_{ma} h_{fg})(T_2 - T_1) \left(\frac{h_m}{h_2} \right) \left(\frac{w_2 - w(\theta)}{\theta} \right) \right]^{-1} \quad (19)$$

The input temperature and relative humidity were used to determine the dewpoint and the rate of condensation by using standard psychrometric equations (ASHRAE [51]).

The overall fin efficiency, η , is defined as the ratio of the actual total heat transfer rate to the maximum total heat transfer rate,

$$\eta = \frac{q_{fin}}{q_{max}} \quad (20)$$

In this case the fin performance is determined by a combination of heat and mass transfer. The actual total heat transfer, q_{fin} must include both the sensible heat transfer and the latent heat transfer originated by mass transfer (condensation). The sensible heat transfer is due to convection from the air to the fin because of the temperature difference between the air and the fin, and the latent heat transfer is caused by the humidity ratio difference between the air and the fin surface. The maximum heat transfer rate, q_{max} corresponds to an ideal fin whose surface temperature equals the temperature at the fin base under wet conditions.

2.3 Results and Discussion

This section describes the heat transfer characteristics of the mathematical model used to perform numerical simulation for conditions found in a typical air conditioner cooling coil under wet condition. The integration of differential equations worked out by the Range-Kutta method with shooting technique [52] corresponds to a characteristic direct expansion cooling coil used in air conditioning applications, some values are kept constant in all simulations such as, $Bi_1 = 1.0$, $Bi_2 = 0.1$, $K=1.0$, $K_f=0.004$, $P = 0.25$, $W = 0.5$, $\Delta = 2 P$, $\Phi = 0.1 P$. These values were chosen using heat transfer coefficients and geometric parameters. Various values of RH, T1, and T2 are represented in Figures 2.7 – 2.9 as a dimensionless temperature Θ versus a dimensionless distance. Figure 2.7 represents the variations of dimensionless temperature with dimensionless distance for changes in the relative humidity. It could be seen that an increase in relative humidity decreases with dimensionless temperature, Θ . The force of water vapor diffusion increases at a larger relative humidity, and as a result, so do the number of molecules of water condensing on the fin surface. Also, a higher latent heat transfer and lower temperature at the fin surface occurs. The figure also demonstrates the significant benefits of water vapor condensation during the heat transfer process, when the temperature profile is compared to that for a dry condition (zero relative humidity).

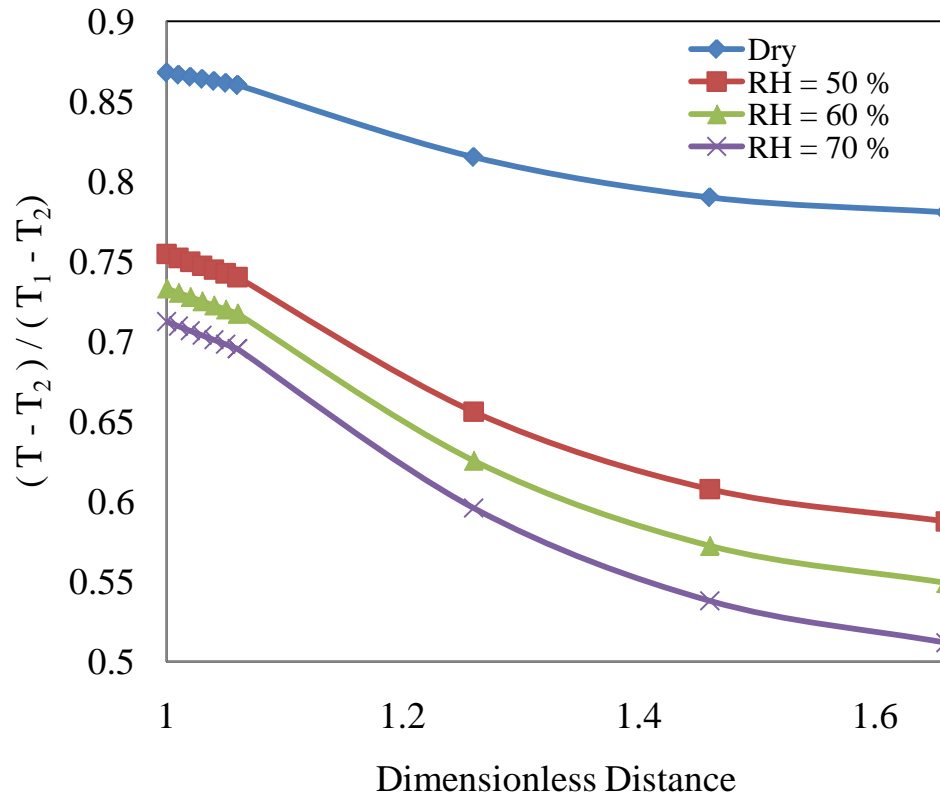


Figure 2.7 Variation of dimensionless temperature distribution with the variation in relative humidity.

Variations of dimensionless temperature with dimensionless distance for changes in the cold fluid temperature T_1 can be seen in Figure 2.8. The figure shows that the fin temperature increases when T_1 increases, and this leads to a decrease in the temperature difference between the fin and its surroundings. Thus, both heat and mass transfer decrease. The condensation comes to an end when T_1 is increased to a value above the air dew point temperature. It can be noted that although the local temperature at the wall and the fin changes with T_1 , the change in the dimensionless temperature Θ is insignificant. Also, there is a large over prediction of the temperature when the fin is assumed to remain dry during the heat transfer process.

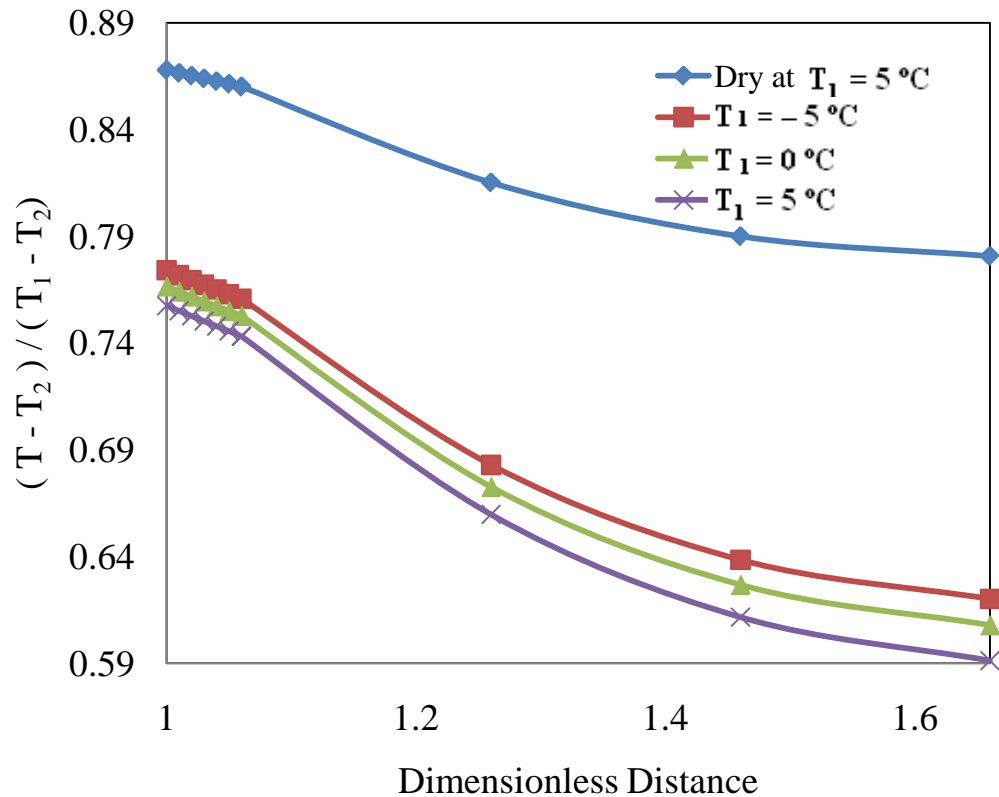


Figure 2.8 Variation of dimensionless temperature distribution with variation in cold fluid temperature at relative humidity 50%.

The dimensionless temperature as a function of the dimensionless distance for the variation in the surrounding temperature T_2 is shown in Figure 2.9. It was noted that an increase in the air side temperature increases the heat transfer rate in the wet fin, and also the dimensionless temperature at the wall as well as in the fin decreases with the increase in T_2 . Pure conduction causes a linear temperature at the wall, after which a larger slope of temperature curve is seen at the fin because of lateral convection. At constant relative humidity, air dry bulb temperature converts to moisture content (humidity ratio). Consequently, both sensible and latent heat transfer increase when at higher

temperatures. Figure 2.9 shows a plot of the dimensionless temperature Θ for artificial dry conditions when the effects of condensation have been ignored, and also shows the discrepancy in the temperature distribution in the fin between wet and dry conditions. The latent heat transfer due to condensation is a significant portion of the total heat transfer and should not be ignored in any cooling coil design.

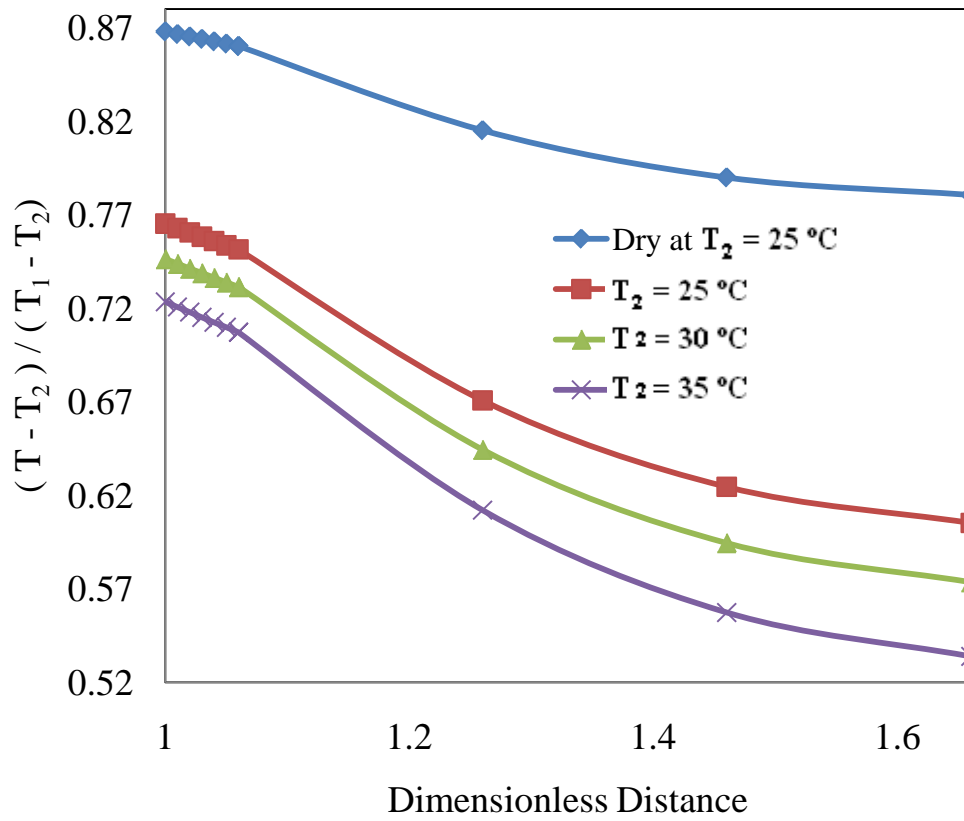


Figure 2.9 Variation of dimensionless temperature distribution with variation in surrounding air dry bulb temperature at relative humidity 50%.

Figure 2.10 shows the variation of dimensionless temperature distribution as a function of the dimensionless distance under two conditions, fin tip with and without insulation at constant relative humidity 50%. It was observed that by leaving the fin tip with no insulation, the area of the surface is increased, which causes better heat dissipation by increasing the fin performance. It can be seen that at insulation fin tip the heat dissipation is less.

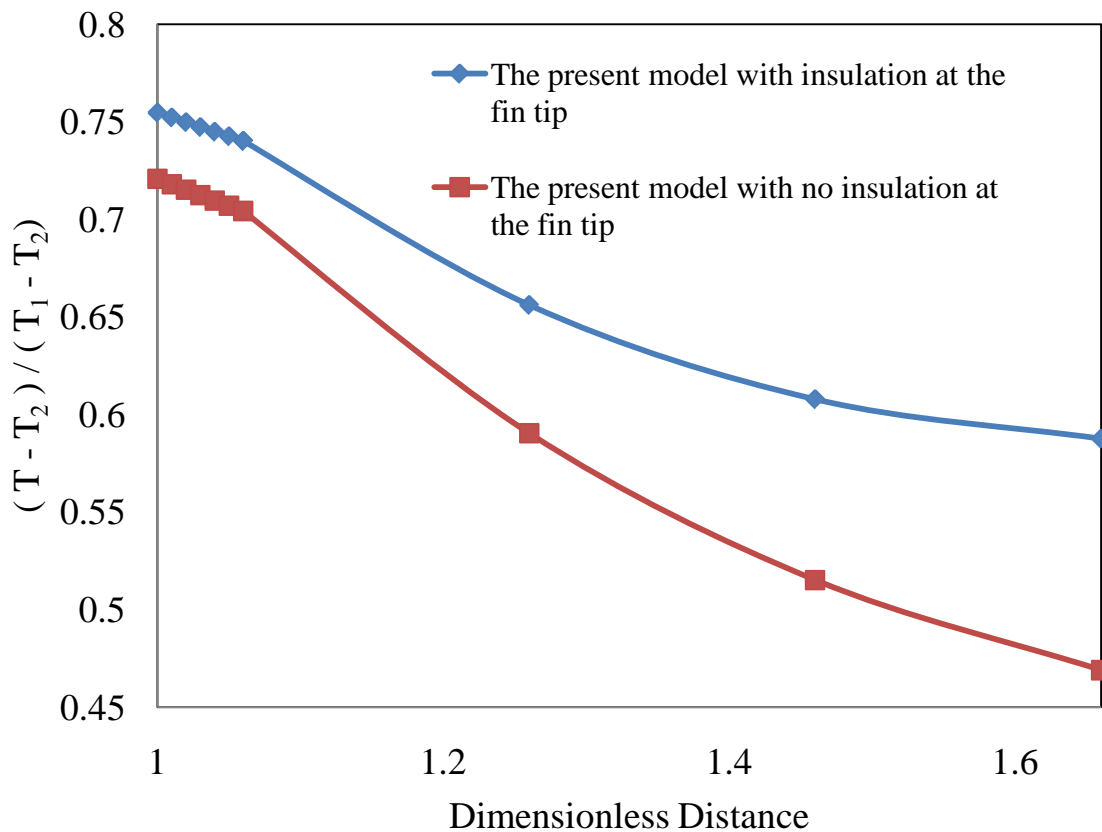


Figure 2.10 The present model with and without insulation in the fin tip, and at 50% RH.

Comparison of rectangular and wavy models for dry bulb temperature and 50% relative humidity RH between wavy model and the model presented by Kazeminejad [6] can be seen in Figure 2.11. A linear relationship between dry bulb temperature and

humidity ratio was assumed in this comparison. It can be observed that there is more agreement in wavy model than in their model. Figure 2.12 shows the comparison between the present model with the models of Kazeminejad [6] and Rosario and Rahman [10]. This comparison shows results of 1-D models for dry and 50 percent relative humidity. Constant thickness film on the fin surface was presented in wavy model. It can be noted that all models show the same tendency of decreasing dimensionless temperature with an increase of relative humidity because of the increase of latent heat transfer due to condensation. Rosario and wavy model represent superior results than the Kazeminejad model, and this demonstrates that to achieve excellent fin performance, one has to design the fin in a radial shape (Rosario) or wavy shape (wavy model).

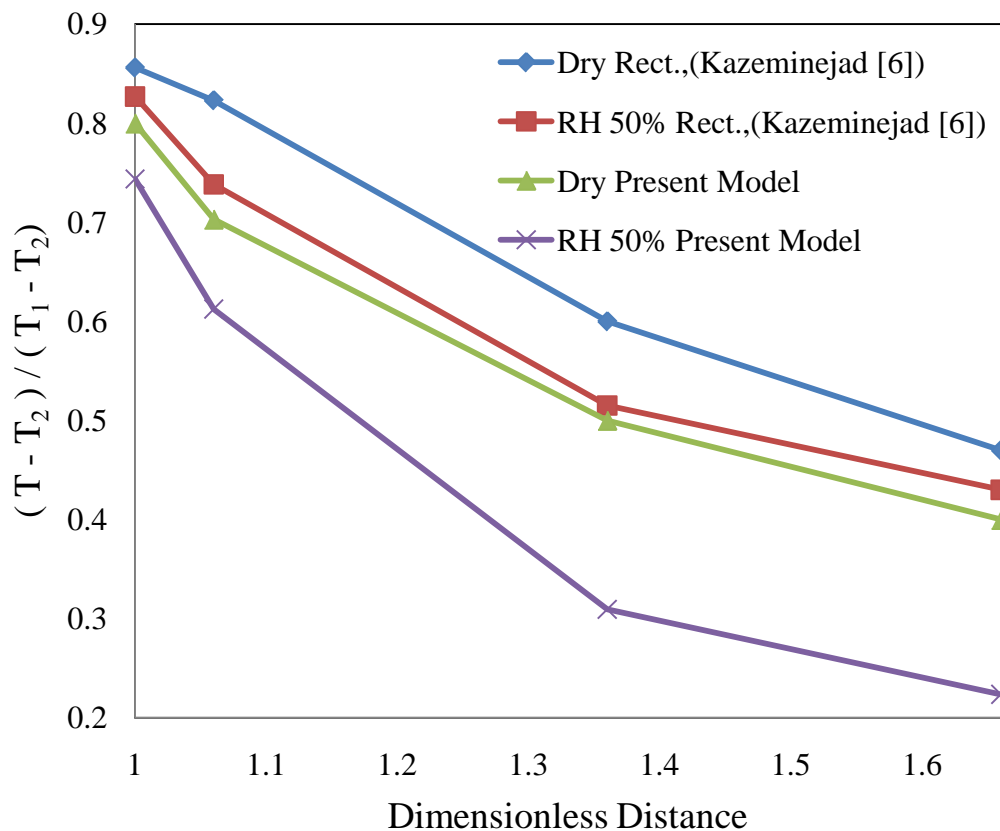


Figure 2.11 Comparison of rectangular and wavy models for dry and 50% RH.

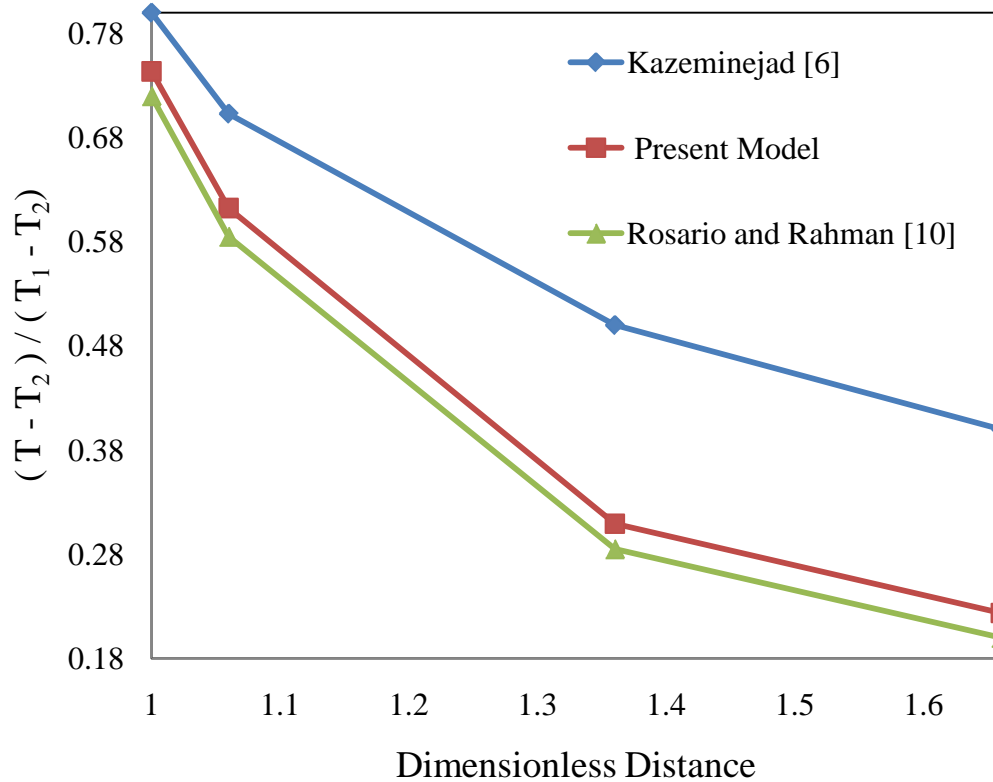


Figure 2.12 Comparison between present model and Kazeminejad [6]; and Rosario and Rahman [10].

Computational results for the heat transfer of the fin assembly with and without dehumidification for various values of T_1 , T_2 , and RH, are plotted in Figures 2.13 – 2.15. The effects of varying these conditions can be studied by plotting $(AUG)_{dry}/(AUG)_{wet}$. The ratio of heat transfer in a finned assembly to heat transfer from the bare tube surface without any fin is defined as augmentation factor. The comparison of enhancement obtained from fins under dry and wet conditions is represented by the ratio of augmentation factor (in other words, the comparison of the efficiency of a fin assembly with and without condensation at the surface). It can be seen that the value of $(AUG)_{dry}/(AUG)_{wet}$ increases with distance and reaches a constant value at dimensionless

distance after 3.5. The value of the augmentation ratio is always greater than 1, demonstrating the descent of fin efficiency with condensation. The insignificant influence of the refrigerant temperature (T_1) on the augmentation ratio is shown in Figure 2.13. The fin efficiency increases in overall heat transfer rate, although it is represented by the fin assembly reduced with condensation. From Figure 2.14 and Figure 2.15, both dry bulb temperature and relative humidity increases significantly with the increase in the augmentation ratio; simultaneously, the fin efficiency decreases with more condensation at the fin surface.

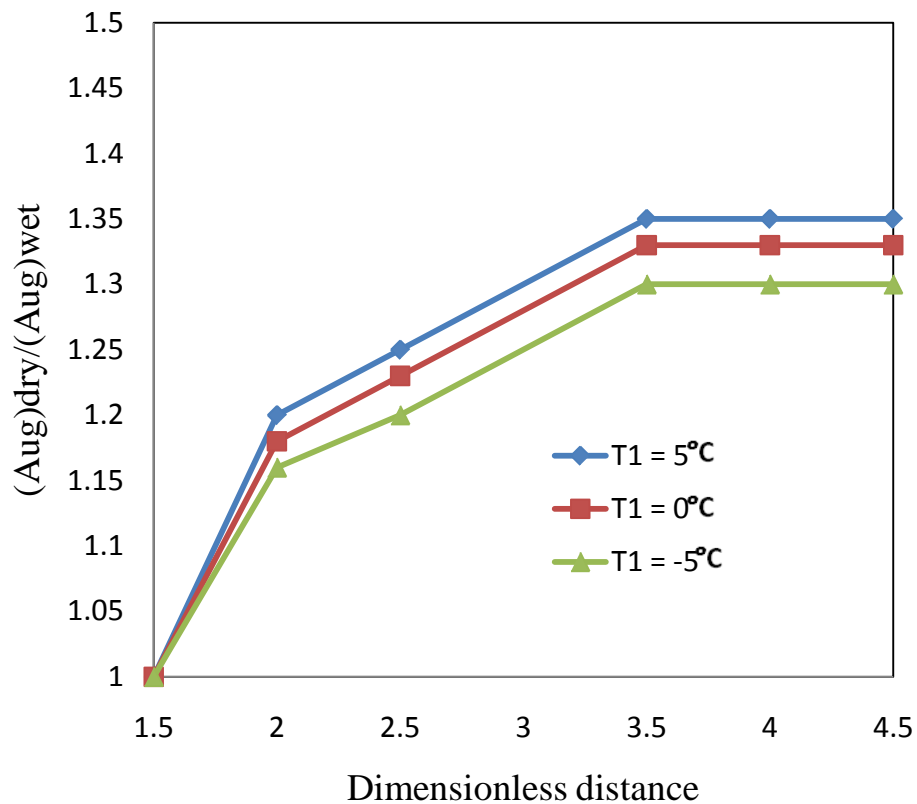


Figure 2.13 $(Aug)_{dry}/(Aug)_{wet}$ variation with change in T_1 .

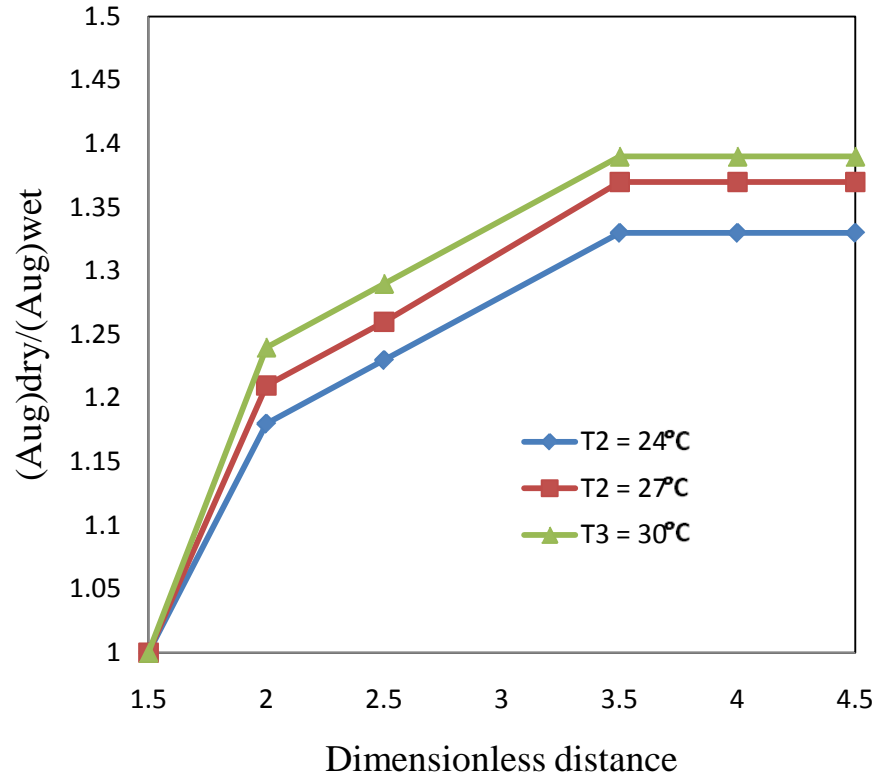


Figure 2.14 $(Aug)_{dry}/(Aug)_{wet}$ variation with change in T_2 .

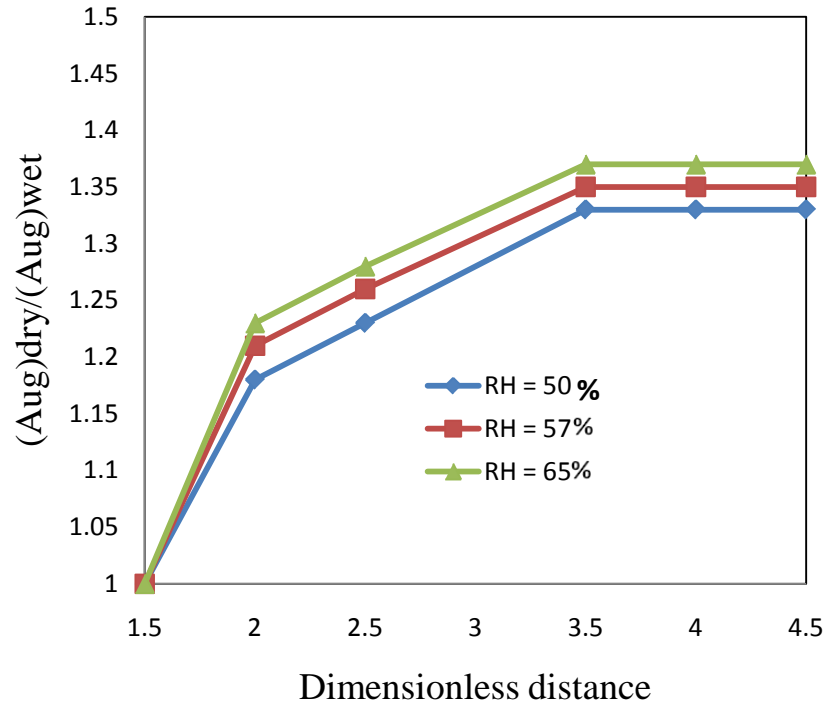


Figure 2.15 $(Aug)_{dry}/(Aug)_{wet}$ variation with change in RH.

The present model and the 2-D model show the same trend as shown in Figure 2.16. It can be seen that the pure conduction in the tube region creates a linear dimensionless temperature, and non-linear in the fin region because of the convection at the fin surfaces. The RH increase creates condensation on the fin surfaces, as a result of which the latent heat transfer increase causes a decrease in the dimensionless temperature. In addition, the 2-D radial geometry is a better representation of the actual cooling coil configuration in most insulation Rosario, and Rahman [53], because it shows a behavior closer to a real heat exchanger.

The comparison of wavy model and the rectangular model under the same conditions can be seen in Figure 2.17. The result of the rectangular model shows a lower heat transfer rate because it has less area. Thus, increasing the fin area is desirable in

order to obtain better fin performance, but there are some physical limitations to building such a fin arrangement. The results demonstrate that the fin performance in the wavy fin depends on the area of the fin, which also indicates that the wavy fin has better performance than the rectangular one which has less area.

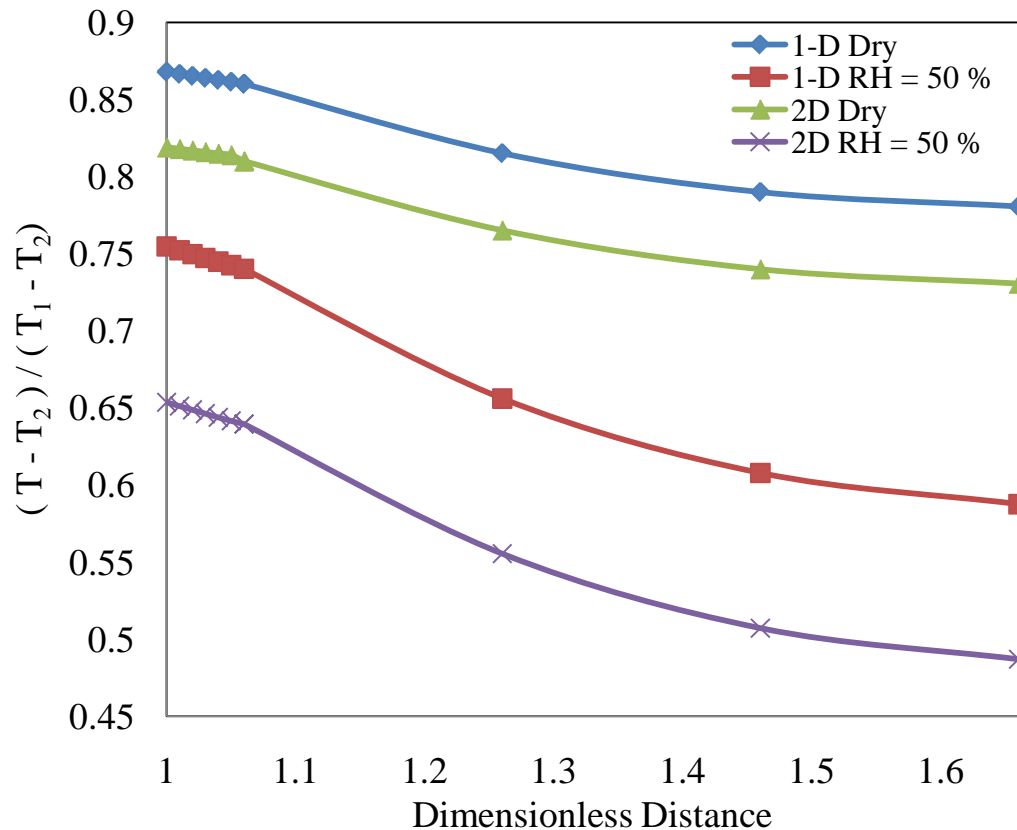


Figure 2.16 Comparison of 1-D and 2-D radial models for dry and 50% RH.

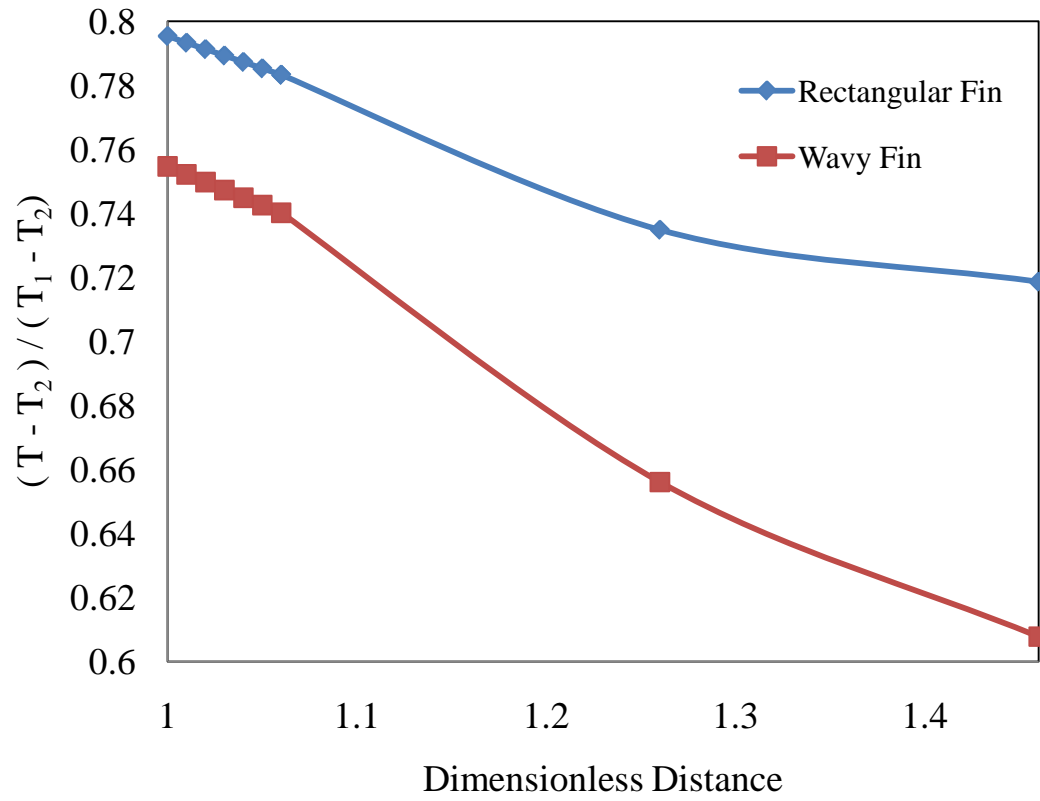


Figure 2.17 Comparison of the wavy model and the converted rectangular model at dry and 50% RH.

Chapter 3: Conjugate Heat Transfer Analysis of a Confined Liquid Jet

Impingement on Concave and Convex Surfaces

3.1 Modeling and Simulation

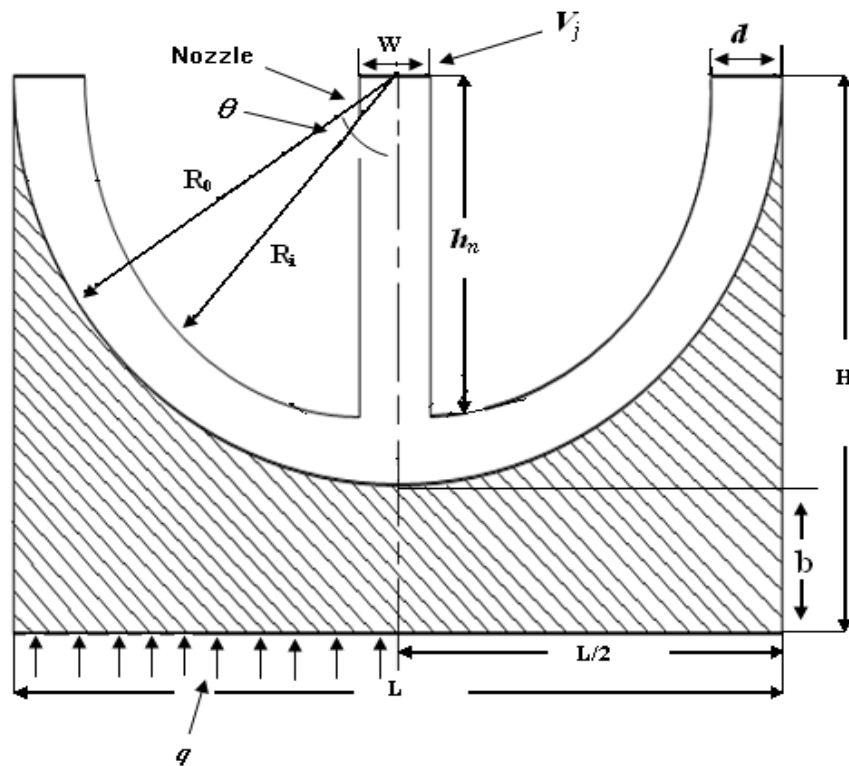


Figure 3.1 Two-dimensional liquid jet impingement on a uniformly heated concave surface.

The physical model corresponds to a two-dimensional confined liquid jet that impinges on a solid curved surface of circular shape, as shown in Figure 3.1. The jet discharges from the nozzle and impinges perpendicularly at the center and top of the

curved body, while its bottom is subjected to a constant heat flux. The fluid is Newtonian and the flow is incompressible and symmetric about the mid-plane under a steady state condition. The $\partial/\partial z$ terms can be omitted as a result of this two-dimensional analysis. The variation of fluid properties with local temperature is taken into account. The equations describing the conservation of mass, momentum (x and y directions respectively), and energy using a Cartesian coordinate system can be written (check Burmeister).

$$\frac{\partial u}{\partial x} + \frac{\partial v}{\partial y} = 0 \quad (21)$$

$$\rho_f \left(u \frac{\partial u}{\partial x} + v \frac{\partial u}{\partial y} \right) = -\frac{\partial p}{\partial x} + \frac{\partial}{\partial x} \left[\mu_f \left(2 \frac{\partial u}{\partial x} - 2 \left(\frac{\partial u}{\partial x} + \frac{\partial v}{\partial y} \right) \right) \right] + \frac{\partial}{\partial y} \left[\mu_f \left(\frac{\partial u}{\partial y} + \frac{\partial v}{\partial x} \right) \right] \quad (22)$$

$$\rho_f \left(u \frac{\partial v}{\partial x} + v \frac{\partial v}{\partial y} \right) = -\frac{\partial p}{\partial y} + \frac{\partial}{\partial y} \left[\mu_f \left(2 \frac{\partial v}{\partial y} - 2 \left(\frac{\partial u}{\partial x} + \frac{\partial v}{\partial y} \right) \right) \right] + \frac{\partial}{\partial x} \left[\mu_f \left(\frac{\partial u}{\partial y} + \frac{\partial v}{\partial x} \right) \right] \quad (23)$$

$$\rho_f \left(u \frac{\partial (C_{p_f} T_f)}{\partial x} + v \frac{\partial (C_{p_f} T_f)}{\partial y} \right) = \frac{\partial}{\partial x} \left(k_f \frac{\partial T_f}{\partial x} \right) + \frac{\partial}{\partial y} \left(k_f \frac{\partial T_f}{\partial y} \right) + 2 \cdot \mu_f \left[\left(\frac{\partial u}{\partial x} \right)^2 + \left(\frac{\partial v}{\partial y} \right)^2 + \frac{1}{2} \left(\frac{\partial v}{\partial x} + \frac{\partial u}{\partial y} \right)^2 - \frac{1}{3} \left(\frac{\partial u}{\partial x} + \frac{\partial v}{\partial y} \right)^2 \right] \quad (24)$$

The variation of thermal conductivity of solids with temperature is not significant. Therefore, the conservation of energy inside the solid can be characterized by the following equation:

$$\frac{\partial^2 T_s}{\partial x^2} + \frac{\partial^2 T_s}{\partial y^2} = 0 \quad (25)$$

The following boundary conditions are used to complete the physical problem formulation.

$$\text{At } x = 0, -H \leq y \leq -R_o : \frac{\partial T_s}{\partial x} = 0 \quad (26)$$

$$x = 0, -R_o \leq y \leq 0 : u = 0, \frac{\partial v}{\partial x} = 0, \frac{\partial T_f}{\partial x} = 0 \quad (27)$$

$$\text{At } y = 0, 0 \leq x \leq \frac{w}{2} : u = 0, v = -V_j, T_f = T_j \quad (28)$$

$$\text{At } x = \frac{w}{2}, -R_i \leq y \leq 0 : u = v = 0, \frac{\partial T_f}{\partial x} = 0 \quad (29)$$

$$\text{At inner curvature, } (x \geq \frac{w}{2}, r = R_i) : u = v = 0, \frac{\partial T_f}{\partial s} = 0$$

$$\text{At outer curvature } (r = R_o) : u = v = 0, T_s = T_f, k_s \frac{\partial T_s}{\partial r} = k_f \frac{\partial T_f}{\partial r}$$

$$\text{At } y = -H, 0 \leq x \leq R_o : q = -k_s \frac{\partial T_s}{\partial y} \quad (30)$$

$$\text{At } y = 0, R_i \leq x \leq R_o : p = p_{\text{atm}} \quad (31)$$

$$\text{At } x = R_o, -H \leq y \leq 0 : u = v = 0, \frac{\partial T_s}{\partial x} = 0 \quad (32)$$

The local heat transfer coefficients can be defined as:

$$h = \frac{1}{(\bar{T}_{\text{int}} - T_j)} \quad (33)$$

The average heat transfer coefficient can be calculated by integrating the local distributing results in the following equation.

$$h_{\text{avg}} = \frac{1}{\theta_{\text{max}} (\bar{T}_{\text{int}} - T_j)} \int_0^{\theta_{\text{max}}} h(T_{\text{int}} - T_j) \cdot d\theta \quad (34)$$

Here, \bar{T}_{int} is the average temperature at the solid-liquid interface. The average temperature is calculated by taking the area-weighted average of the local interface

temperature. The local and average Nusselt numbers are calculated according to the following expressions:

$$Nu = \frac{h \cdot w}{k_f} \quad (35)$$

$$Nu_{avg} = \frac{h_{avg} \cdot w}{k_f} \quad (36)$$

The governing equations (1–5) along with the boundary conditions (6–14) are solved using the Galerkin finite element method as demonstrated by Fletcher [54]. Four node quadrilateral elements are used. In each element, the velocity, pressure, and temperature fields are approximated, which leads to a set of equations which define the continuum.

The number of elements required for accurate results is determined from a grid independence study. A structured grid is used in which the size of the elements near the solid–fluid interface is made smaller, to adequately capture large variations in velocity and temperature in that region. The solution of the resulting nonlinear differential equations is carried out using the Newton–Raphson method. Due to the non–linear nature of the governing transport equations, an iterative procedure is used to arrive at the solution for the velocity and temperature fields. The solution is considered converged when the field value does not change from one iteration to the next and the sum of the residuals for all the dependent variables is less than a predefined tolerance value; in this case, 10^{-6} .

The values of Reynolds number is limited to a maximum of 2000 to stay within the laminar region. The nozzle opening and the solid plate have a length of 3 and 30 mm respectively. The heat flux (q) is kept constant at a value of 125 kW/m^2 . The incoming

fluid jet temperature (T_j) is 310 K for water. The base thickness of the solid plate (b) is varied over the following values: 10, 20, 30, 40, 50 mm. The channel spacing height or gap is set to the following values: 1, 2, 3, 4, 5 mm. The radius of curvature (R_O) is extended from 30 to 34 mm. The range of Reynolds number is varied from 750 to 2000. All runs used in the paper check out to be laminar. The simulation is carried out for a number of disk materials: aluminum, Constantan, copper, and silicon. The properties of solid materials are obtained from Özisik [55]. Fluid properties for H₂O are obtained from Bejan [56]. The properties of the above fluids are correlated according to the following equations:

- water, between $300\text{ K} < T < 411\text{ K}$;
- $C_{p_f} = 9.5 \times 10^{-3} \cdot T^2 - 5.9299 \cdot T + 5098.1$;
- $k_f = -7.0 \times 10^{-6} \cdot T^2 + 5.8 \times 10^{-3} \cdot T - 0.4765$;
- $\rho_f = -2.7 \times 10^{-3} \cdot T^2 + 1.3104 \cdot T + 848.07$; and
- $\ln(\mu_f) = -3.27017 - 0.0131 \cdot T$.

3.2 Results and Discussion

This section describes the heat transfer characteristics of a confined liquid jet impingement under flat, concave, and convex surfaces. The velocity vector distribution remains uniform at the potential core region of the confined liquid jet through the curvature, as shown in Figure 3.2. The direction of motion of the fluid particles shifts by more than 90° in a concave surface, 90° in the flat surface, and less than 90° in the convex surface.

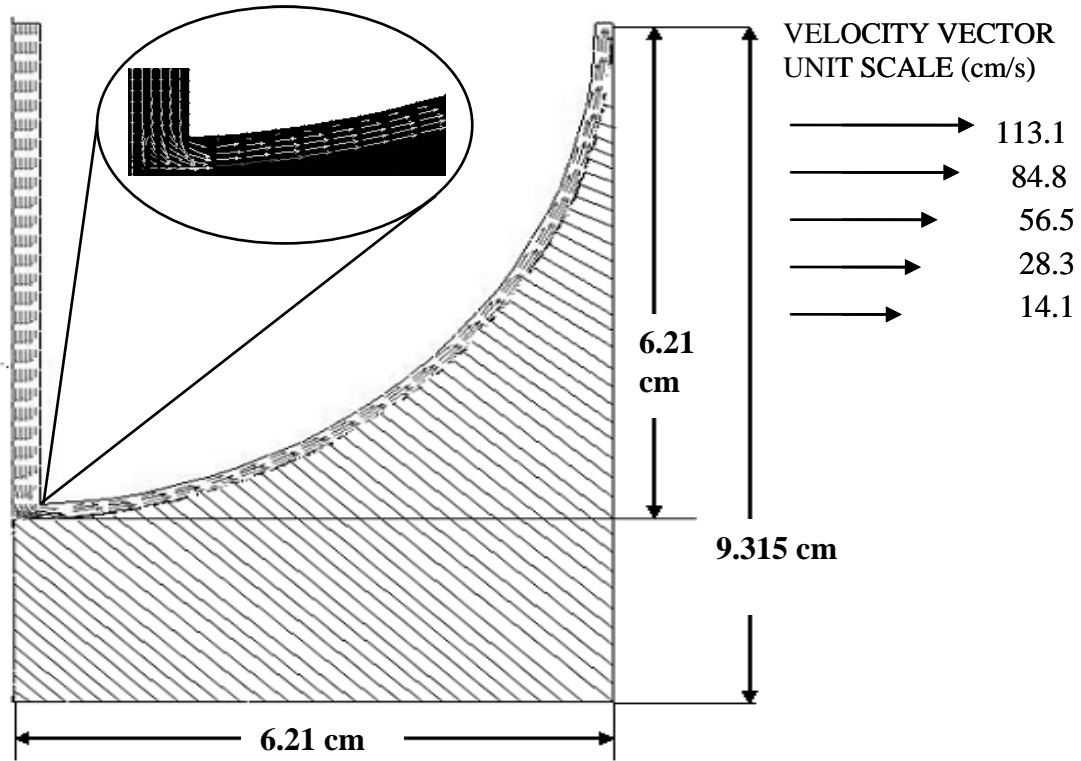


Figure 3.2 Velocity vector distribution for jet impingement on a curved copper plate.

Thereafter, the fluid strikes the solid surface at which point there is a rapid deceleration, while the flow changes direction along the surface. After this, there is a brief acceleration starting the development of boundary layer. It can be noted that the boundary layer thickness increases along the radius of curvature, and the frictional resistance from the wall is eventually transmitted to the fluid flow. The fluid between the boundary layer zone and confined top plate has much smaller flow velocity compared to the inlet velocity. This is due to frictional resistance from the solid body, as well as the confined plate.

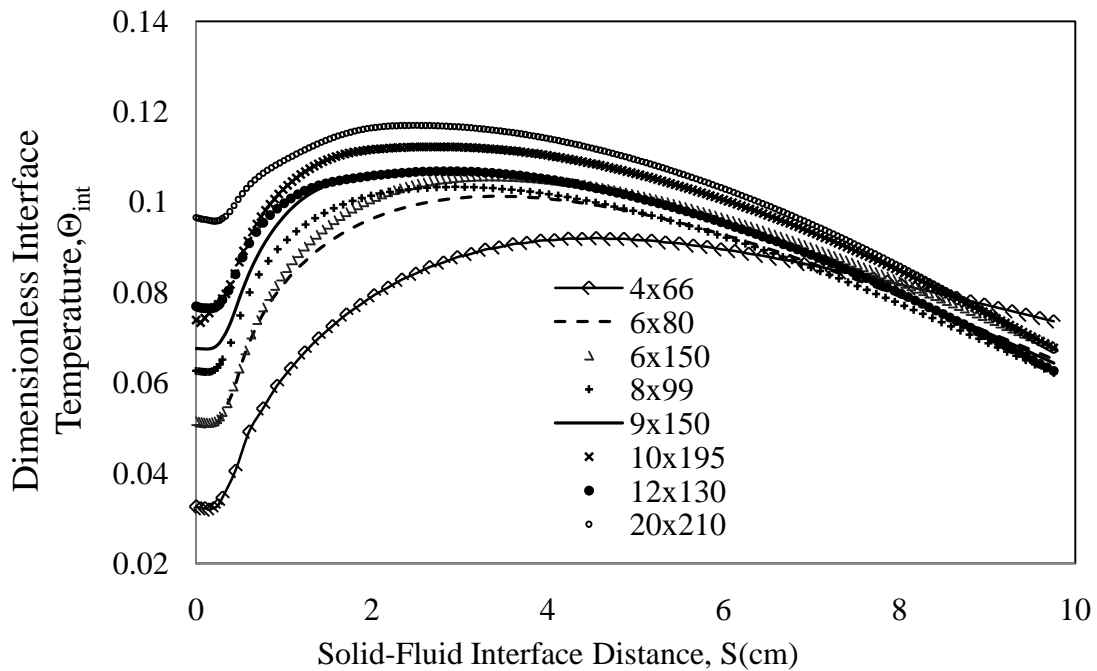


Figure 3.3 Solid–fluid interface temperature for different number of elements in x and y directions ($Re = 1,000$, $b = 30$, $w = 0.6$ cm).

The solid–fluid dimensionless interface temperatures for different number of grids are plotted in Figure 3.3. Several grids are used to determine the number of elements needed for accurate numerical solution. It is observed that the numerical solution becomes grid independent when the grids reach a number of divisions equal to 12x130 in

(y) and (x) directions, respectively. Numerical results for a 12x130 grid gave almost identical results compared to 10x195 and 9x150 grids for an impingement height (h_n) equal to 30 mm. Therefore, the chosen grid is 12x130, which carries an average margin error of 0.163%; all further computations are carried out using this grid distribution. The size of the elements varies with denser distribution at the solid–fluid interface and at the nozzle axis.

Figure 3.4a and Figure 3.4b show the variation of solid–fluid dimensionless interface temperature plots and local Nusselt number distributions at different Reynolds numbers for concave and convex surfaces respectively, with water as a cooling fluid and copper as the solid body material. The plots reveal that dimensionless interface temperature decreases with jet velocity (or Reynolds number) for either type of plate configuration. At any Reynolds number, the dimensionless interface temperature has a low value at the stagnation point and increases radially along the radius of curvature, reaching the highest value at the solid fluid interface distance (S) (approximately equal to 2.52 cm) and decreases to its lowest value at the end of the concave curvature, as shown on Figure 3.4a. A new behavior occurs along the upright concave surface, causing the dimensionless temperature to drop. This is due to an energy balance, where more of the heat dissipates at the interface along the jet impingement region that is closer to the base of the plate, under a uniform heat flux boundary condition that gradually moves far away at constant flow rate conditions. At this condition, the thickness of the thermal boundary layer decreases along the radius of curvature, causing the interface temperature to drop along the radial distance. This allows the heat to dissipate faster and results in a lower interface temperature at the end of the concave plate.

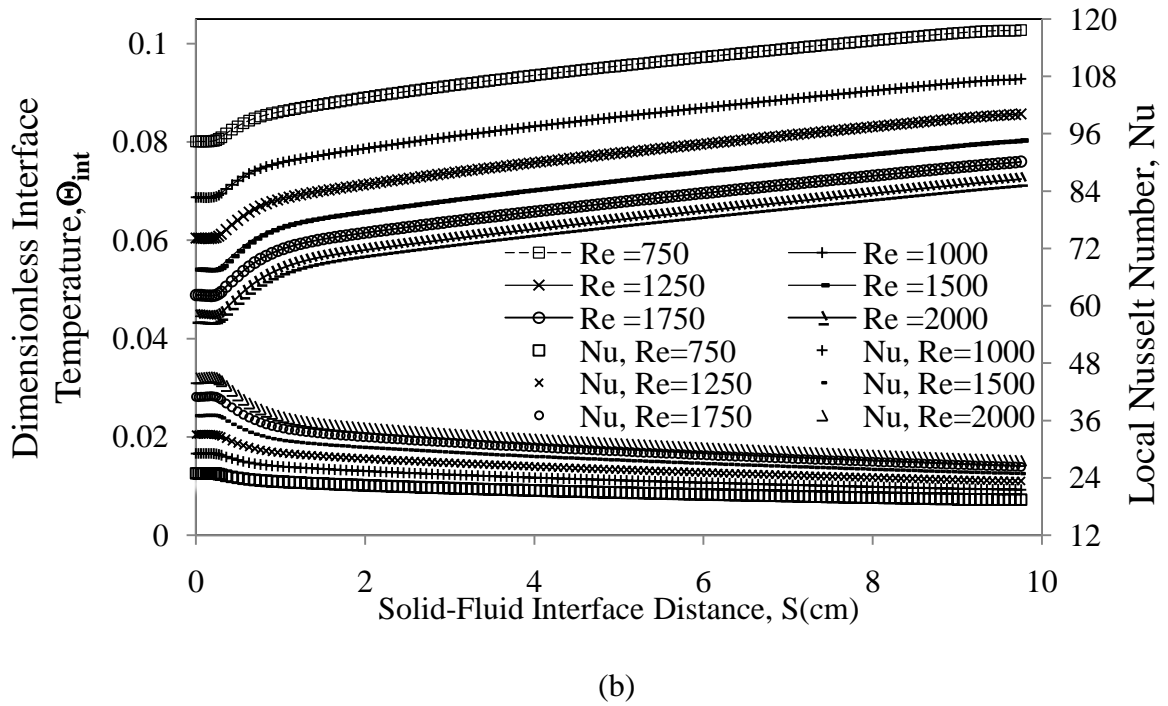
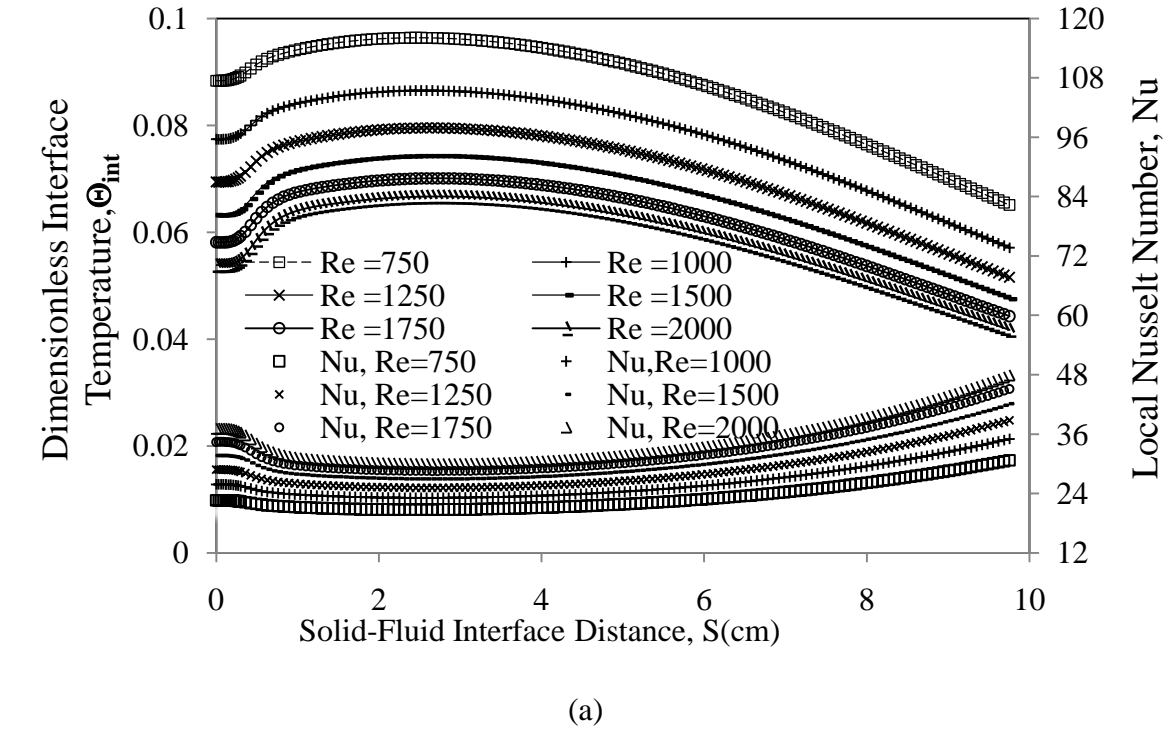
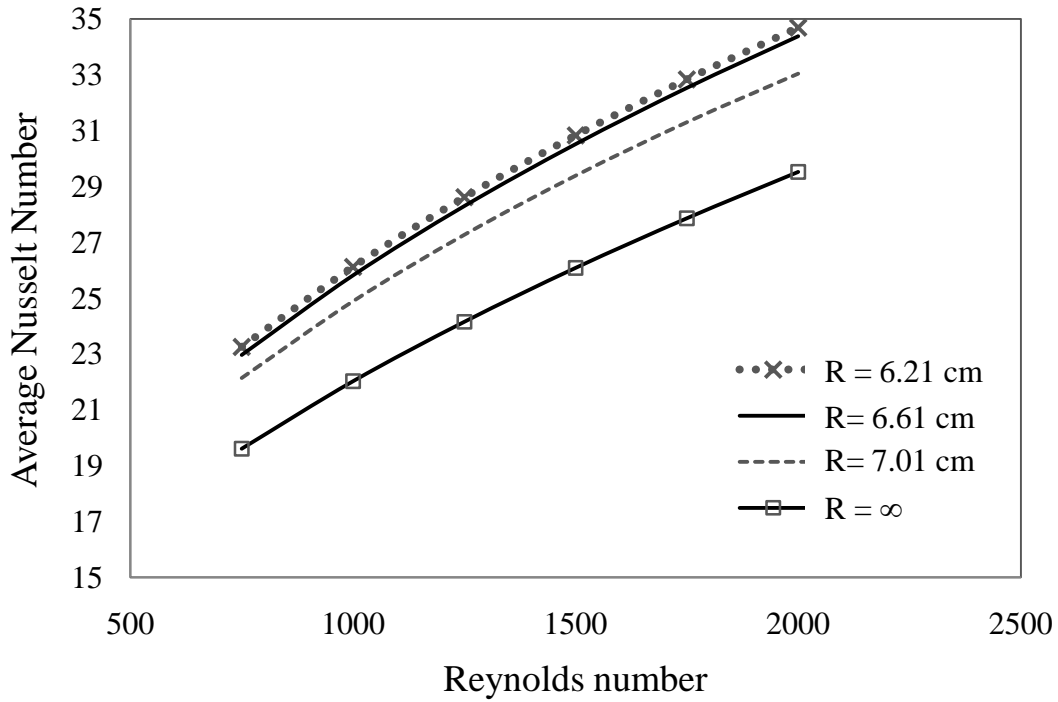


Figure 3.4 Dimensionless interface temperature and Local Nusselt number distribution for (a) concave and (b) convex copper plate at different Reynolds numbers and water as the cooling fluid.

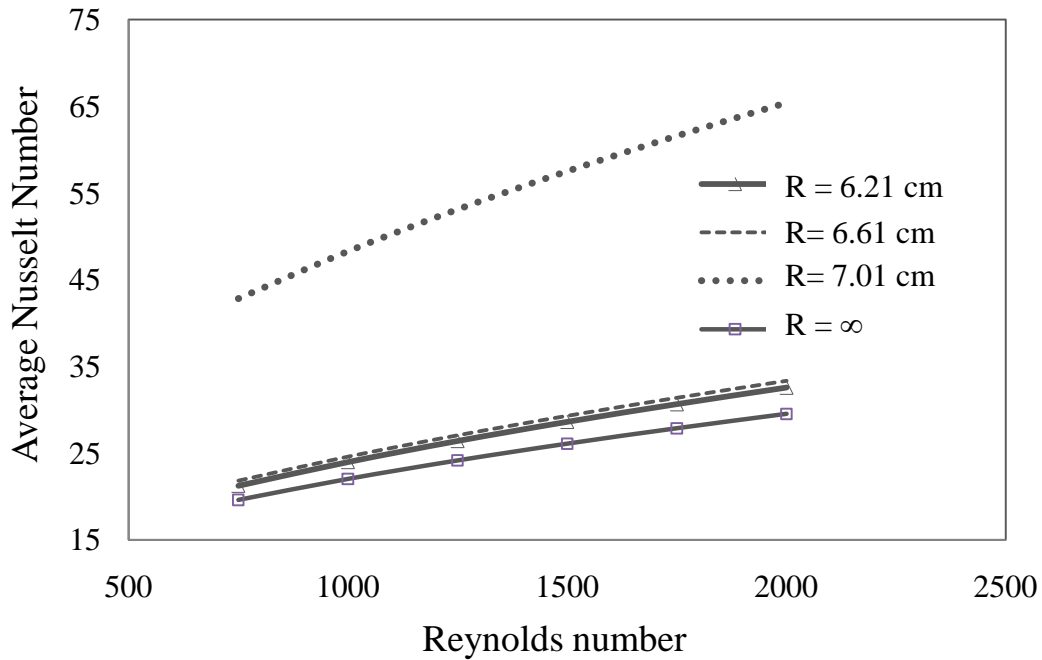
Conversely, the dimensionless interface temperature for the convex plate has the lowest value at the stagnation point (underneath the center of the axial opening) and increases radially downstream, reaching the highest value at the end of the curvature, as shown in Figure 3.4b. The thickness of the thermal boundary layer increases along the radius of curvature of the convex plate and causes the interface temperature to increase due to the proximity of the solid-fluid interface to the heat flux boundary condition.

Local Nusselt number distributions of Figure 3.4a are half-bell shaped with a peak at the stagnation point and gradually increase along the concave surface, reaching the highest value at the end of the radius of curvature. Contrarily, all local Nusselt number distributions of Figure 3.4b show a half-bell profile with a peak at the stagnation point and a decrease along the radius of curvature of the convex plate. Figures 3.4a and 3.4b confirm how an increasing Reynolds number contributes to more effective cooling. Similar profiles shown in Figure 3.4b have been documented by Ma et al. [34], and Garimella and Nenaydykh [35].

Figures 3.5a and 3.5b present the average Nusselt number as a function of Reynolds number and different radius of curvature. It can be seen that the average Nusselt number increases according to the Reynolds number. As the flow rate (or Reynolds number) increases, the magnitude of fluid velocity near the solid-fluid interface that controls the convective heat transfer rate increases. Furthermore, at a particular Reynolds number, the Nusselt number decreases with the increment of the radius of curvature. In figure 3.5b we can see that at radius 7.01 cm the average Nusselt number is highest, this because the concave is more closer to the heat flux.



(a)

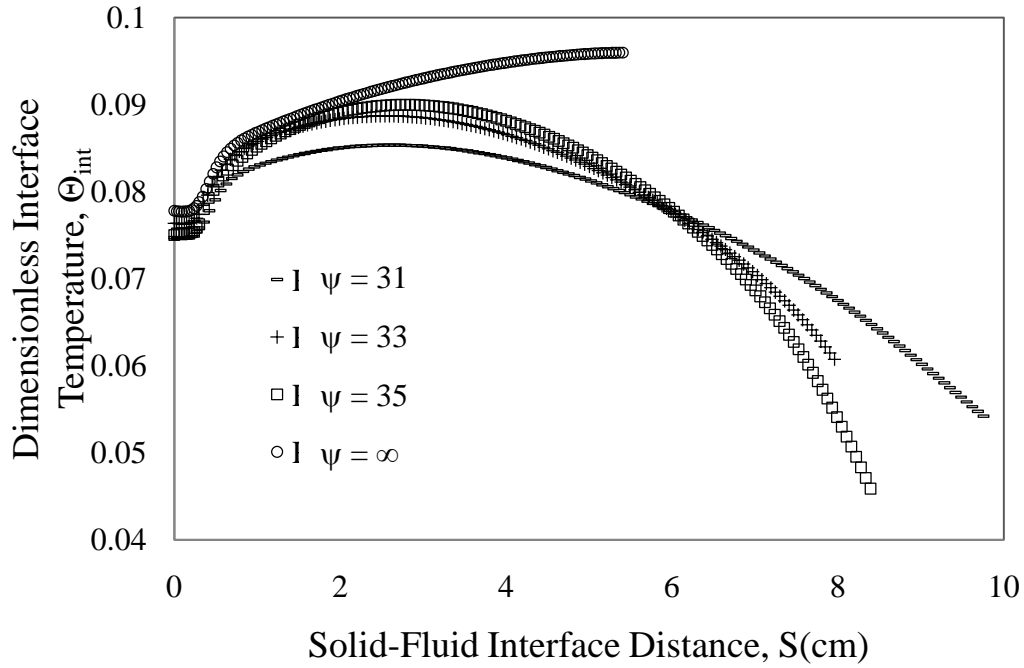


(b)

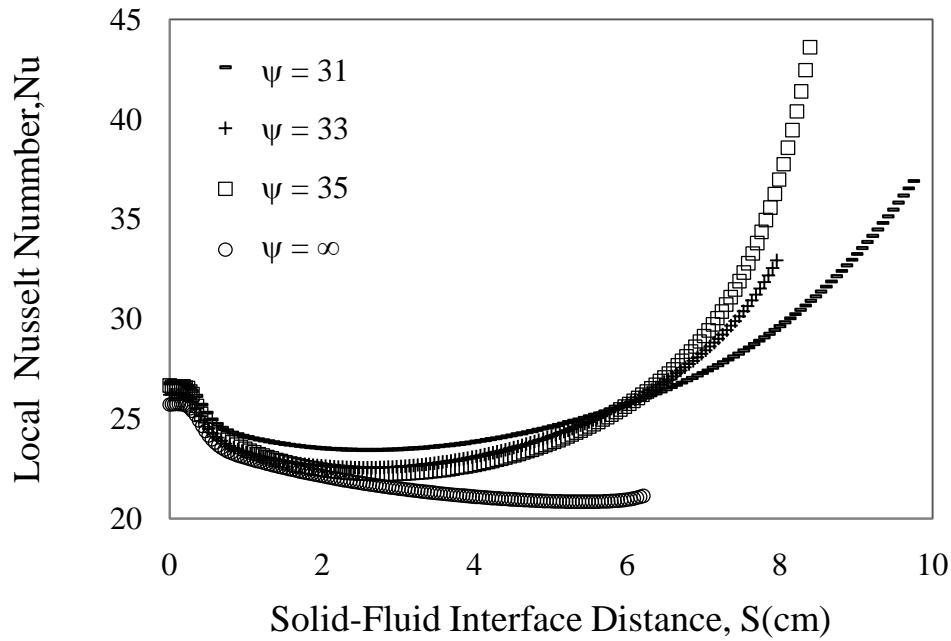
Figure 3.5 Average Nusselt number at different Reynolds numbers for (a) concave (b) convex copper plate with water as the cooling fluid ($R = 6.21, 6.61, 7.01, \text{ and } \infty, \text{ cm}$).

In addition, it can be seen that the average Nusselt number plots get closer to each other as the radius of curvature decreases. This behavior confirms the positive influence of the radius of curvature (ψ) on the average Nusselt number down to $\psi=62.1$, which corresponds to an outer radius of curvature of 6.21 cm.

The radius of curvature effects on the dimensionless interface temperature and local Nusselt number are shown in Figure 3.6a and Figure 3.6b for concave and Figures 3.7a and 3.7b for convex. The dimensionless solid–fluid interface distance increases for the concave from the impingement region all the way to the end at the infinite radius, and increases to the peak point at the highest solid thickness region and drops down to the lowest at the shortest solid thickness for other radiuses as shown in Figure 3.6a. We observe in Figure 3.7a better results for convex during the increase in temperature from the impingement region all the way to the end at all radiuses. The higher outflow temperature occurs when the temperature is lower at the stagnation region. This is fairly estimated, since the total heat transferred to the curvature as well as the fluid flow rates are the same for all cases. For the concave, as shown in Figure 3.6b, the local Nusselt number decreases with the solid-fluid interface distance for a rate of radius of curvature (ψ) from $31.05 - \infty$ at Reynolds number of 1000 at maximum of thickness and starts increasing to highest at the minimum of thickness.

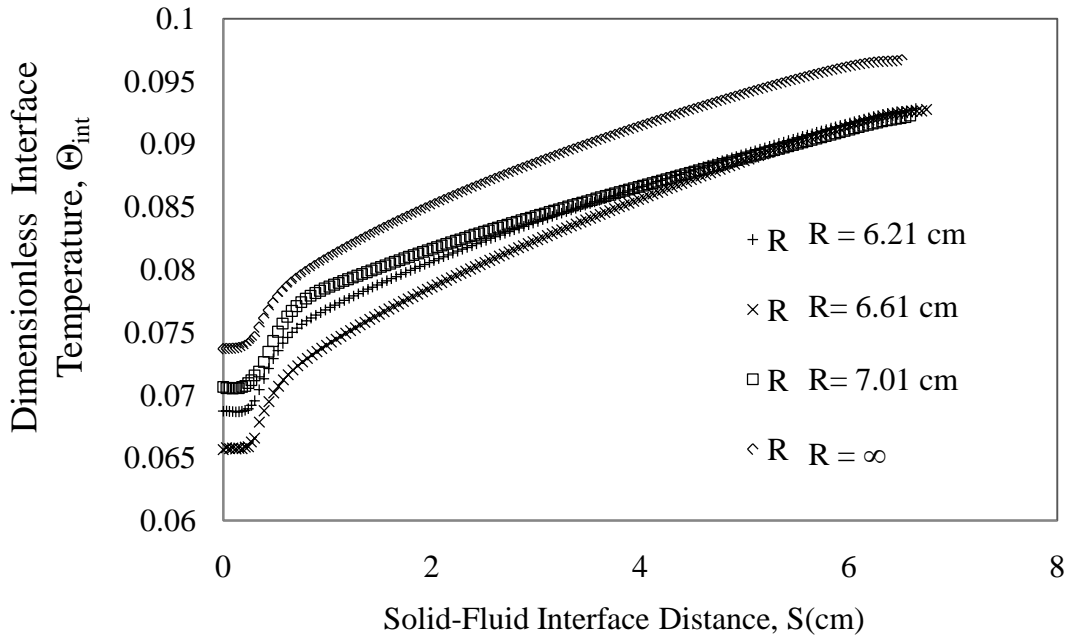


(a)

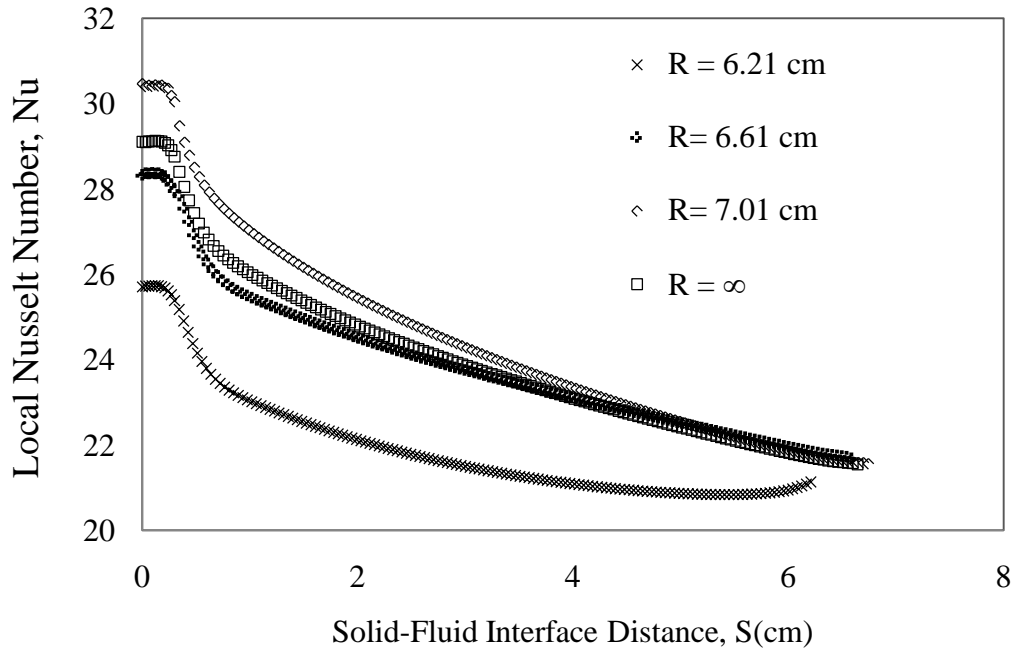


(b)

Figure 3.6 Solid–fluid interface distance and (a) dimensionless interface temperature distribution (b) Local Nusselt number distribution for a concave copper wafer at different radius, and water as the cooling fluid ($R= 6.21, 6.61, 7.01, \text{ and } \infty \text{ cm}$).



(a)

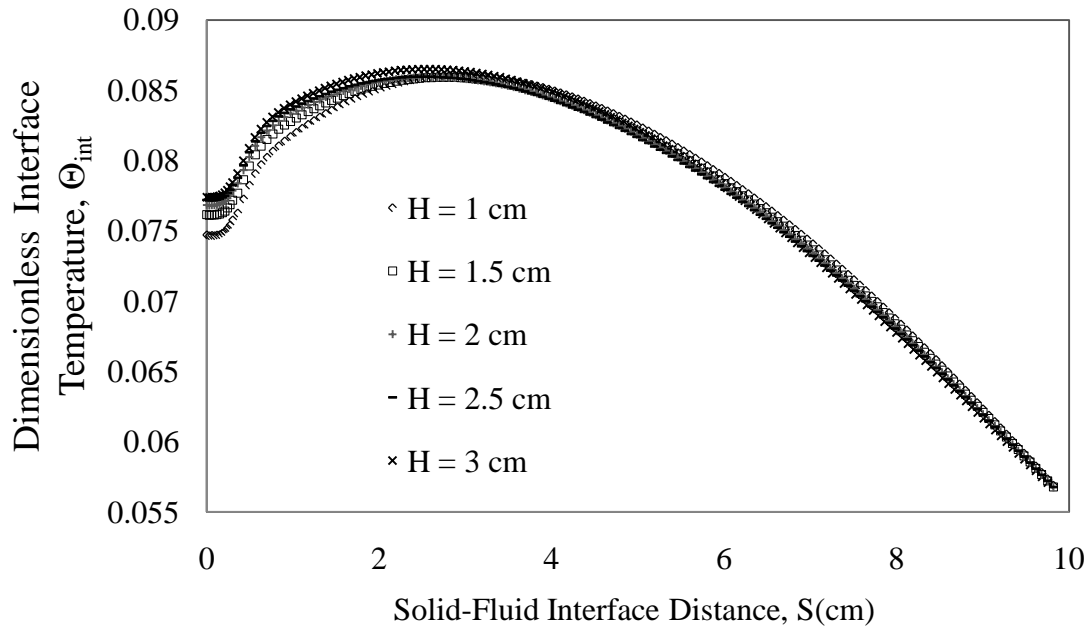


(b)

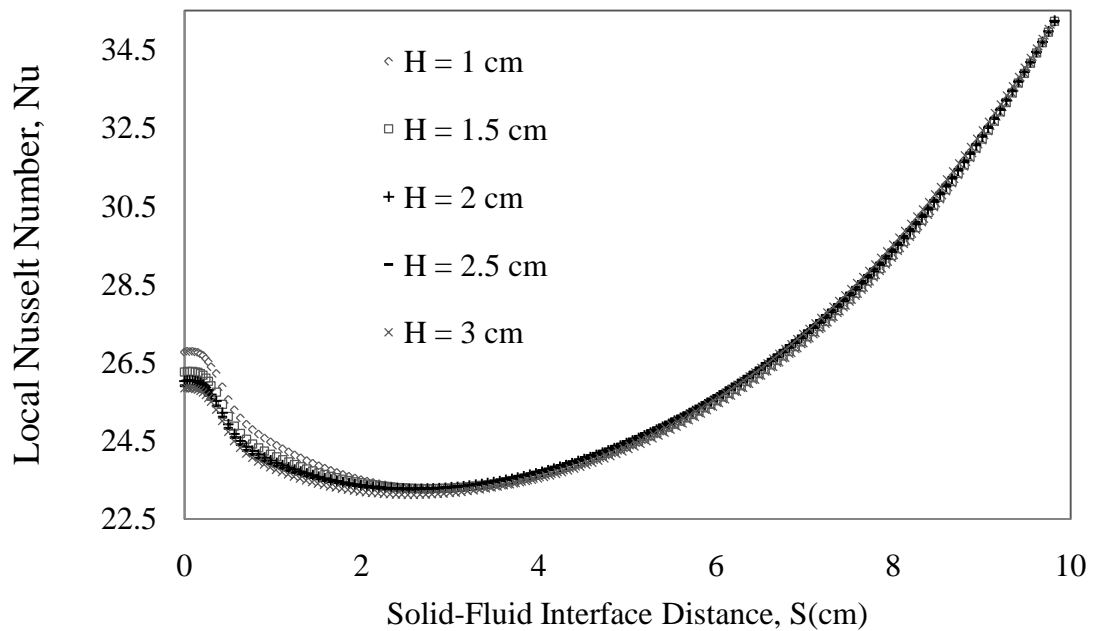
Figure 3.7 Solid–fluid interface distance and (a) dimensionless interface temperature distribution (b) Local Nusselt number distribution for a convex copper wafer at different radius, and water as the cooling fluid ($R = 6.21, 6.61, 7.01,$ and ∞ cm).

Figure 3.8b illustrates superior consequences for convex compared with concave throughout the decrease of Nusselt number all the way to the end, without changing due to the difference of thicknesses. The local fluid velocity adjacent to the heated material surface creates an enhancement of Nusselt number due to the confined impingement jet. Copper has been used as the solid material and water as the cooling fluid for a Reynolds number of 1000 and solid thickness to curvature ratio of 0.161 – 0.5.

The difference of solid thickness to curvature spacing ratios (Φ) from 0.161 – 0.5 are modeled for water as the coolant and copper as the solid material. The effects of solid thickness to the spacing of curvature on the local Nusselt number and dimensionless interface temperature at a Reynolds number of 1000 are shown in Figures 3.8a and 3.8b. It may be noted that the solid thickness insignificantly affects the local Nusselt number distribution particularly at the end; however there is a minor change at the stagnation region.



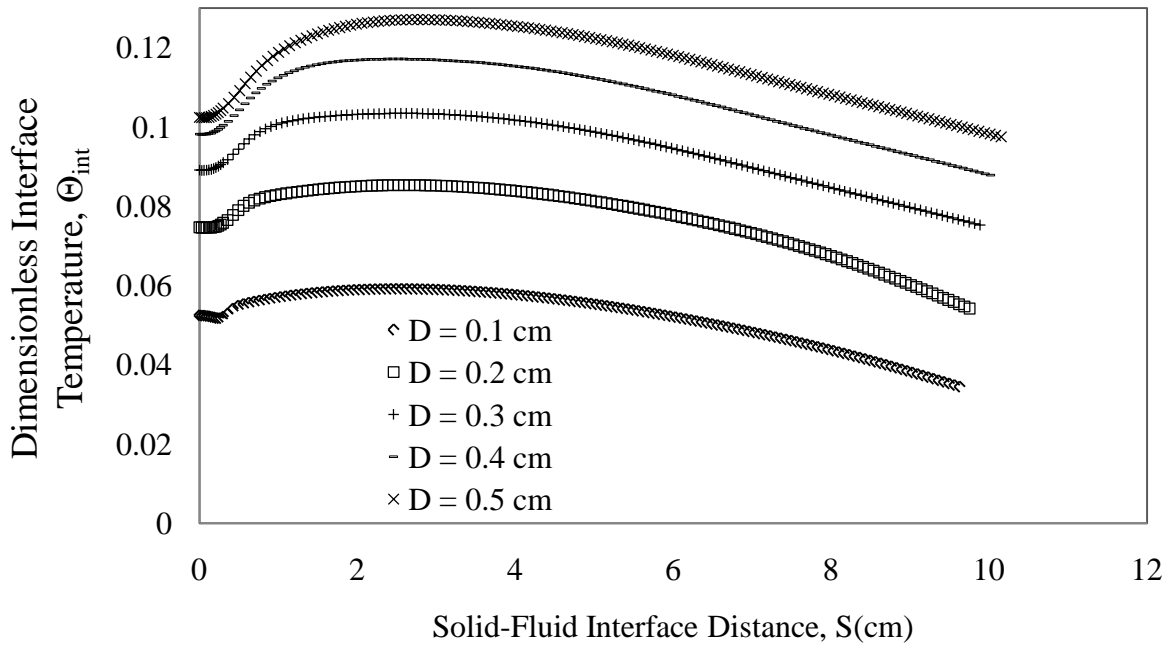
(a)



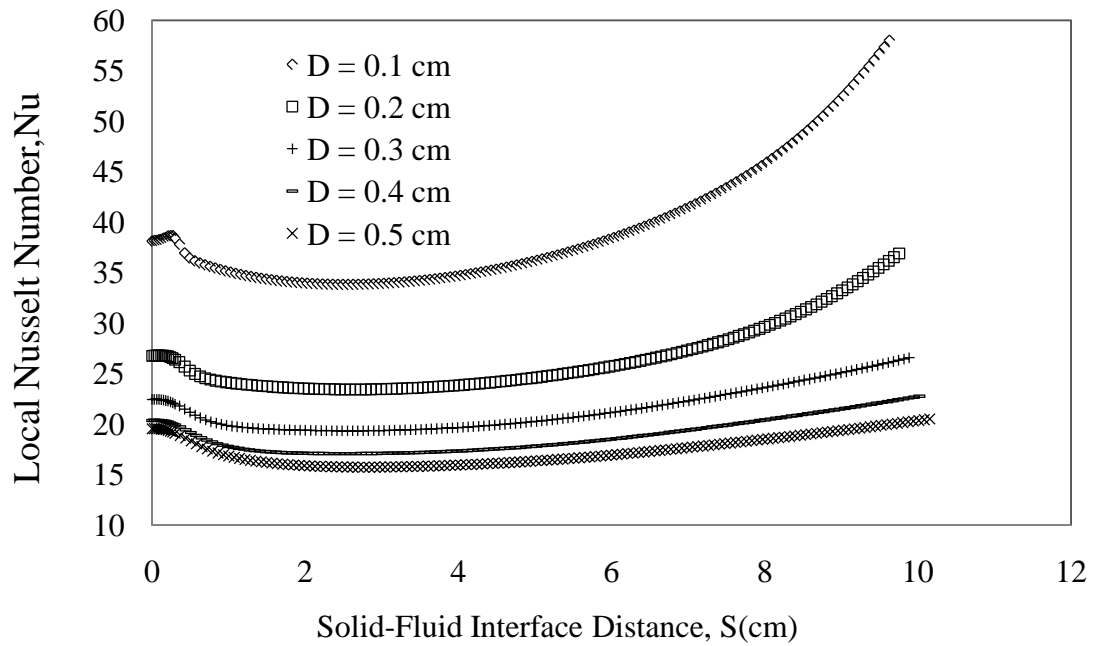
(b)

Figure 3.8 Solid–fluid interface distance and (a) dimensionless interface temperature distribution (b) Local Nusselt number distribution for different material thickness ($H = 1, 1.5, 2, 2.5,$ and 3 cm).

The solid–fluid dimensionless interface temperature and local Nusselt number distributions for five different spacing of curvature for water as the cooling fluid and Reynolds number of 1000 are shown in Figures 3.9 (a and b) and 3.10 (a and b), respectively. Due to the higher jet momentum at impingement at the end of the nozzle, the temperature at the solid–fluid interface decreases, causing higher velocity of fluid particles adjacent to the plate, enhances the heat transfer. In Figures 3.9 and 3.10, a higher Nusselt number is seen all along the arc length at all radii of different spacing, and also the Nusselt number increases by increasing the spacing of curvature (from 0.1 - 0.5 cm). Also, we have seen that the impingement height affects the Nusselt number more at the stagnation region and the early part of the boundary layer region. For larger spacing (0.5 cm), the values get closer for all impingement heights. Hence, it can be concluded that the jet momentum more strongly affects the areas subjected to direct impingement. Because of the fast traveling of heat at less material, it can be noted that the Nusselt number increases at all radii of different spacing.

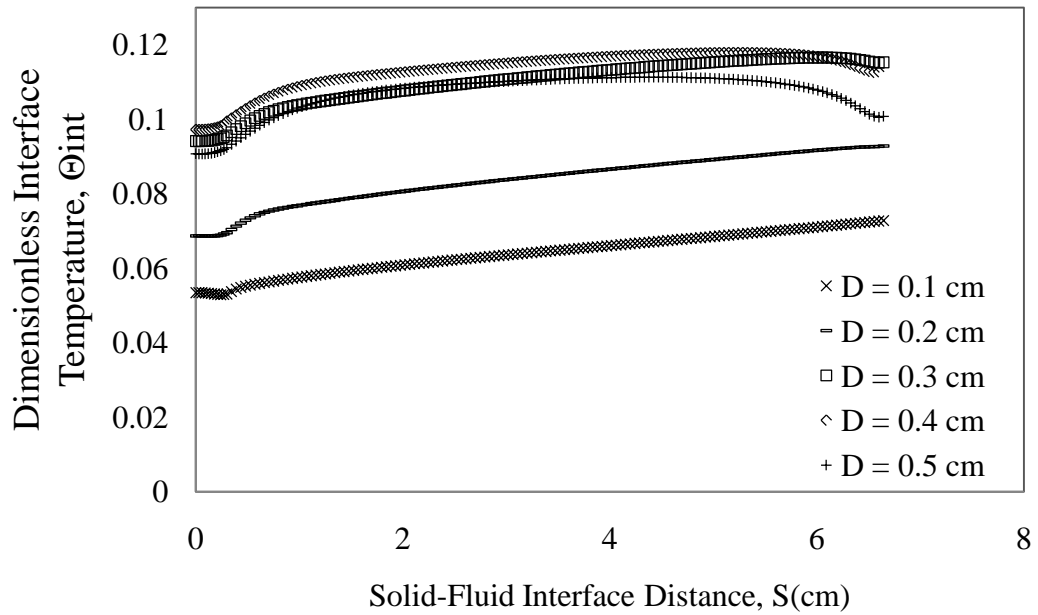


(a)

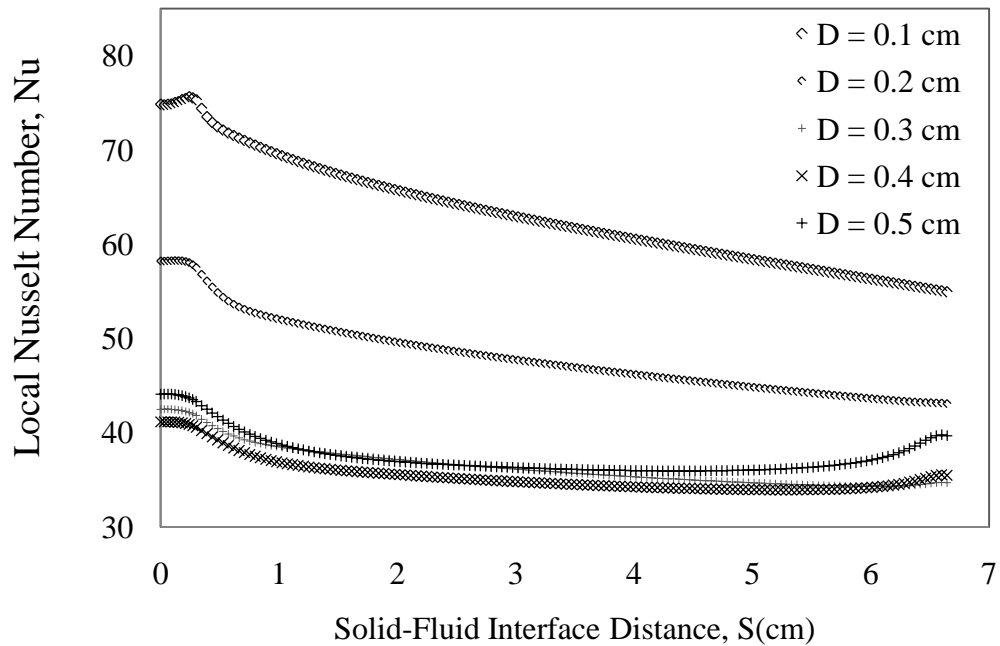


(b)

Figure 3.9 Solid–fluid interface distance and (a) dimensionless interface temperature distribution (b) Local Nusselt number distribution for different spacing of concave curvature ($D = 0.1, 0.2, 0.3, 0.4,$ and 0.5 cm).



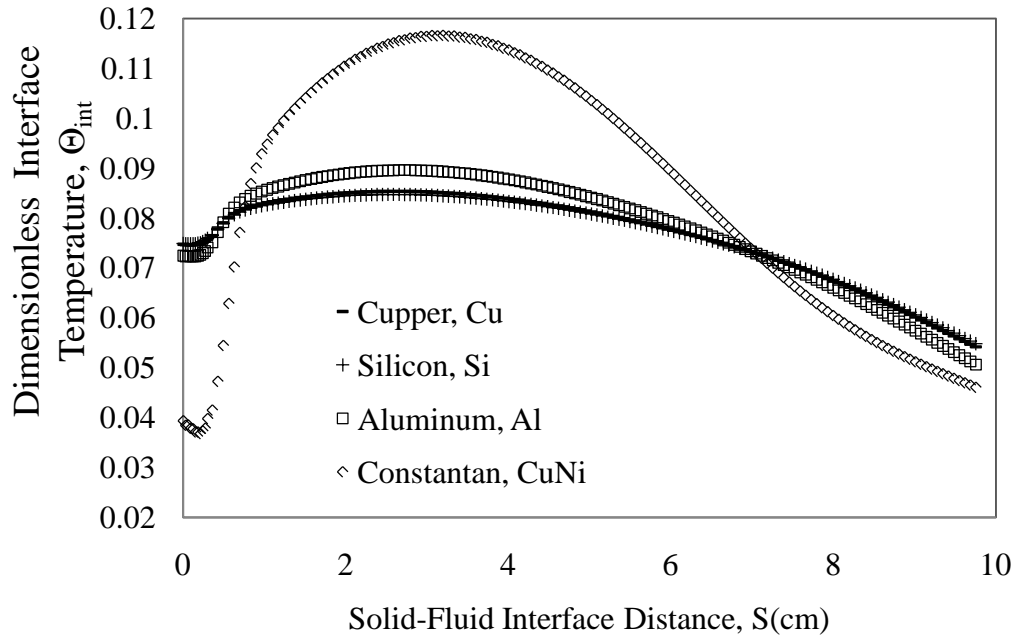
(a)



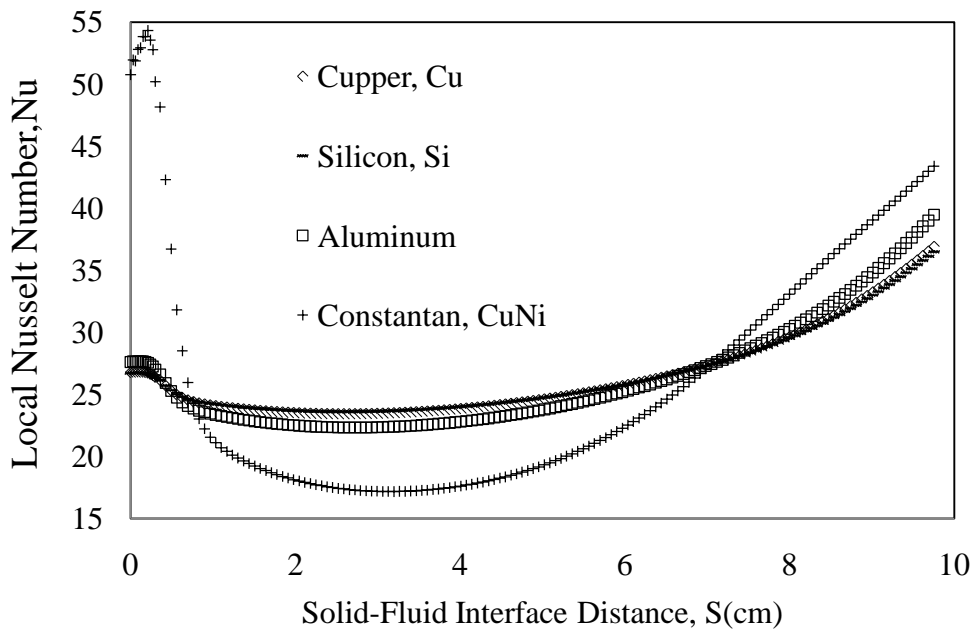
(b)

Figure 3.10 Solid–fluid interface distance and (a) dimensionless interface temperature distribution (b) Local Nusselt number distribution for different spacing of convex curvature ($D = 0.1, 0.2, 0.3, 0.4,$ and 0.5 cm).

Figures 3.11a and 3.11b show the dimensionless solid-fluid interface temperature and local Nusselt number distribution plots respectively as a function of the dimensionless radial distance measured from mid-plane axis for different solid materials, with water as the working fluid. The numerical simulation is carried for a set of materials: aluminum, copper, Constantan and silicon, which all have different thermo-physical properties. The temperature distribution plots reveal how the thermal conductivity of the solids affects the heat flux distribution that controls the local interface temperature. It may be noted that Constantan has the lowest temperature at the impingement axis and the highest at the inner radial distance of the concave plate. This large interface temperature variation is due to its lower thermal conductivity. As the thermal conductivity increases, the thermal resistance within the solid becomes lower and the interface temperature becomes more uniform, as seen in the plots corresponding to copper and silicon. The cross-over of the curves of the four materials occurs due to a constant fluid flow and heat flux rate that provides a constant thermal energy transfer for all circumstances. Narrow and elevated bell shape pattern for local Nusselt number distributions are seen in Figure 3.11b for all solid materials with low thermal conductivity. Conversely, high thermal conductivity materials such as aluminum and copper portray a more uniform local Nusselt number distribution in general.



(a)



(b)

Figure 3.11 Solid–fluid interface distance and (a) dimensionless interface temperature distribution (b) Local Nusselt number distribution for different materials (copper, silicon, aluminum, and Constantan).

Figure 3.12a and Figure 3.12b show the variation of solid–fluid dimensionless interface temperature plots and local Nusselt number distributions at different Reynolds numbers for concave and convex surfaces respectively, with water as a cooling fluid and silicon as a material. It can be seen that there is no significant change in the results between copper and silicon. The same plots reveal that dimensionless interface temperature decreases with jet velocity (or Reynolds number) for either type of plate configuration. Also, at any Reynolds number, the dimensionless interface temperature has a low value at the stagnation point and increases radially along the radius of curvature, reaching the highest value at the solid fluid interface distance, (S) (approximately equal to 3.00 cm) and decreases to its lowest value at the end of the concave curvature, as shown on Figure 3.12a. The difference is ± 0.48 cm. This behavior is due to the development of a thermal boundary layer as the fluid moves downstream from the center of the concave curvature, and the difference between the thermal conductivity of the material. The thickness of the thermal boundary layer increases along the radius of curvature and causes the interface temperature to increase; subsequently the area of curvature diminishes along the radial distance, allowing the heat to dissipate faster, resulting in a lower interface temperature at the end of the concave plate. This also makes a difference in the local Nusselt number, within a range of about ± 48 . On the other hand, the dimensionless interface temperature for the convex plate has the lowest value at the stagnation point (underneath the center of the axial opening) and increases radially downstream, reaching the highest value at the end of the curvature, as shown in Figure 3.12b. The thickness of the thermal boundary layer increases along the radius of curvature of the convex plate and causes the interface temperature to increase. This is

caused by the proximity of the solid-fluid interface due to the heat flux boundary condition.

Local Nusselt number distributions of Figure 3.12a are half-bell shaped with a peak at the stagnation point and gradually increase along the concave surface, reaching the highest value at the end of the radius of curvature. Contrarily, all local Nusselt number distributions of Figure 3.12b show a half-bell profile with a peak at the stagnation point and decrease along the radius of curvature of the convex plate.

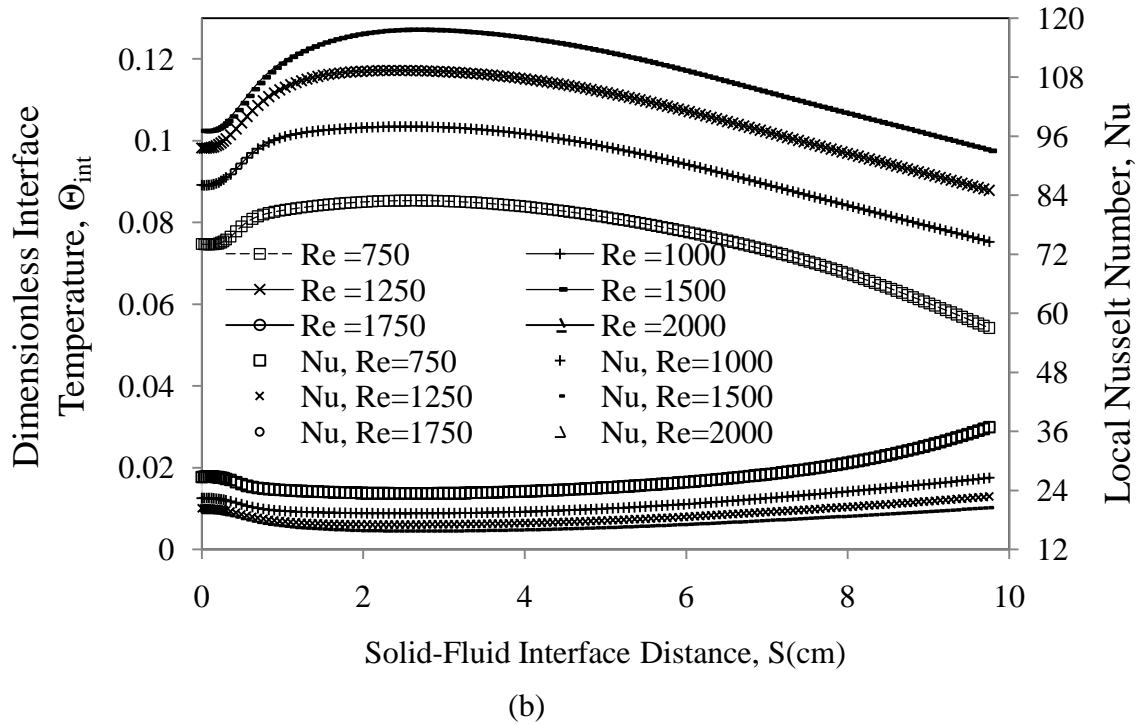
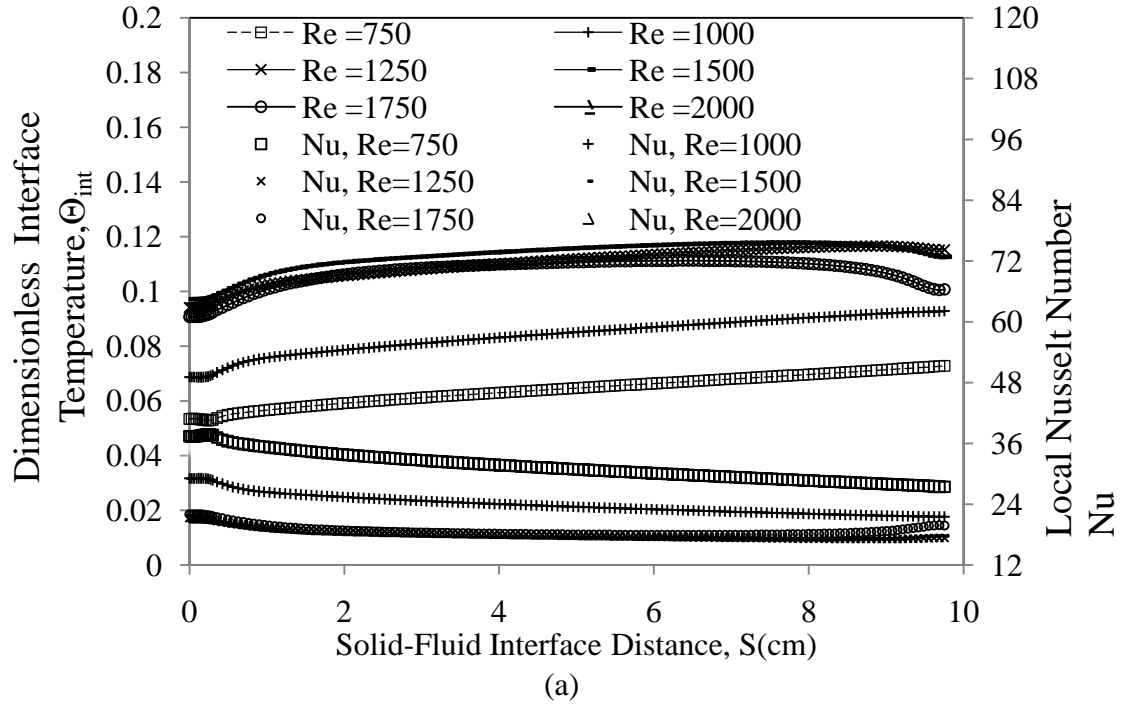


Figure 3.12 Dimensionless interface temperature and Local Nusselt number distribution for (a) concave and (b) convex silicon plates at different Reynolds numbers and water as the cooling fluid.

Papers used for the validation of this numerical study included analytical works by Inoue et al.[40] and Inoue et al.[41] using fluids with Reynolds numbers between 500 – 200. The fluids were tested for heat removal under confined liquid jet impingement on a heated flat surface maintained at uniform heat flux. The graphical representation of actual numerical average Nusselt number results at the stagnation point at different Reynolds numbers are shown in Figure 3.13. The local Nusselt number under Reynolds numbers of 750, 1,000, 1,250, 1,500, 1,750, and 2000 correlates with an average difference margin of 17.95%, 12.1%, 11.11%, 10.35%, 12.7%, and 12.12% respectively. The results shown in Figure 3.13 were on average within 34.29% of Rahman et al. [49] within 35% of A. Inoue et al. [40], and within 33.33% for the current work. Considering the inherent discretization and round off errors, this comparison of Nusselt numbers at the stagnation point is quite satisfactory.

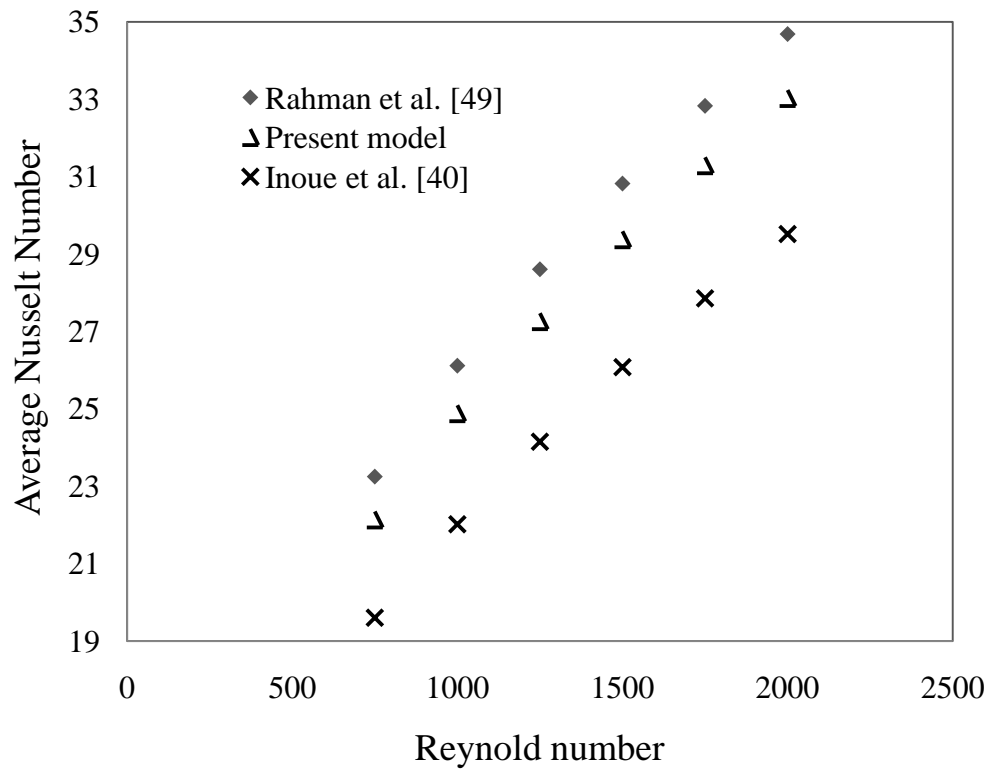


Figure 3.13 Stagnation Nusselt number comparison of Rahman et al. [49], Inoue et al. [40], with actual numerical results under different Reynolds numbers ($w = 4$ mm, $d = 2$ mm).

Chapter 4: Conclusions

The analytical model for a one-dimensional wavy fin assembly under fully wet conditions has been developed. The model was considered with and without insulation at the fin tip under the same conditions. The same model has been converted to straight radial (rectangular) fin, and the results revealed that at the insulation fin tip the heat dissipation is less. We also found that under the same operating conditions; the radial wavy fin provides better heat transfer performance than the radial rectangular one. The cooling and dehumidification fin assembly heat transfer performance has been carried out when synchronous mass and heat transfer take place. The results show that generally the fin efficiency depends on the condition of the surface and the area of the fin under wet condition. The heat transfer characteristics have been carried out at variations of T_1 , T_2 , and RH. The latent heat transfer under wet condition during the condensation process enhances the heat transfer rate to a fin assembly when dehumidification occurs, at a rate which is always higher than the dry fin assembly. Under fully wet conditions, the dimensionless temperature, Θ decreases with temperature and relative humidity of the surrounding air, thus the fin efficiency changes rapidly with air relative to humidity. The study of the effects of differences in cold fluid temperature (T_1), air side temperature (T_2), and relative humidity (RH) has led to a better understanding of heat and mass transfer occurring in the air-conditioning dehumidification coils. The results show that at any increase in the air side temperature (T_2), while the cold fluid temperature and relative

humidity remain constant, both sensible and latent heat transfer increases at the coil. The heat and mass transfer decrease by increasing the fin temperature when the cold fluid temperature (T_1) increases, and the air side temperature (T_2) and the relative humidity (RH) remain constant. Due to a larger condensation rate at the fin surface, the dimensionless temperature decreases when the relative humidity increases. At all results, the heat transfer rate of the fin assembly is higher than that of a dry fin assembly when dehumidification occurs. The variations of cold fluid temperature (T_1) enhance the augmentation factor of the wet fin assembly compared to the dry surface condition. The increase in the amount of dehumidification makes a reduction in the wet augmentation factor. The increment in the area of the fin surface, air side temperature (T_2), and the relative humidity (RH), illustrate the increase in the ratio of the dry to wet augmentation factor. The findings of the current work demonstrate that the overall fin efficiency is dependent on the relative humidity of the surrounding air and the area of the fin. The efficiency depends on the fin surface area; The increase in surface area causes better heat dissipation by increasing the fin performance. However, even though an increase in fin surface area is desirable in order to obtain better fin performance, there are some physical limitations involved in building such a fin arrangement. Covering dry, partially wet, and fully wet conditions gives us a complete understanding of heat transfer phenomenon for an efficient design of dehumidification apparatus.

The solid–fluid dimensionless interface temperature and local and average Nusselt number for concave, convex, and flat surfaces show a strong dependence on Reynolds number, curvature spacing, length of radius, impingement height, and solid material properties. The increment of Reynolds number increases the local heat transfer

coefficient distribution values over the entire solid-fluid interface for all different materials. The results showed that decreasing the nozzle width increases the local Nusselt number at the core region. Decreasing the channel spacing, plate thickness, or plate inner radius of curvature all enhanced the local Nusselt number. It can be seen that implementation of confined liquid jet impingement over a convex surface is more effective compared to flat or concave surface cooling methods. The ongoing contrivance harvests low cost and accurate prediction of processes which involve jet impingement cooling. This approach is useful for the design of relevant cooling applications which enhance the heat transfer removal encountered on high heat flux of concave and convex surfaces. Numerical simulation results are validated by comparison with the experimental measurements of flat and concave surfaces.

References

- [1] Lunardini JV, Aziz A (1995) Effect of Condensation on Performance and Design of Extended Surfaces. CRREL Report 95-20.
- [2] Kays WM, London AL (1964) *Compact Heat Exchangers*, McGraw Hill, New York.
- [3] Wang C, Hsieh Y, and Lin Y (1997) Performance of Plate Finned Tube Heat Exchangers Under Dehumidifying Conditions. *Journal of Heat Transfer* Vol. 119, pp. 109-117.
- [4] Leu J, Chen S, and Yuhjang J (2004) Heat Transfer and Fluid Flow in Rectangular Fin and Elliptic Tube Heat Exchangers Under Dry and Dehumidifying Conditions. *Journal of Enhanced Heat Transfer* Vol. 11, No. 1, pp. 43-60.
- [5] Webb RL (1994) *Principles of Enhanced Heat Transfer*. John Wiley & Sons, New York.
- [6] Kazeminejad H (1995) Analysis of One-Dimensional Fin Assembly Heat Transfer with Dehumidification. *International Journal of Heat and Mass Transfer* Vol. 38, No. 3, pp. 455-462.
- [7] Salah El-Din MM (1998) Performance Analysis of Partially Wet Fin Assembly. *Applied Thermal Engineering* Vol. 18, No. 5, pp. 337-349.
- [8] Liang SY, Wong, TN, and Nathan GK (2000) *Comparison of One-Dimensional and Two-Dimensional Models for Wet Surface Efficiency of a Plate-Fin-Tube Heat Exchanger*. *Applied Thermal Engineering* Vol. 20, pp. 941-962.
- [9] Rosario L, Rahman MM (1998) Overall Efficiency of a Radial Fin Assembly Under Dehumidifying Conditions. *Journal of Energy Resources Technology* Vol. 120, No. 4, pp. 299-304.
- [10] Rosario L, Rahman MM (1999) Analysis of Heat Transfer in a Partially Wet Radial Fin Assembly During Dehumidification. *International Journal of Heat and Fluid Flow* Vol. 20, pp. 642-648.

- [11] Threlkeld JL (1970) *Thermal Environmental Engineering*. Prentice-Hall, New York.
- [12] ARI Standard 410-81 (1972) *Forced Circulation Air-Cooling and Air-Heating Coils*. Air Conditioning and Refrigeration Institute.
- [13] McQuiston FC (1975) Fin Efficiency with Combined Heat and Mass Transfer. *ASHRAE Transactions* Vol. 81, No. 1, pp. 350-355.
- [14] Coney JER, Sheppard CGW, and El-Shafei EAM (1989) Fin Performance with Condensation from Humid Air: a Numerical Investigation. *International Journal of Heat and Fluid Flow* Vol. 10, No. 3, pp. 224-231.
- [15] Srinivasan V, Shah RK (1997) Fin Efficiency of Extended Surfaces in Two-Phase Flow. *International Journal of Heat and Fluid Flow* Vol. 18, No. 4, pp. 419-429.
- [16] Elmahdy AH, Biggs RC (1983) Efficiency of Extended Surfaces with Simultaneous Heat and Mass Transfer. *ASHRAE Transactions* Vol. 89, No. 1A, pp. 135-143.
- [17] McQuiston FC, Parker JD (1994) *Heating, Ventilating, and Air Conditioning*, John Wiley & Sons, New York.
- [18] Schmidt TE (1949) *Heat Transfer Calculations for Extended Surfaces*. Refrigerating Engineering, pp. 351-357.
- [19] Hong TK, Webb RL (1996) Calculation of Fin Efficiency for Wet and Dry Fins. *International Journal of HVAC and Research*, Vol. 2, No. 1, pp. 27-41.
- [20] Lin Y, Hsu K, Chang Y, and Wang C (2001) Performance of Rectangular Fin in Wet Conditions: Visualization and Wet Fin Efficiency. *Journal of Heat Transfer* Vol. 123, No. 5, pp. 827-836.
- [21] Heggs P J, Ooi TH (2004) Design Charts for Radial Rectangular Fins in Terms of Performance Ratio and Maximum Effectiveness. *Applied Thermal Engineering* Vol. 24, pp. 1341-1351.
- [22] Lin CN, Jang JY (2002) A Two-Dimensional Fin Efficiency Analysis of Combined Heat and Mass Transfer in Elliptic Fins. *International Journal of Heat and Mass Transfer* Vol. 45, pp. 3839-3847.
- [23] Martin, H (1977) Heat and Mass Transfer Between Impinging Gas Jets and Solid Surfaces, *Adv. Heat Mass Transfer*, Vol.13, pp.1-60.
- [24] Viskanta, R, (1993) Heat Transfer to Impinging Isothermal Gas and Flames Jets. *Thermal and Fluid Science*, Vol. 2, pp. 111-134.

- [25] Hong, SK, Lee, DH, and Cho, HH, (2008) Heat/Mass Transfer Measurement on Concave Surface in Rotating Jet Impingement, *Journal of Mechanical Science and Technology*, Vol. 22, No. 10, pp.1952-1958.
- [26] Glauert, M.B. The Wall Jet, *Journal of Fluid Mechanics*, Vol.1, No.6, 1956, pp. 625–643.
- [27] McMurray, D.C., Myers, P.S., and Uyehara, O.A., “Influence of Impinging Jet Variables on Local Heat Transfer Coefficients Along a Flat Surface with Constant Heat Flux,” *Proc. of the 3rd Inter. Heat Transfer Conference*, Chicago, IL, Vol. 2, 1966, pp. 292–299.
- [28] Metzger, D.E., Cummings, K.N., and Ruby, W.A., “Effects of Prandtl Number on Heat Transfer Characteristics of Impinging Liquid Jets,” *Proc. of the 5th Inter. Heat Transfer Conference*, Tokyo, Vol. 2, 1974, pp. 20–24.
- [29] Thomas, S., Faghri, A., and Hankey, W.L., “Experimental Analysis and Flow Visualization of a Thin Liquid Film on a Stationary and Rotating Disk,” *Journal of Fluids Engineering*, Vol. 113, No.1, 1991, pp.73–80.
- [30] Faghri, A., Thomas, S., and Rahman, M.M., “Conjugate Heat Transfer from a Heated Disk to a Thin Liquid Film formed by a Controlled Impinging Jet,” *Journal of Heat Transfer*, Vol.115, No.1, 1993, pp. 116–123.
- [31] Hung, Y.H., and Lin, Z.H., “Effect of Confinement Plate on Heat Transfer Characteristics of a Circular Jet Impingement,” *Proc. of the ASME Fundamentals of Heat Transfer in Forced Convection*, HTD–Vol. 285, 1994, pp.101–109.
- [32] Garimella, S.V., and Rice, R., “Confined and Submerged Liquid Jet Impingement Heat Transfer,” *Journal of Heat Transfer*, Vol. 117, No. 4, 1995, pp. 871–877.
- [33] Webb, B.W., and Ma, C.F., “Single-phase Liquid Jet Impingement Heat Transfer,” *Advances in Heat Transfer*, 26(1), 1995, pp. 105–117.
- [34] Ma, C.F., Zheng, Q., Lee, S.C., and Gomi, T., “Impingement Heat Transfer and Recovery Effect with Submerged Jets of Large Prandtl Number Liquid 2. Initially Laminar Confined Slot Jets,” *International Journal of Heat and Mass Transfer*, Vol. 40, No.6, 1997, pp. 1491–1500.
- [35] Garimella, S.V., and Nenaydykh, B., “Nozzle-Geometry Effects in Liquid Jet Impingement Heat Transfer,” *International Journal of Heat and Mass Transfer*, Vol. 39, No. 14, 1996, pp. 2915–2923.

- [36] Li, D.Y., Guo, Z.Y., and Ma, C.F., “Relationship Between the Recovery Factor and the Viscous Dissipation in a Confined, Impinging, Circular Jet of High–Prandtl Number Liquid,” *International Journal of Heat and Fluid Flow*, Vol. 18, No.6, 1997, pp. 585–590.
- [37] Fitzgerald, J.A., and Garimella, S.V., “A Study of the Flow Field of a Confined and Submerged Impinging Jet,” *International Journal of Heat and Mass Transfer*, Vol. 41, No. 8–9, 1998, pp. 1025–1034.
- [38] Morris G.K., and Garimella, S.V., “Orifice and Impingement Flow Fields in Confined Jet Impingement,” *Journal of Electronic Packaging*, Vol. 120, No. 1, 1998, pp. 68–72.
- [39] Tzeng, P.Y. Soong, C.Y. and Hsieh, C.D. Numerical Investigation of Heat Transfer Under Confined Impinging Turbulent Slot Jets, *Numerical Heat Transfer, Part A*, Vol.35, No.8, pp. 903–924, 1999.
- [40] Inoue, A., Ui, A., Yamazaki, Y., Matsusita, H., and Lee, S.R., “Studies on a Cooling of High Heat Flux Surface in Fusion Reactor by Impinging Planar Jet Flow”, *Fusion Engineering and Design* , Vol. 51–52, 2000, pp. 781–787.
- [41] Inoue, A., Ui, A., Yamazaki, and Lee, S.R., “Studies on Cooling by Two-dimensional Confined Jet Flow of High Heat Flux Surface in Fusion Reactor”, *Nuclear Engineering and Design* , Vol. 200, 2000, pp. 317–329.
- [42] Li, C.Y., and Garimella, S.V., “Prandtl–Number Effects and Generalized Correlations for Confined and Submerged Jet Impingement,” *Inter. Journal of Heat and Mass Transfer*, Vol. 44, No.18, 2001, pp. 3471–3480.
- [43] Rahman, M.M., Dontaraju, P., and Ponnappan, R., “Confined Jet Impingement Thermal Management using Liquid Ammonia as the Working Fluid,” *Proc. of the ASME Inter. Mechanical Engineering Congress and Expo.*, New Orleans, Louisiana, 2002, pp. 1–10.
- [44] Ichimiya, K., and Yamada, Y., “Three–Dimensional Heat Transfer of a Confined Circular Impinging Jet with Buoyancy Effects,” *Journal of Heat Transfer*, Vol. 125, No.2, 2003, pp. 250–256.
- [45] Dano, B., Liburdy, J.A., and Kanokjaruvijit, K., “Flow Characteristics and Heat Transfer Performances of a Semi–confined Impinging Array of Jets: Effect of Nozzle Geometry,” *Inter. Journal of Heat and Mass Transfer*, Vol. 48, No. 3–4, 2005, pp.691–701.
- [46] Rahman, M.M., and Mukka, S. K., “Confined Liquid Jet Impingement on a Plate with Discrete Heating Elements,” *Proc. of the ASME Summer Heat Transfer Conference*, Vol.4, 2005, pp. 637–647.

- [47] Robinson, A.J., and Schnitzler, E. “An Experimental Investigation of Free and Submerged Miniature Liquid Jet Array Impingement Heat Transfer”, *Experimental Thermal and Fluid Science*, Vol. 32, No.1, 2007, pp.1–13.
- [48] Whelan, B.P., and Robinson A.J., “Nozzle Geometry Effects in Liquid Jet Array Impingement”, *Applied Thermal Engineering*, Vol. 29, No. 11–12, 2009, pp. 2211–22.
- [49] Rahman, M.M., Hernandez, C., and Lallave, J.C., “Free Liquid Jet Impingement From a Slot Nozzle to a Curved Plate”, *Numerical Heat Transfer, Part A*, Vol. 57, No. 11, 2010, pp.799–821.
- [50] Chang, S., and Liou, H., 2009 “Heat Transfer of Impinging Jet-array onto Concave- and Convex-dimpled Surfaces with Effusion” *International Journal of Heat and Mass Transfer*, Vol.52, 2009, pp.4484–4499.
- [51] Wang C, Lee S, Sheu J W, and Chang J Y (2002) A comparison of the airside performance of the fin-and-tube heat exchangers in wet conditions; with and without hydrophilic coating. *Applied Thermal Engineering*, v 22, n 3, p 267-78.
- [52] Sharma JN (2004) *Numerical methods for engineers and scientists*. Alpha Science International, Ltd. Pangbourne, UK. 231-237.
- [53] L. Rosario and M.M. Rahman, “A Two-Dimensional Numerical Study of Heat Transfer in a Finned Tube Assembly during Axisymmetric Dehumidification,” *ASME Journal of Energy Resources Technology*, Vol.121, No.4, pp. 247-253, 1999.
- [54] Fletcher, C.A.J., *Computational Galerkin Methods*, Springer Verlag, New York, 1984, pp. 27 and 205.
- [55] Özisik, M.N., *Heat Conduction*, 2nd ed., John Wiley and Sons, New York, 1993, Appendix 1, pp. 657–660.
- [56] Bejan, A., *Convection Heat Transfer*, 2nd ed., John Wiley & Sons, New York, 1995, Appendix C, pp. 595–602.

Appendices

Appendix A: Q-Basic Heat Transfer Code of a Wavy Fin Analysis

```
'MUTASIM AN ROSARIO - Research Basic program'  
'this program solves the ordinary differential equations'  
'For the radial fin assembly heat transfer with dehumification.'  
'X is the adimensional radius variable for fin portion.'  
'Y is the derivative of F for fin portion.'  
'F is the adimensional temperature for fin portion.'  
DIM X(1 TO 100), Y(1 TO 100), F(1 TO 100)  
'X1 is the adimensional radius variable for wall portion.'  
'Y1 is the derivative of F1 for wall portion.'  
'F1 is the adimensional temperature for portion.'  
DIM X1(1 TO 100), Y1(1 TO 100), F1(1 TO 100)  
'T is the temperature used to calculate ratio of sensible to  
total heat.'  
'pws saturation pressure.'  
'pw partial pressure of water vapor.'  
'w humidity ratio.'  
'the procedure used to calculate the humidity ratio taken from  
ASHRAE.'  
DIM T(1 TO 100), pws(1 TO 100), pw(1 TO 100), w(1 TO 100), CON(1  
TO 100), R(1 TO 100)  
'initial guess -0.01 Sept 14 97  
HR = .50  
cpa = .24  
rma = .075  
hfg = 1076  
T1 = 32  
T2 = 75.2
```

Appendix A: (Continued)

```
C8 = -1.04404 * 10000
C9 = -1.129465 * 10
C10 = -2.702235 / 100
C11 = 1.289036 / 100000
C12 = -2.478068 / 1000000000
C13 = 6.545967
CON2 = C8 / (T2 + 460) + C9 + C10 * (T2 + 460) + C11 * ((T2 +
460) ^ 2) + C12 * ((T2 + 460) ^ 3) + C13 * LOG(T2 + 460)
pws2 = EXP(CON2)
pw2 = HR * pws2
w2 = .62198 * pw2 / (14.7 - pw2)
' "INPUT PARAMETERS" '
BI1 = 1
BI2 = .1
' "PLEASE INPUT STEP SIZE H "; H for the fin calculation'
H = .1
'INPUT "PLEASE INPUT DIMENSION OF Y AND F ND "; ND for fin
calculation'
ND = 11
'INPUT "PLEASE INPUT NUMBER OF STEPS N "; N for fin calculation'
N = 11
' "N SHOULD BE LESS THAN OR EQUAL TO DIMENSION OF Y AND F"'
' INPUT CONVERGENCE CRITERION EPS "; EPS'
EDGE = H * N + 1.5 P
RINT "EDGE =", EDGE
' PARAMETERS'
'INPUT "PLEASE INPUT P"; P'
```

Appendix A: (Continued)

```
P = .25

'INPUT "PLEASE INPUT THETA";THETA

THETA = 3.1416 / 4

'INPUT "PLEASE INPUT STEP SIZE H1 "; H1 for wall calculation'

H1 = .05

'INPUT "PLEASE INPUT DIMENSION OF Y1 AND F1  ND1 "; ND1 for wall'

ND1 = 11

'INPUT "PLEASE INPUT NUMBER OF STEPS N1 "; N1 for wall'

N1 = 11

      'PRINT "N1 SHOULD BE LESS THAN OR EQUAL TO DIMENSION OF Y1
AND F1"'

'INPUT "PLEASE INPUT K'

K = 1

BI = BI2 * P / K

B = (BI / ((P ^ 2)))

EDGE1 = H1 * N1 + 1

PRINT "EDGE1 =", EDGE1

'SET INITIAL CONDITIONS'

100 INPUT "INITIAL GUESS `FOR Y1(1)= A1"; A1

PRINT A1

IF (A1 < -1000) THEN

GOTO 100

ELSE

END IF

40 Y1(1) = A1

'BOUNDARY CONDITION'

F1(1) = 1 + (Y1(1) / BI1)
```


Appendix A: (Continued)

```
X1(1) = 1
X(1) = 1.5
FOR IT = 1 TO 2
FOR I = 1 TO (N1 - 1)
RK11 = H1 * Y1(1)
RK21 = H1 * (Y1(I) + (RK11 / 2))
RK31 = H1 * (Y1(I) + (RK21 / 2))
RK41 = H1 * (Y1(I) + RK31)
F1(I + 1) = F1(I) + (RK11 + 2 * RK21 + 2 * RK31 + RK41) / 6
RK1P1 = H1 * 0
RK2P1 = H1 * ((RK1P1 / 2) / (H1 / 2))
RK3P1 = H1 * ((RK2P1 / 2) / (H1 / 2))
RK4P1 = H1 * ((RK3P1) / (H1))
Y1(I + 1) = Y1(I) + (RK1P1 + 2 * RK2P1 + 2 * RK3P1 + RK4P1) / 6
X1(I + 1) = X1(I) + H1
NEXT I
'to calculate Rb at base'
I = N1
T(I) = (T1 - T2) * F1(I) + T2
CON(I) = C8 / (T(I) + 460) + C9 + C10 * (T(I) + 460) + C11 *
((T(I) + 460) ^ 2) + C12 * ((T(I) + 460) ^ 3) + C13 * LOG((T(I) +
460))
pws(I) = EXP(CON(I))
pw(I) = HR * pws(I)
w(I) = .62198 * pw(I) / (14.7 - pw(I))
R(I) = 1 / (1 + (1 * hfg * (1 / (T2 - T1)) * (w2 - w(I)) /
((F1(I) * cpa))))
```

Appendix A: (Continued)

```
F(1) = F1(N1)

'BOUNDARY CONDITION'

Y(1) = (Y1(N1) + (BI2 / R(N1)) * (1 - P) * F1(N1)) / (K * P)

FOR I = 1 TO (N - 1)

RK1 = H * Y(I)

RK2 = H * (Y(I) + (RK1 / 2))

RK3 = H * (Y(I) + (RK2 / 2))

RK4 = H * (Y(I) + RK3)

F(I + 1) = F(I) + (RK1 + 2 * RK2 + 2 * RK3 + RK4) / 6

T(I) = (T1 - T2) * F(I) + T2

CON(I) = C8 / (T(I) + 460) + C9 + C10 * (T(I) + 460) + C11 *
((T(I) + 460) ^ 2) + C12 * ((T(I) + 460) ^ 3) + C13 * LOG((T(I) +
460))

pws(I) = EXP(CON(I))

pw(I) = HR * pws(I)

w(I) = .62198 * pw(I) / (14.7 - pw(I))

R(I) = 1 / (1 + (1 * hfg * (1 / (T2 - T1)) * (w2 - w(I)) / (F(I)
* cpa)))

RK1P = H * (B * COS(THETA) * F(I) / R(I))

T(I) = (T1 - T2) * (F(I) + RK1 / 2) + T2

CON(I) = C8 / (T(I) + 460) + C9 + C10 * (T(I) + 460) + C11 *
((T(I) + 460) ^ 2) + C12 * ((T(I) + 460) ^ 3) + C13 * LOG((T(I) +
460))

pws(I) = EXP(CON(I))

pw(I) = HR * pws(I)

w(I) = .62198 * pw(I) / (14.7 - pw(I))
```

Appendix A: (Continued)

```
R(I) = 1 / (1 + (1 * hfg * (1 / (T2 - T1)) * (w2 - w(I)) / ((F(I)
+ RK1 / 2) * cpa)))
RK2P = H * (B * COS(THETA) * (F(I) + RK1 / 2) / R(I) + (RK1P / 2)
/ (H / 2))
T(I) = (T1 - T2) * (F(I) + RK2 / 2) + T2
CON(I) = C8 / (T(I) + 460) + C9 + C10 * (T(I) + 460) + C11 *
((T(I) + 460) ^ 2) + C12 * ((T(I) + 460) ^ 3) + C13 * LOG((T(I) +
460))
pws(I) = EXP(CON(I))
pw(I) = HR * pws(I)
w(I) = .62198 * pw(I) / (14.7 - pw(I))
R(I) = 1 / (1 + (1 * hfg * (1 / (T2 - T1)) * (w2 - w(I)) / ((F(I)
+ RK2 / 2) * cpa)))
RK3P = H * (B * COS(THETA) * (F(I) + RK2 / 2) / R(I) + (RK2P / 2)
/ (H / 2))
CON(I) = C8 / (T(I) + 460) + C9 + C10 * (T(I) + 460) + C11 *
((T(I) + 460) ^ 2) + C12 * ((T(I) + 460) ^ 3) + C13 * LOG((T(I) +
460))
pws(I) = EXP(CON(I))
pw(I) = HR * pws(I)
w(I) = .62198 * pw(I) / (14.7 - pw(I))
R(I) = 1 / (1 + (1 * hfg * (1 / (T2 - T1)) * (w2 - w(I)) / ((F(I)
+ RK3) * cpa)))
RK4P = H * (B * cos(THETA) * (F(I) + RK3) / R(I) + (RK3P) / (H))
Y(I + 1) = Y(I) + (RK1P + 2 * RK2P + 2 * RK3P + RK4P) / 6
X(I + 1) = X(I) + H
NEXT I
```

Appendix A: (Continued)

```
IF (IT = 1) THEN
S1 = Y(N)
DA1 = A1 / 50000
A1 = A1 + DA1
Y1(1) = A1
ELSE
S2 = Y(N)
END IF
NEXT IT
T(N) = (T1 - T2) * (F(N)) + T2
CON(N) = C8 / (T(N) + 460) + C9 + C10 * (T(N) + 460) + C11 *
((T(N) + 460) ^ 2) + C12 * ((T(N) + 460) ^ 3) + C13 * LOG((T(N) +
460))
pws(N) = EXP(CON(N))
pw(N) = HR * pws(N)
w(N) = .62198 * pw(N) / (14.7 - pw(N))
R(N) = 1 / (1 + (1 * hfg * (1 / (T2 - T1)) * (w2 - w(N)) /
((F(N)) * cpa)))
'BOUNDARY CONDITION'
YEND = -(BI * F(N)) / (R(N) * P)
PRINT "YEND=", YEND
S12 = (S2 - S1) / DA1
IF (S12 = 0) THEN
GOTO 50
ELSE
END IF
A1 = Y1(1) + (YEND - Y(N)) / S12
```

Appendix A: (Continued)

```
IF (A1 < -1000) THEN
PRINT "TRY ANOTHER GUESS FOR A1"
GOTO 100
ELSE
END IF
IF (ABS(Z - A1) < EPS) THEN
GOTO 50
ELSE
END IF
Z = A1
GOTO 40
50 X(1) = 1.5
PRINT "T1="; T1; "T2="; T2; "HR="; HR
FOR I = 1 TO N1 STEP 1
PRINT I, X1(I), Y1(I), F1(I)
NEXT I
FOR I = 1 TO N STEP 2
PRINT I, X(I), Y(I), F(I)
NEXT I
END
```

Appendix B: FIDAP Code for Analysis of Heat Transfer by Jet Impingement

B.1 Using Copper "Cu" at Re = 100

```
FI-GEN( ELEM = 1, POIN = 1, CURV = 1, SURF = 1, NODE = 0, MEDG =
1, MLOO = 1,
MFAC = 1, BEDG = 1, SPAV = 1, MSHE = 1, MSOL = 1, COOR = 1, TOLE
= 0.0001 )
/POINTS
POINT( ADD, COOR, X = 0, Y = 0 )
POINT( ADD, COOR, X = -3.1125, Y = 0 )
POINT( ADD, COOR, X = -3.3125, Y = 0 )
POINT( ADD, COOR, X = -9.315, Y = 0 )
POINT( ADD, COOR, X = -9.315, Y = 0.3 )
POINT( ADD, COOR, X = -3.3125, Y = 0.3 )
POINT( ADD, COOR, X = -5.0653, Y = 4.2497 )
POINT( ADD, COOR, X = -9.315, Y = 6.01 )
POINT( ADD, COOR, X = -9.315, Y = 6.21 )
POINT( ADD, COOR, X = -4.9239, Y = 4.3911 )
POINT( ADD, COOR, X = -3.1125, Y = 0.3 )
POINT( ADD, COOR, X = 0, Y = 6.21 )
POINT( ADD, COOR, X = 0, Y = 0.3 )
/LINES
POINT ( SELE, ID )
1      6
CURVE( ADD, LINE )
POINT( SELE, ID )
6      8
CURVE( ADD, ARC )
POINT ( SELE, ID )
```

Appendix B: (Continued)

8 9
CURVE(ADD, LINE)
POINT(SELE, ID)
9 11
CURVE(ADD, ARC)
POINT (SELE, ID)
11
2
CURVE(ADD, LINE)
POINT (SELE, ID)
11
6
CURVE(ADD, LINE)
POINT (SELE, ID)
6
3
CURVE(ADD, LINE)
POINT (SELE, ID)
12
9
CURVE(ADD, LINE)
POINT (SELE, ID)
12
13
CURVE(ADD, LINE)
POINT (SELE, ID)
13

Appendix B: (Continued)

```
11
CURVE( ADD, LINE )
POINT ( SELE, ID )
13
1
CURVE( ADD, LINE )
/SURFACE
POINT ( SELE, ID )
1
4
12
9
SURFACE ( ADD, POIN, ROWW = 2, NOAD )
//MESH EDGES
CURVE( SELE, ID = 1 )
MEDGE( ADD, SUCC, INTE = 10, RATI = 0, 2RAT = 0, PCEN = 0 )
CURVE( SELE, ID = 2 )
MEDGE( ADD, SUCC, INTE = 9, RATI = 0, 2RAT = 0, PCEN = 0 )
CURVE( SELE, ID = 3 )
MEDGE( ADD, SUCC, INTE = 80, RATI = 0, 2RAT = 0, PCEN = 0 )
CURVE( SELE, ID = 4 )
MEDGE( ADD, SUCC, INTE = 10, RATI = 0, 2RAT = 0, PCEN = 0 )
CURVE( SELE, ID = 5 )
MEDGE( ADD, SUCC, INTE = 80, RATI = 0, 2RAT = 0, PCEN = 0 )
CURVE( SELE, ID = 6 )
MEDGE( ADD, SUCC, INTE = 140, RATI = 0, 2RAT = 0, PCEN = 0 )
CURVE( SELE, ID = 7 )
```


Appendix B: (Continued)

```
MEDGE( ADD, SUCC, INTE = 9, RATI = 0, 2RAT = 0, PCEN = 0 )
CURVE( SELE, ID = 8 )

MEDGE( ADD, SUCC, INTE = 140, RATI = 0, 2RAT = 0, PCEN = 0 )
CURVE( SELE, ID = 9 )

MEDGE( ADD, SUCC, INTE = 10, RATI = 0, 2RAT = 0, PCEN = 0 )
CURVE( SELE, ID = 10 )

MEDGE( ADD, SUCC, INTE = 9, RATI = 0, 2RAT = 0, PCEN = 0 )
CURVE( SELE, ID = 11 )

MEDGE( ADD, SUCC, INTE = 10, RATI = 0, 2RAT = 0, PCEN = 0 )
CURVE( SELE, ID = 12 )

MEDGE( ADD, SUCC, INTE = 10, RATI = 0, 2RAT = 0, PCEN = 0 )
CURVE( SELE, ID = 13 )

MEDGE( ADD, SUCC, INTE = 140, RATI = 1.1, 2RAT = 0, PCEN = 0 )
CURVE( SELE, ID = 14 )

MEDGE( ADD, SUCC, INTE = 10, RATI = 0, 2RAT = 0, PCEN = 0 )
CURVE( SELE, ID = 15 )

MEDGE( ADD, SUCC, INTE = 10, RATI = 0, 2RAT = 0, PCEN = 0 )

/LOOP 1

CURVE( SELE, ID )

1
9
14
15

MLOOP( ADD, MAP, VISI, NOSH, EDG1 = 1, EDG2 = 1, EDG3 = 1, EDG4 =
1 )

/LOOP 2

CURVE( SELE, ID )
```

Appendix B: (Continued)

14

8

12

13

```
MLOOP( ADD, MAP, VISI, NOSH, EDG1 = 1, EDG2 = 1, EDG3 = 1, EDG4 =  
1 )
```

```
/LOOP 3
```

```
CURVE( SELE, ID )
```

10

6

7

8

```
MLOOP( ADD, MAP, VISI, NOSH, EDG1 = 1, EDG2 = 1, EDG3 = 1, EDG4 =  
1 )
```

```
/LOOP 4
```

```
CURVE( SELE, ID )
```

2

11

10

9

```
MLOOP( ADD, MAP, VISI, NOSH, EDG1 = 1, EDG2 = 1, EDG3 = 1, EDG4 =  
1 )
```

```
/LOOP 5
```

```
CURVE( SELE, ID )
```

3

4

5

Appendix B: (Continued)

```
11
MLOOP( ADD, MAP, VISI, NOSH, EDG1 = 1, EDG2 = 1, EDG3 = 1, EDG4 =
1 )
//ADDING MESH FACE
SURFACE( SELE, ID = 1 )
MLOOP( SELE, ID = 1 )
MFACE( ADD )
//ADDING MESH FACE
SURFACE( SELE, ID = 1 )
MLOOP( SELE, ID = 2 )
MFACE( ADD )
//ADDING MESH FACE
SURFACE( SELE, ID = 1 )
MLOOP( SELE, ID = 3 )
MFACE( ADD )
//ADDING MESH FACE
SURFACE( SELE, ID = 1 )
MLOOP( SELE, ID = 4 )
MFACE( ADD )
//ADDING MESH FACE
SURFACE( SELE, ID = 1 )
MLOOP( SELE, ID = 5 )
MFACE( ADD )
// MESHING
MFACE( SELE, ID )
1
2
```

Appendix B: (Continued)

```
ELEMENT( SETD, QUAD, NODE = 4 )
MFACE( MESH, MAP, NOSM, ENTI = "Cu" )
MFACE( SELE, ID )
3
4
5
ELEMENT( SETD, QUAD, NODE = 4 )
MFACE( MESH, MAP, ENTI = "water" )
/MESH MAP ELEMENT ID
ELEMENT( SETD, EDGE, NODE = 2 )
MEDGE( SELE, ID = 4 )
MEDGE( MESH, MAP, ENTI = "inlet" )
MEDGE( SELE, ID = 7 )
MEDGE( MESH, MAP, ENTI = "outlet" )
MEDGE( SELE, ID = 5 )
MEDGE( MESH, MAP, ENTI = "surf1" )
MEDGE( SELE, ID = 6 )
MEDGE( MESH, MAP, ENTI = "surf2" )
MEDGE( SELE, ID )
13
15
MEDGE( MESH, MAP, ENTI = "bottom" )
MEDGE( SELE, ID )
1
2
3
MEDGE( MESH, MAP, ENTI = "axis" )
```

Appendix B: (Continued)

```
MEDGE( SELE, ID = 12 )

MEDGE( MESH, MAP, ENTI = "sides" )

MEDGE( SELE, ID )

8

9

MEDGE( MESH, MAP, ENTI = "interface" )

END( )

FIPREP( )

//Fluid and solid properties

/WATER PROPERTIES

DENSITY( ADD, SET = "water", CONS = 0.996 )

CONDUCTIVITY( ADD, SET = "water", CONS = 0.0014699 )

VISCOSITY( ADD, SET = "water", CONS = 0.00798 )

SPECIFICHEAT( ADD, SET = "water", CONS = 0.998137 )

SURFACETENSION( ADD, SET = "water", CONS = 73 )

/CU PROPERTIES

DENSITY( SET = "Cu", CONS = 8.954 )

CONDUCTIVITY( SET = "Cu", CONS = 0.922562 )

SPECIFICHEAT( SET = "Cu", CONS = 0.0915019 )

ENTITY( ADD, NAME = "Cu", SOLI, PROP = "Cu" )

ENTITY( ADD, NAME = "water", FLUI, PROP = "water" )

ENTITY( ADD, NAME = "inlet", PLOT )

ENTITY( ADD, NAME = "outlet", PLOT )

ENTITY( ADD, NAME = "surfl", PLOT )

ENTITY( ADD, NAME = "surf2", PLOT )

ENTITY( ADD, NAME = "bottom", PLOT )

ENTITY( ADD, NAME = "axis", PLOT )
```

Appendix B: (Continued)

```
ENTITY( ADD, NAME = "sides", PLOT )
ENTITY( ADD, NAME = "interface", PLOT, ATTA = "Cu", NATT =
"water" )
BODYFORCE( ADD, CONS, FX = 981, FY = 0, FZ = 0 )
PRESSURE( ADD, MIXE = 1e-11, DISC )
DATAPRINT( ADD, CONT )
EXECUTION( ADD, NEWJ )
PRINTOUT( ADD, NONE, BOUN )
OPTIONS (ADD, UPWI )
UPWINDING (ADD, STRE )
/You can try different ones to see which one works
RELAXATION( )
    0.3, 0.3, 0.3, 0, 0.05, 0.25, 0.25
    /0.6, 0.6, 0.6, 0, 0.3, 0.3, 0.3
    /0.5, 0.5, 0.5, 0, 0.75, 0.75, 0.75
BCNODE( ADD, URC, ENTI = "axis", ZERO )
BCNODE( ADD, URC, ENTI = "inlet", ZERO )
BCNODE( ADD, UZC, ENTI = "inlet", CONS = 50 )
BCNODE( ADD, TEMP, ENTI = "inlet", CONS = 37 )
BCNODE( ADD, VELO, ENTI = "surf1", ZERO )
BCNODE( ADD, VELO, ENTI = "surf2", ZERO )
BCNODE( ADD, VELO, ENTI = "sides", ZERO )
BCNODE( ADD, VELO, ENTI = "bottom", ZERO )
BCFLUX( ADD, HEAT, ENTI = "bottom", CONS = 5.971 )
BCNODE( ADD, VELO, ENTI = "interface", ZERO )
BCNODE( ADD, VELO, ENTI = "Cu", ZERO )
/ICNODE( VELO, STOKES )
```

Appendix B: (Continued)

```
/PROBLEM DEFINITION

PROBLEM( ADD, 2-D, INCO, STEA, LAMI, NONL, NEWT, MOME, ENER,
FIXE, SING )

SOLUTION( ADD, S.S. = 1500, VELC = 1e-5, RESC = 1e-5 )

CLIPPING( ADD, MINI )

      0,      0,      0,      0,      37,      0

END( )

CREATE( FISO )

RUN( FISOLV, BACK, AT = "", TIME = "NOW", COMP )
```

B.2 Using Copper "Cu" at Re = 750

```
FI-GEN( ELEM = 1, POIN = 1, CURV = 1, SURF = 1, NODE = 0, MEDG =
1, MLOO = 1,
MFAC = 1, BEDG = 1, SPAV = 1, MSHE = 1, MSOL = 1, COOR = 1, TOLE
= 0.0001 )

/POINTS

POINT( ADD, COOR, X = 0, Y = 0 )

POINT( ADD, COOR, X = -3.1125, Y = 0 )

POINT( ADD, COOR, X = -3.3125, Y = 0 )

POINT( ADD, COOR, X = -9.315, Y = 0 )

POINT( ADD, COOR, X = -9.315, Y = 0.3 )

POINT( ADD, COOR, X = -3.3125, Y = 0.3 )

POINT( ADD, COOR, X = -5.0653, Y = 4.2497 )

POINT( ADD, COOR, X = -9.315, Y = 6.01 )

POINT( ADD, COOR, X = -9.315, Y = 6.21 )

POINT( ADD, COOR, X = -4.9239, Y = 4.3911 )

POINT( ADD, COOR, X = -3.1125, Y = 0.3 )
```

Appendix B: (Continued)

```
POINT( ADD, COOR, X = 0, Y = 6.21 )
POINT( ADD, COOR, X = 0, Y = 0.3 )

/LINES

POINT ( SELE, ID )
1      6

CURVE( ADD, LINE )
POINT( SELE, ID )
6      8

CURVE( ADD, ARC )
POINT ( SELE, ID )
8      9

CURVE( ADD, LINE )
POINT( SELE, ID )
9      11

CURVE( ADD, ARC )
POINT ( SELE, ID )
11
2

CURVE( ADD, LINE )
POINT ( SELE, ID )
11
6

CURVE( ADD, LINE )
POINT ( SELE, ID )
6
3

CURVE( ADD, LINE )
```


Appendix B: (Continued)

```
POINT ( SELE, ID )
12
9
CURVE( ADD, LINE )
POINT ( SELE, ID )
12
13
CURVE( ADD, LINE )
POINT ( SELE, ID )
13
11
CURVE( ADD, LINE )
POINT ( SELE, ID )
13
1
CURVE( ADD, LINE )
/SURFACE
POINT ( SELE, ID )
1
4
12
9
SURFACE ( ADD, POIN, ROWW = 2, NOAD )
//MESH EDGES
CURVE( SELE, ID = 1 )
MEDGE( ADD, SUCC, INTE = 20, RATI = 0, 2RAT = 0, PCEN = 0 )
CURVE( SELE, ID = 2 )
```

Appendix B: (Continued)

MEDGE(ADD, SUCC, INTE = 10, RATI = 0, 2RAT = 0, PCEN = 0)
CURVE(SELE, ID = 3)
MEDGE(ADD, SUCC, INTE = 100, RATI = 0, 2RAT = 0, PCEN = 0)
CURVE(SELE, ID = 4)
MEDGE(ADD, SUCC, INTE = 10, RATI = 0, 2RAT = 0, PCEN = 0)
CURVE(SELE, ID = 5)
MEDGE(ADD, SUCC, INTE = 100, RATI = 0, 2RAT = 0, PCEN = 0)
CURVE(SELE, ID = 6)
MEDGE(ADD, SUCC, INTE = 200, RATI = 0, 2RAT = 0, PCEN = 0)
CURVE(SELE, ID = 7)
MEDGE(ADD, SUCC, INTE = 10, RATI = 0, 2RAT = 0, PCEN = 0)
CURVE(SELE, ID = 8)
MEDGE(ADD, SUCC, INTE = 200, RATI = 0, 2RAT = 0, PCEN = 0)
MEDGE(ADD, SUCC, INTE = 10, RATI = 0, 2RAT = 0, PCEN = 0)
CURVE(SELE, ID = 10)
MEDGE(ADD, SUCC, INTE = 10, RATI = 0, 2RAT = 0, PCEN = 0)
CURVE(SELE, ID = 11)
MEDGE(ADD, SUCC, INTE = 10, RATI = 0, 2RAT = 0, PCEN = 0)
CURVE(SELE, ID = 12)
MEDGE(ADD, SUCC, INTE = 20, RATI = 0, 2RAT = 0, PCEN = 0)
CURVE(SELE, ID = 13)
MEDGE(ADD, SUCC, INTE = 200, RATI = 1.1, 2RAT = 0, PCEN = 0)
CURVE(SELE, ID = 14)
MEDGE(ADD, SUCC, INTE = 20, RATI = 0, 2RAT = 0, PCEN = 0)
CURVE(SELE, ID = 15)
MEDGE(ADD, SUCC, INTE = 10, RATI = 0, 2RAT = 0, PCEN = 0)
CURVE(SELE, ID = 9)

Appendix B: (Continued)

```
/LOOP 1
CURVE( SELE, ID )
1
9
14
15
MLOOP( ADD, MAP, VISI, NOSH, EDG1 = 1, EDG2 = 1, EDG3 = 1, EDG4 =
1 )
/LOOP 2
CURVE( SELE, ID )
14
8
12
13
MLOOP( ADD, MAP, VISI, NOSH, EDG1 = 1, EDG2 = 1, EDG3 = 1, EDG4 =
1 )
/LOOP 3
CURVE( SELE, ID )
10
6
7
8
MLOOP( ADD, MAP, VISI, NOSH, EDG1 = 1, EDG2 = 1, EDG3 = 1, EDG4 =
1 )
/LOOP 4
CURVE( SELE, ID )
2
```

Appendix B: (Continued)

```
11
10
9
MLOOP( ADD, MAP, VISI, NOSH, EDG1 = 1, EDG2 = 1, EDG3 = 1, EDG4 =
1 )
/LOOP 5
CURVE( SELE, ID )
3
4
5
11
MLOOP( ADD, MAP, VISI, NOSH, EDG1 = 1, EDG2 = 1, EDG3 = 1, EDG4 =
1 )
//ADDING MESH FACE
SURFACE( SELE, ID = 1 )
MLOOP( SELE, ID = 1 )
MFACE( ADD )
//ADDING MESH FACE
SURFACE( SELE, ID = 1 )
MLOOP( SELE, ID = 2 )
MFACE( ADD )
//ADDING MESH FACE
SURFACE( SELE, ID = 1 )
MLOOP( SELE, ID = 3 )
MFACE( ADD )
//ADDING MESH FACE
SURFACE( SELE, ID = 1 )
```

Appendix B: (Continued)

```
MLOOP( SELE, ID = 4 )

MFACE( ADD )

//ADDING MESH FACE

SURFACE( SELE, ID = 1 )

MLOOP( SELE, ID = 5 )

MFACE( ADD )

// MESHING

MFACE( SELE, ID )

1

2

ELEMENT( SETD, QUAD, NODE = 4 )

MFACE( MESH, MAP, NOSM, ENTI = "Cu" )

MFACE( SELE, ID )

3

4

5

ELEMENT( SETD, QUAD, NODE = 4 )

MFACE( MESH, MAP, ENTI = "water" )

/MESH MAP ELEMENT ID

ELEMENT( SETD, EDGE, NODE = 2 )

MEDGE( SELE, ID = 4 )

MEDGE( MESH, MAP, ENTI = "inlet" )

MEDGE( SELE, ID = 7 )

MEDGE( MESH, MAP, ENTI = "outlet" )

MEDGE( SELE, ID )

5

6
```

Appendix B: (Continued)

```
MEDGE( MESH, MAP, ENTI = "surface" )
MEDGE( SELE, ID )
13
15
MEDGE( MESH, MAP, ENTI = "bottom" )
MEDGE( SELE, ID )
1
2
3
MEDGE( MESH, MAP, ENTI = "axis" )
MEDGE( SELE, ID = 12 )
MEDGE( MESH, MAP, ENTI = "sides" )
MEDGE( SELE, ID )
8
9
MEDGE( MESH, MAP, ENTI = "interface" )
END( )
FIPREP( )
//Fluid and solid properties
/WATER PROPERTIES
DENSITY( ADD, SET = "water", CONS = 0.996 )
CONDUCTIVITY( ADD, SET = "water", CONS = 0.0014699 )
VISCOSITY( ADD, SET = "water", CONS = 0.00798 )
SPECIFICHEAT( ADD, SET = "water", CONS = 0.998137 )
SURFACETENSION( ADD, SET = "water", CONS = 73 )
/SILICON PROPERTIES
/DENSITY( ADD, SET = "silicon", CONS = 2.33 )
```

Appendix B: (Continued)

```
/CONDUCTIVITY( ADD, SET = "silicon", CONS = 0.334608 )
/SPECIFICHEAT( ADD, SET = "silicon", CONS = 0.17006 )
/CU PROPERTIES
DENSITY( SET = "Cu", CONS = 8.954 )
CONDUCTIVITY( SET = "Cu", CONS = 0.922562 )
SPECIFICHEAT( SET = "Cu", CONS = 0.0915019 )
ENTITY( ADD, NAME = "Cu", SOLI, PROP = "Cu" )
ENTITY( ADD, NAME = "water", FLUI, PROP = "water" )
ENTITY( ADD, NAME = "inlet", PLOT )
ENTITY( ADD, NAME = "outlet", PLOT )
ENTITY( ADD, NAME = "surface", PLOT )
ENTITY( ADD, NAME = "bottom", PLOT )
ENTITY( ADD, NAME = "axis", PLOT )
ENTITY( ADD, NAME = "sides", PLOT )
ENTITY( ADD, NAME = "interface", PLOT, ATTA = "Cu", NATT =
"water" )
BODYFORCE( ADD, CONS, FX = 981, FY = 0, FZ = 0 )
PRESSURE( ADD, MIXE = 1e-11, DISC )
DATAPRINT( ADD, CONT )
EXECUTION( ADD, NEWJ )
PRINTOUT( ADD, NONE, BOUN )
OPTIONS (ADD, UPWI )
UPWINDING (ADD, STRE )
/You can try different ones to see which one works
RELAXATION( )
0.3, 0.3, 0.3, 0, 0.05, 0.25, 0.25
/0.6, 0.6, 0.6, 0, 0.3, 0.3, 0.3
```

Appendix B: (Continued)

```
/0.5, 0.5, 0.5, 0, 0.75, 0.75, 0.75
BCNODE( ADD, URC, ENTI = "axis", ZERO )
BCNODE( ADD, URC, ENTI = "inlet", ZERO )
BCNODE( ADD, UZC, ENTI = "inlet", CONS = 50 )
BCNODE( ADD, TEMP, ENTI = "inlet", CONS = 37 )
BCNODE( ADD, VELO, ENTI = "surface", ZERO )
/BCNODE( ADD, VELO, ENTI = "surf2", ZERO )
BCNODE( ADD, VELO, ENTI = "sides", ZERO )
BCNODE( ADD, VELO, ENTI = "bottom", ZERO )
BCFLUX( ADD, HEAT, ENTI = "bottom", CONS = 5.971 )
BCNODE( ADD, VELO, ENTI = "interface", ZERO )
BCNODE( ADD, VELO, ENTI = "Cu", ZERO )
/ICNODE( VELO, STOKES )
/PROBLEM DEFINITION
PROBLEM( ADD, 2-D, INCO, STEA, LAMI, NONL, NEWT, MOME, ENER,
FIXE, SING )
SOLUTION( ADD, S.S. = 1500, VELC = 1e-5, RESC = 1e-5 )
CLIPPING( ADD, MINI )
      0,      0,      0,      0,      37,      0
END( )
CREATE( FISO )
RUN( FISOLV, BACK, AT = "", TIME = "NOW", COMP )
```

B.3 Using Silicon "Si"

EXAMPLE 1

```
FI-GEN( ELEM = 1, POIN = 1, CURV = 1, SURF = 1, NODE = 0,
MEDG = 1, MLOO = 1,
```


Appendix B: (Continued)

```
MFAC = 1, BEDG = 1, SPAV = 1, MSHE = 1, MSOL = 1, COOR = 1,
TOLE = 0.0001 )
/POINTS
POINT( ADD, COOR, X = 0, Y = 0 )
POINT( ADD, COOR, X = -3.1125, Y = 0 )
POINT( ADD, COOR, X = -3.3125, Y = 0 )
POINT( ADD, COOR, X = -9.315, Y = 0 )
POINT( ADD, COOR, X = -9.315, Y = 0.3 )
POINT( ADD, COOR, X = -3.3125, Y = 0.3 )
POINT( ADD, COOR, X = -5.0653, Y = 4.2497 )
POINT( ADD, COOR, X = -9.315, Y = 6.01 )
POINT( ADD, COOR, X = -9.315, Y = 6.21 )
POINT( ADD, COOR, X = -4.9239, Y = 4.3911 )
POINT( ADD, COOR, X = -3.1125, Y = 0.3 )
POINT( ADD, COOR, X = 0, Y = 6.21 )
POINT( ADD, COOR, X = 0, Y = 0.3 )
/LINES
POINT ( SELE, ID )
1      6
CURVE( ADD, LINE )
POINT( SELE, ID )
6      8
CURVE( ADD, ARC )
POINT ( SELE, ID )
8      9
CURVE( ADD, LINE )
POINT( SELE, ID )
```

Appendix B: (Continued)

9 11
CURVE(ADD, ARC)
POINT (SELE, ID)
11
2
CURVE(ADD, LINE)
POINT (SELE, ID)
11
6
CURVE(ADD, LINE)
POINT (SELE, ID)
6
3
CURVE(ADD, LINE)
POINT (SELE, ID)
12
9
CURVE(ADD, LINE)
POINT (SELE, ID)
12
13
CURVE(ADD, LINE)
POINT (SELE, ID)
13
11
CURVE(ADD, LINE)
POINT (SELE, ID)

Appendix B: (Continued)

```
13
1
CURVE( ADD, LINE )
/SURFACE
POINT ( SELE, ID )
1
4
12
9
SURFACE ( ADD, POIN, ROWW = 2, NOAD )
//MESH EDGES
CURVE( SELE, ID = 1 )
MEDGE( ADD, SUCC, INTE = 40, RATI = 0, 2RAT = 0, PCEN = 0 )
CURVE( SELE, ID = 2 )
MEDGE( ADD, SUCC, INTE = 8, RATI = 0, 2RAT = 0, PCEN = 0 )
CURVE( SELE, ID = 3 )
MEDGE( ADD, SUCC, INTE = 80, RATI = 0, 2RAT = 0, PCEN = 0 )
CURVE( SELE, ID = 4 )
MEDGE( ADD, SUCC, INTE = 10, RATI = 0, 2RAT = 0, PCEN = 0 )
CURVE( SELE, ID = 5 )
MEDGE( ADD, SUCC, INTE = 80, RATI = 0, 2RAT = 0, PCEN = 0 )
CURVE( SELE, ID = 6 )
MEDGE( ADD, SUCC, INTE = 140, RATI = 0, 2RAT = 0, PCEN = 0 )
CURVE( SELE, ID = 7 )
MEDGE( ADD, SUCC, INTE = 8, RATI = 0, 2RAT = 0, PCEN = 0 )
CURVE( SELE, ID = 8 )
MEDGE( ADD, SUCC, INTE = 140, RATI = 0, 2RAT = 0, PCEN = 0 )
```

Appendix B: (Continued)

```
CURVE( SELE, ID = 9 )
MEDGE( ADD, SUCC, INTE = 10, RATI = 0, 2RAT = 0, PCEN = 0 )
CURVE( SELE, ID = 10 )
MEDGE( ADD, SUCC, INTE = 8, RATI = 0, 2RAT = 0, PCEN = 0 )
CURVE( SELE, ID = 11 )
MEDGE( ADD, SUCC, INTE = 10, RATI = 0, 2RAT = 0, PCEN = 0 )
CURVE( SELE, ID = 12 )
MEDGE( ADD, SUCC, INTE = 40, RATI = 0, 2RAT = 0, PCEN = 0 )
CURVE( SELE, ID = 13 )
MEDGE( ADD, SUCC, INTE = 140, RATI = 1.1, 2RAT = 0, PCEN = 0 )
CURVE( SELE, ID = 14 )
MEDGE( ADD, SUCC, INTE = 40, RATI = 0, 2RAT = 0, PCEN = 0 )
CURVE( SELE, ID = 15 )
MEDGE( ADD, SUCC, INTE = 10, RATI = 0, 2RAT = 0, PCEN = 0 )
/LOOP 1
CURVE( SELE, ID )
1
9
14
15
MLOOP( ADD, MAP, VISI, NOSH, EDG1 = 1, EDG2 = 1, EDG3 = 1, EDG4 =
1 )
/LOOP 2
CURVE( SELE, ID )
14
8
12
```

Appendix B: (Continued)

13

```
MLOOP( ADD, MAP, VISI, NOSH, EDG1 = 1, EDG2 = 1, EDG3 = 1, EDG4 =  
1 )
```

```
/LOOP 3
```

```
CURVE( SELE, ID )
```

10

6

7

8

```
MLOOP( ADD, MAP, VISI, NOSH, EDG1 = 1, EDG2 = 1, EDG3 = 1, EDG4 =  
1 )
```

```
/LOOP 4
```

```
CURVE( SELE, ID )
```

2

11

10

9

```
MLOOP( ADD, MAP, VISI, NOSH, EDG1 = 1, EDG2 = 1, EDG3 = 1, EDG4 =  
1 )
```

```
/LOOP 5
```

```
CURVE( SELE, ID )
```

3

4

5

11

```
MLOOP( ADD, MAP, VISI, NOSH, EDG1 = 1, EDG2 = 1, EDG3 = 1, EDG4 =  
1 )
```

Appendix B: (Continued)

```
//ADDING MESH FACE
SURFACE( SELE, ID = 1 )
MLOOP( SELE, ID = 1 )
MFACE( ADD )

//ADDING MESH FACE
SURFACE( SELE, ID = 1 )
MLOOP( SELE, ID = 2 )
MFACE( ADD )

//ADDING MESH FACE
SURFACE( SELE, ID = 1 )
MLOOP( SELE, ID = 3 )
MFACE( ADD )

//ADDING MESH FACE
SURFACE( SELE, ID = 1 )
MLOOP( SELE, ID = 4 )
MFACE( ADD )

//ADDING MESH FACE
SURFACE( SELE, ID = 1 )
MLOOP( SELE, ID = 5 )
MFACE( ADD )

// MESHING
MFACE( SELE, ID )

1
2

ELEMENT( SETD, QUAD, NODE = 4 )
MFACE( MESH, MAP, NOSM, ENTI = "Cu" )
MFACE( SELE, ID )
```

Appendix B: (Continued)

```
3
4
5
ELEMENT( SETD, QUAD, NODE = 4 )
MFACE( MESH, MAP, ENTI = "water" )
/MESH MAP ELEMENT ID
ELEMENT( SETD, EDGE, NODE = 2 )
MEDGE( SELE, ID = 4 )
MEDGE( MESH, MAP, ENTI = "inlet" )
MEDGE( SELE, ID = 7 )
MEDGE( MESH, MAP, ENTI = "outlet" )
MEDGE( SELE, ID = 5 )
MEDGE( MESH, MAP, ENTI = "surf1" )
MEDGE( SELE, ID = 6 )
MEDGE( MESH, MAP, ENTI = "surf2" )
MEDGE( SELE, ID )
13
15
MEDGE( MESH, MAP, ENTI = "bottom" )
MEDGE( SELE, ID )
1
2
3
MEDGE( MESH, MAP, ENTI = "axis" )
MEDGE( SELE, ID = 12 )
MEDGE( MESH, MAP, ENTI = "sides" )
MEDGE( SELE, ID )
```

Appendix B: (Continued)

8

9

```
MEDGE( MESH, MAP, ENTI = "interface" )  
  
END( )  
  
FIPREP( )  
  
//Fluid and solid properties  
  
/WATER PROPERTIES  
  
DENSITY( ADD, SET = "water", CONS = 0.996 )  
  
CONDUCTIVITY( ADD, SET = "water", CONS = 0.0014699 )  
  
VISCOSITY( ADD, SET = "water", CONS = 0.00798 )  
  
SPECIFICHEAT( ADD, SET = "water", CONS = 0.998137 )  
  
SURFACETENSION( ADD, SET = "water", CONS = 73 )  
  
/SILICON PROPERTIES  
  
/DENSITY( ADD, SET = "silicon", CONS = 2.33 )  
  
/CONDUCTIVITY( ADD, SET = "silicon", CONS = 0.334608 )  
  
/SPECIFICHEAT( ADD, SET = "silicon", CONS = 0.17006 )  
  
/CU PROPERTIES  
  
DENSITY( SET = "Cu", CONS = 8.954 )  
  
CONDUCTIVITY( SET = "Cu", CONS = 0.922562 )  
  
SPECIFICHEAT( SET = "Cu", CONS = 0.0915019 )  
  
ENTITY( ADD, NAME = "Cu", SOLI, PROP = "Cu" )  
  
ENTITY( ADD, NAME = "water", FLUI, PROP = "water" )  
  
ENTITY( ADD, NAME = "inlet", PLOT )  
  
ENTITY( ADD, NAME = "outlet", PLOT )  
  
ENTITY( ADD, NAME = "surfl", PLOT )  
  
ENTITY( ADD, NAME = "surf2", PLOT )  
  
ENTITY( ADD, NAME = "bottom", PLOT )
```


Appendix B: (Continued)

```
ENTITY( ADD, NAME = "axis", PLOT )
ENTITY( ADD, NAME = "sides", PLOT )
ENTITY( ADD, NAME = "interface", PLOT, ATTA = "Cu", NATT =
"water" )
BODYFORCE( ADD, CONS, FX = 981, FY = 0, FZ = 0 )
PRESSURE( ADD, MIXE = 1e-11, DISC )
DATAPRINT( ADD, CONT )
EXECUTION( ADD, NEWJ )
PRINTOUT( ADD, NONE, BOUN )
OPTIONS (ADD, UPWI )
UPWINDING (ADD, STRE )
/You can try different ones to see which one works
RELAXATION( )
    0.3, 0.3, 0.3, 0, 0.05, 0.25, 0.25
    /0.6, 0.6, 0.6, 0, 0.3, 0.3, 0.3
    /0.5, 0.5, 0.5, 0, 0.75, 0.75, 0.75
BCNODE( ADD, URC, ENTI = "axis", ZERO )
BCNODE( ADD, URC, ENTI = "inlet", ZERO )
BCNODE( ADD, UZC, ENTI = "inlet", CONS = 13.35341 )
BCNODE( ADD, TEMP, ENTI = "inlet", CONS = 37 )
BCNODE( ADD, VELO, ENTI = "surfl", ZERO )
BCNODE( ADD, VELO, ENTI = "surf2", ZERO )
BCNODE( ADD, VELO, ENTI = "sides", ZERO )
BCNODE( ADD, VELO, ENTI = "bottom", ZERO )
BCFLUX( ADD, HEAT, ENTI = "bottom", CONS = 2.9855 )
BCNODE( ADD, VELO, ENTI = "interface", ZERO )
BCNODE( ADD, VELO, ENTI = "Cu", ZERO )
```

Appendix B: (Continued)

```
/ICNODE( VELO, STOKES )

/PROBLEM DEFINITION

PROBLEM( ADD, 2-D, INCO, STEA, LAMI, NONL, NEWT, MOME, ENER,
FIXE, SING )

SOLUTION( ADD, S.S. = 1500, VELC = 1e-5, RESC = 1e-5 )

CLIPPING( ADD, MINI )

      0,      0,      0,      0,      37,      0

END( )

CREATE( FISO )

RUN( FISOLV, BACK, AT = "", TIME = "NOW", COMP )
```

B.4 Using Titanium "CuNi"

```
EXAMPLE 1

FI-GEN( ELEM = 1, POIN = 1, CURV = 1, SURF = 1, NODE = 0, MEDG =
1, MLOO = 1,
MFAC = 1, BEDG = 1, SPAV = 1, MSHE = 1, MSOL = 1, COOR = 1, TOLE
= 0.0001 )

/POINTS

POINT( ADD, COOR, X = 0, Y = 0 )

POINT( ADD, COOR, X = -3.1125, Y = 0 )

POINT( ADD, COOR, X = -3.3125, Y = 0 )

POINT( ADD, COOR, X = -9.315, Y = 0 )

POINT( ADD, COOR, X = -9.315, Y = 0.3 )

POINT( ADD, COOR, X = -3.3125, Y = 0.3 )

POINT( ADD, COOR, X = -5.0653, Y = 4.2497 )

POINT( ADD, COOR, X = -9.315, Y = 6.01 )

POINT( ADD, COOR, X = -9.315, Y = 6.21 )
```

Appendix B: (Continued)

```
POINT( ADD, COOR, X = -4.9239, Y = 4.3911 )
POINT( ADD, COOR, X = -3.1125, Y = 0.3 )
POINT( ADD, COOR, X = 0, Y = 6.21 )
POINT( ADD, COOR, X = 0, Y = 0.3 )

/LINES

POINT ( SELE, ID )
1      6
CURVE( ADD, LINE )
POINT( SELE, ID )
6      8
CURVE( ADD, ARC )
POINT ( SELE, ID )
8      9
CURVE( ADD, LINE )
POINT( SELE, ID )
9      11
CURVE( ADD, ARC )
POINT ( SELE, ID )
11
2
CURVE( ADD, LINE )
POINT ( SELE, ID )
11
6
CURVE( ADD, LINE )
POINT ( SELE, ID )
6
```

Appendix B: (Continued)

```
3
CURVE( ADD, LINE )
POINT ( SELE, ID )
12
9
CURVE( ADD, LINE )
POINT ( SELE, ID )
12
13
CURVE( ADD, LINE )
POINT ( SELE, ID )
13
11
CURVE( ADD, LINE )
POINT ( SELE, ID )
13
1
CURVE( ADD, LINE )
/SURFACE
POINT ( SELE, ID )
1
4
12
9
SURFACE ( ADD, POIN, ROWW = 2, NOAD )
//MESH EDGES
```

Appendix B: (Continued)

CURVE(SELE, ID = 1)
MEDGE(ADD, SUCC, INTE = 40, RATI = 0, 2RAT = 0, PCEN = 0)
CURVE(SELE, ID = 2)
MEDGE(ADD, SUCC, INTE = 8, RATI = 0, 2RAT = 0, PCEN = 0)
CURVE(SELE, ID = 3)
MEDGE(ADD, SUCC, INTE = 80, RATI = 0, 2RAT = 0, PCEN = 0)
CURVE(SELE, ID = 4)
MEDGE(ADD, SUCC, INTE = 10, RATI = 0, 2RAT = 0, PCEN = 0)
CURVE(SELE, ID = 5)
MEDGE(ADD, SUCC, INTE = 80, RATI = 0, 2RAT = 0, PCEN = 0)
CURVE(SELE, ID = 6)
MEDGE(ADD, SUCC, INTE = 140, RATI = 0, 2RAT = 0, PCEN = 0)
CURVE(SELE, ID = 7)
MEDGE(ADD, SUCC, INTE = 8, RATI = 0, 2RAT = 0, PCEN = 0)
CURVE(SELE, ID = 8)
MEDGE(ADD, SUCC, INTE = 140, RATI = 0, 2RAT = 0, PCEN = 0)
CURVE(SELE, ID = 9)
MEDGE(ADD, SUCC, INTE = 10, RATI = 0, 2RAT = 0, PCEN = 0)
CURVE(SELE, ID = 10)
MEDGE(ADD, SUCC, INTE = 8, RATI = 0, 2RAT = 0, PCEN = 0)
CURVE(SELE, ID = 11)
MEDGE(ADD, SUCC, INTE = 10, RATI = 0, 2RAT = 0, PCEN = 0)
CURVE(SELE, ID = 12)
MEDGE(ADD, SUCC, INTE = 40, RATI = 0, 2RAT = 0, PCEN = 0)
CURVE(SELE, ID = 13)
MEDGE(ADD, SUCC, INTE = 140, RATI = 1.1, 2RAT = 0, PCEN = 0)
CURVE(SELE, ID = 14)

Appendix B: (Continued)

```
MEDGE( ADD, SUCC, INTE = 40, RATI = 0, 2RAT = 0, PCEN = 0 )
CURVE( SELE, ID = 15 )
MEDGE( ADD, SUCC, INTE = 10, RATI = 0, 2RAT = 0, PCEN = 0 )
/LOOP 1
CURVE( SELE, ID )
1
9
14
15
      MLOOP( ADD, MAP, VISI, NOSH, EDG1 = 1, EDG2 = 1, EDG3 = 1,
EDG4 = 1 )
/LOOP 2
CURVE( SELE, ID )
14
8
12
13
MLOOP( ADD, MAP, VISI, NOSH, EDG1 = 1, EDG2 = 1, EDG3 = 1, EDG4 =
1 )
/LOOP 3
CURVE( SELE, ID )
10
6
7
8
MLOOP( ADD, MAP, VISI, NOSH, EDG1 = 1, EDG2 = 1, EDG3 = 1, EDG4 =
1 )
```

Appendix B: (Continued)

```
/LOOP 4
CURVE( SELE, ID )
2
11
10
9
MLOOP( ADD, MAP, VISI, NOSH, EDG1 = 1, EDG2 = 1, EDG3 = 1, EDG4 =
1 )
/LOOP 5
CURVE( SELE, ID )
3
4
5
11
MLOOP( ADD, MAP, VISI, NOSH, EDG1 = 1, EDG2 = 1, EDG3 = 1, EDG4 =
1 )
//ADDING MESH FACE
SURFACE( SELE, ID = 1 )
MLOOP( SELE, ID = 1 )
MFACE( ADD )
//ADDING MESH FACE
SURFACE( SELE, ID = 1 )
MLOOP( SELE, ID = 2 )
MFACE( ADD )
//ADDING MESH FACE
SURFACE( SELE, ID = 1 )
MLOOP( SELE, ID = 3 )
```

Appendix B: (Continued)

```
MFACE( ADD )

//ADDING MESH FACE

SURFACE( SELE, ID = 1 )

MLOOP( SELE, ID = 4 )

MFACE( ADD )

//ADDING MESH FACE

SURFACE( SELE, ID = 1 )

MLOOP( SELE, ID = 5 )

MFACE( ADD )

// MESHING

MFACE( SELE, ID )

1

2

ELEMENT( SETD, QUAD, NODE = 4 )

MFACE( MESH, MAP, NOSM, ENTI = "CuNi" )

MFACE( SELE, ID )

3

4

5

ELEMENT( SETD, QUAD, NODE = 4 )

MFACE( MESH, MAP, ENTI = "water" )

/MESH MAP ELEMENT ID

ELEMENT( SETD, EDGE, NODE = 2 )

MEDGE( SELE, ID = 4 )

MEDGE( MESH, MAP, ENTI = "inlet" )

MEDGE( SELE, ID = 7 )

MEDGE( MESH, MAP, ENTI = "outlet" )
```


Appendix B: (Continued)

```
MEDGE( SELE, ID = 5 )
MEDGE( MESH, MAP, ENTI = "surf1" )
MEDGE( SELE, ID = 6 )
MEDGE( MESH, MAP, ENTI = "surf2" )
MEDGE( SELE, ID )
13
15
MEDGE( MESH, MAP, ENTI = "bottom" )
MEDGE( SELE, ID )
1
2
3
MEDGE( MESH, MAP, ENTI = "axis" )
MEDGE( SELE, ID = 12 )
MEDGE( MESH, MAP, ENTI = "sides" )
MEDGE( SELE, ID )
8
9
MEDGE( MESH, MAP, ENTI = "interface" )
END( )
FIPREP( )
//Fluid and solid properties
/WATER PROPERTIES
DENSITY( ADD, SET = "water", CONS = 0.996 )
CONDUCTIVITY( ADD, SET = "water", CONS = 0.0014699 )
VISCOSITY( ADD, SET = "water", CONS = 0.00798 )
SPECIFICHEAT( ADD, SET = "water", CONS = 0.998137 )
```

Appendix B: (Continued)

```
SURFACETENSION( ADD, SET = "water", CONS = 73 )

/Constantan (CuNi)PROPERTIES

DENSITY( ADD, SET = "CuNi", CONS = 8.9 )

CONDUCTIVITY( ADD, SET = "CuNi", CONS = 0.04657497 )

SPECIFICHEAT( ADD, SET = "CuNi", CONS = 0.39 )

/SILICON PROPERTIES

/DENSITY( ADD, SET = "silicon", CONS = 2.33 )

/CONDUCTIVITY( ADD, SET = "silicon", CONS = 0.334608 )

/SPECIFICHEAT( ADD, SET = "silicon", CONS = 0.17006 )

/CU PROPERTIES

/DENSITY( SET = "Cu", CONS = 8.954 )

/CONDUCTIVITY( SET = "Cu", CONS = 0.922562 )

/SPECIFICHEAT( SET = "Cu", CONS = 0.0915019 )

ENTITY( ADD, NAME = "CuNi", SOLI, PROP = "CuNi" )

ENTITY( ADD, NAME = "water", FLUI, PROP = "water" )

ENTITY( ADD, NAME = "inlet", PLOT )

ENTITY( ADD, NAME = "outlet", PLOT )

ENTITY( ADD, NAME = "surf1", PLOT )

ENTITY( ADD, NAME = "surf2", PLOT )

ENTITY( ADD, NAME = "bottom", PLOT )

ENTITY( ADD, NAME = "axis", PLOT )

ENTITY( ADD, NAME = "sides", PLOT )

ENTITY( ADD, NAME = "interface", PLOT, ATTA = "CuNi", NATT =

"water" )

BODYFORCE( ADD, CONS, FX = 981, FY = 0, FZ = 0 )

PRESSURE( ADD, MIXE = 1e-11, DISC )

DATAPRINT( ADD, CONT )
```

Appendix B: (Continued)

```
EXECUTION( ADD, NEWJ )

PRINTOUT( ADD, NONE, BOUN )

OPTIONS (ADD, UPWI )

UPWINDING (ADD, STRE )

/You can try different ones to see which one works

RELAXATION( )

    0.3, 0.3, 0.3, 0, 0.05, 0.25, 0.25

    /0.6, 0.6, 0.6, 0, 0.3, 0.3, 0.3

    /0.5, 0.5, 0.5, 0, 0.75, 0.75, 0.75

BCNODE( ADD, URC, ENTI = "axis", ZERO )

BCNODE( ADD, URC, ENTI = "inlet", ZERO )

BCNODE( ADD, UZC, ENTI = "inlet", CONS = 13.35341 )

BCNODE( ADD, TEMP, ENTI = "inlet", CONS = 37 )

BCNODE( ADD, VELO, ENTI = "surf1", ZERO )

BCNODE( ADD, VELO, ENTI = "surf2", ZERO )

BCNODE( ADD, VELO, ENTI = "sides", ZERO )

BCNODE( ADD, VELO, ENTI = "bottom", ZERO )

BCFLUX( ADD, HEAT, ENTI = "bottom", CONS = 2.9855 )

BCNODE( ADD, VELO, ENTI = "interface", ZERO )

BCNODE( ADD, VELO, ENTI = "CuNi", ZERO )

/ICNODE( VELO, STOKES )

/PROBLEM DEFINITION

    PROBLEM( ADD, 2-D, INCO, STEA, LAMI, NONL, NEWT, MOME,

ENER, FIXE, SING )

SOLUTION( ADD, S.S. = 1500, VELC = 1e-5, RESC = 1e-5 )

CLIPPING( ADD, MINI )

    0,    0,    0,    0,    37,    0
```

Appendix B: (Continued)

```
END( )
```

```
CREATE( FISO )
```

```
RUN( FISOLV, BACK, AT = "", TIME = "NOW", COMP )
```